Palaeoproductivity reconstruction for the Northern Indian Ocean utilizing lipid biomarkers

A Thesis submitted to Goa University for the award of the Degree of
DOCTOR OF PHILOSOPHY

in
MARINE SCIENCE

By

Vikesano Rosaline Punyu

Research Guide

Dr. Virupaxa K. Banakar

Goa University,
Taleigao, Goa
(2015)

CHAPTER 1

INTRODUCTION

"The farther backwards you can look; the farther forward you are likely to see"-Winston Churchill

1.1. Palaeoclimatology

The natural changes in the global climate primarily is governed by astronomical parameters (Earth's orbital configuration), which bring-in complex interactions between atmosphere, oceans and continents. The regional and local ocean-atmosphere-biosphere-cryosphere-lithosphere dynamics are superimposed on these primary parameters which together produce resultant effect known as climate variability. The climatic system has undergone several changes since the formation of the earth around 4.5 billion years ago. The climate change varies in magnitude and rate and processes and mechanisms. These involve highly complex feedbacks between its various components. Understanding the interconnections between various components of the climate system is a challenging job where many components are yet to be uncovered.

The word "palaeoclimate" has been derived from the Greek words "palaeo" meaning "long ago" and "climate" meaning "weather". The palaeoclimatology, in its simplest definition, is the study of changes in climate that have occurred in the geological past. Bradley (1991) defined it as the study of climate "prior to the period of instrumental measurements". The goal of palaeoclimate studies may vary from description and interpretation of climate at a given time to the nature and rate of climatic changes during specific time intervals (Brassell, 1993).

From documented records, it is known that the climate has always been dynamic throughout Earth's geological history. Around 650 my ago, the earth was believed to be completely covered with ice (Snow Ball Earth: Kirschvink, 1992), while around 55 my ago, it witnessed extremely warm temperature and became totally ice-free, which is popularly known as Paleocene-Eocene Thermal Maximum (Kenneth and Stott, 1991).

Lately at around 2 my ago a rhythmic cycle of cold-and-warm climate repeating approximately at every 100,000 years began (Milankovitch, 1938). Around 20,000 years ago (last glacial period) many parts of North America, Northern Europe and high-latitude Asia were covered with ice sheets. We are now in the recent-most warm period called the Holocene. Again, within the present Holocene period, the earth experienced the mini cold spells known as the "Younger Dryas" (12,800 -11,500 B.P) and the "Little Ice Age" (1400-1860 A.D).

Today, the significance of climate change is at the peak-of-concern of the world, mainly because of the phenomenon called 'global warming'. Due to human induced warming of the climate, the planet is witnessing rapid rise in global average temperatures since the 19^{th} century causing significant melting of glaciers and ice-sheets, measurable sea-level rises, changing weather patterns and increased frequency of storms and cyclones and other catastrophic events. This warming phenomenon has come as a warning siren to us, simply, because it can possibly bring about disturbances to the earth system beyond our comprehension and may severly affect the very existence of human race that has not yet proved its adaptability to extreme climates. So far, observed fluctuations in climate system and associated catastrophic extreme events remind us that the climatic change is inevitable but also may be unpredictable.

The solar radiation received at the earth's surface (insolation) is not constant over the entire surface of the planet due to its shape, and not remained constant through time due to its changing orbital ellipticity and tilt in its rotational axis. As solar energy is the primary fuel for all climate-related processes, a slightest change in the Earth's orbital parameters can change the insolation significantly causing climate change. A network of global measurement of solar radiation was documented during the International Geophysical Year in 1957/58. The results of this study indicated that

the Sun's energy at the surface of the Earth has undergone significant variation which, in turn, affected the climate through decades. Eddy (1976) for the first time provided a detailed account of the correlation of long term climatic variation and solar radiation. A classic example of Sun's variation is the appearance and disappearance of sunspots. Periodicity of sunspot cycles spans ~11 years (Schwabe, 1843). Interestingly, satellite measurements of irradiance have shown that there is a positive correlation between the number of sunspots and total solar irradiance. During periods such as the Maunder Minimum (1645-1715), the Sporer Minimum (1460-1550), and the Dalton Minimum (1795-1820) when sunspots were rare or absent, lower than average global temperature was observed. More recently, Sirocko et al. (2012) observed that over the last 230 years, 10 out of the 14 "freezings" of the Rhine River in Europe occurred during low sunspot activity. Such observations indicate the connection between solart activity and climate. As already mentioned, the major causes modulating the variation of solar radiation reaching the earth surface are the Milankovitch Cycles (Figure 1).

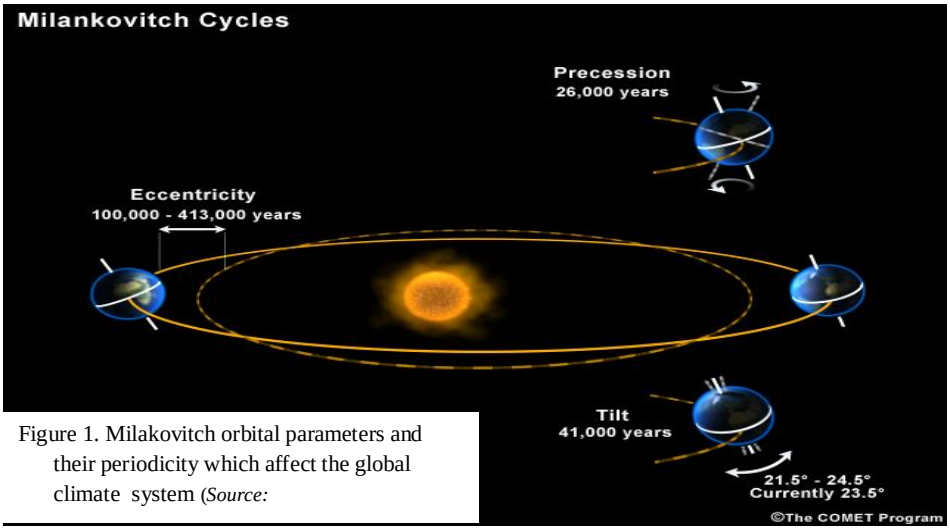

Figure 1. Milakovitch orbital parameters and their periodicity which affect the global climate system (*Source:*

The link between astronomical parameters and climate change was earlier proposed by Adhemar (1842) and Croll (1875). Milankovitch (1920) provided an accurate mathematical basis for this link which became a basis for paleoclimatology popularly known as Milankovitch Orbital Theory of Climate Change. The Milankovitch Cycles are considered as the pacemakers of glacial-interglacial cycles during most of the Pleistocene, which is also known as the 'Ice Age'.

The eccentricity of Earth's orbit around the sun, the obliquity (angle from the vertical position of the rotation axis) and precession or wobbling of the rotation axis (see Figure 1) produce ~100,000, ~40,000 and ~20,000 years cycles in the climate variability (Milankovitch, 1920). The insolation changes due to changes in these orbital parameters at a given point of time are a cumulative effect emerging out of superimposition of all these three parameters.

There are several factors which contribute to palaeoclimatic changes in addition to the primary pace-maker, the insolation. For instance, the major cause of the cold "Younger Dryas" is thought to be the shutdown of formation of deep-waters in North Atlantic, i.e., the North Atlantic Deep Water (NADW), due to which inter-hemispheric heat exchange driven by NADW (Global Thermohaline Conveyor) had reduced significantly. As a result, the entire Europe came under freezing conditions caused by the weakening of warm westerlies flowing from north Atlantic over the Europe, thus resulting in the Younger Dryas between 12,800-11,500 years BP. In the present time, the role of atmospheric carbon dioxide (CO_2) and other anthropogenic greenhouse gases are believed to play major roles in enhancing global temperature. This issue is elaborately discussed in the Intergovernmental Panel on Climate change (IPCC) Report-2007. The IPCC points out that the natural systems are being affected by regional changes and attributed the cause of global warming to 'greenhouse gas

emissions due to human activities'. The same report gives an estimate of around 70 % increase in these anthropogenic components was between 1970 and 2004.

The data collected from Greenland Ice have shown that CO_2 levels in the pre-industrial era was ~280 ppmv after which it rose abruptly to ~365 ppmv (Wahlen et al., 1991; Smith et al., 1997a,b; Tschumi and Stauffer, 2000). Similarly, the Antarctic ice cores also have shown similar range for pre-anthropogenic variability in atmospheric CO_2 since ~800,000 years (Epica Community Members, 2006). The atmospheric CO_2 recorded in excess of the maximum natural level of 280 ppmv is caused by the human activity particularly from the beginning of industrial era. Emissions from automobiles, industries, massive deforestation, and phenomenal changes in land use and land cover are largely held responsible for the global warming. Therefore, it is important to look into the natural variability of the past climate in order to improve our understanding of the anthropogenic forcing.

The knowledge of palaeoclimate has increased greatly since 1970s with the discovery of 'Little Ice Age' (~400 years ago: Matthews, 1939) and the "Medieval Warm Period" (~1000-1300 A.D: Lamb, 1965). However, uncertainties and unexplained mechanisms still exist about these events. The efforts are on to develop new robust palaeoclimate proxies to unravel the past events on precise time-scale so as to provide baseline of natural changes over which the human induced changes are imprinted. This is necessary to develop predictive models of future climate.

1.2. Palaeoclimate proxies

The proxies for palaeoclimate reconstructions range from direct measurements such as gas contents in ice cores and indirect measurements using various organic and inorganic proxies sensitive to climate which are well-preserved in different types of repositories. In simple terms, a climate proxy may be defined as a component in nature which 'contains a climatic signal' (Bradley, 1991).

The organic proxies include OM or C_{org}, lipids, pollen grains, vegetation type, tree rings, bacterial biomass etc. Reconstruction of palaeoclimate using proxies is a tedious task. The potential proxy should have two essential qualities. Firstly, the component should be sensitive to changes in its ambient environment. Secondly, the proxy should have the ability to incorporate that change and store it for long time. A compilation of various sources of paleoclimate proxy is presented in Table 1 [*Source*: Bradley (1991)].

Glaciological	**Geological**		**Biological**
	Marine	**Terrestrial**	
Geochemical tracers -Gas content in air bubbles -Trace elements and microparticle concentration	Biogenic Sediments -Oxygen isotope -Faunal and floral abundance -Morphological variations -Alkenones	Glacial deposits and features of glacial erosion	Tree rings
		Periglacial features	Pollen
		Shorelines	Plant Microfossils
Physical properties (e.g., ice fabric)		Aeolian deposits	Insects
		Lacustrine sediments and erosional features	Corals
	Inorganic Sediments -terrestrial (aeolian dust) and ice rafted debris -clays	Pedological features	Diatoms, Ostracods and other biota in lake sediments
		Speleothems	Modern population distribution

The proxies such as OM, stable isotopes, microfossils, elements and their isotopes etc in marine deposits (sediments and authigenic minerals) not only contain records of climatological variables, but also contain information on changes in the weathering history of adjacent land masses (Banakar et al., 2003), and provide insights into the history of climate and vegetation cover (Sukumar et al., 1995; Galy et al., 2008). Some of the major parameters of ocean dynamics and the proxies that are employed to study them are listed below:

- *Sea surface temperature (SST):* Proxies such as oxygen isotopes and Mg/Ca ratios and clumped-isotopes of planktic foraminifera, alkenone unsaturation index in sedimentary-OM ($U^{k'}_{37}$) etc., are used for reconstructing the past SST. A relatively recent SST proxy which is widely used is the Tetraether Index with 86 carbon atoms (TEX_{86}) based on membrane lipid of mesophilic marine Thaurmarchaeota (Shouten et al., 2000). Proxies such as long chain alkenones ($U^{k'}_{37}$) and TEX_{86} are particularly useful in palaeo-SST reconstructions at high latitude locations, where conventional proxies based on carbonate geochemistry is often difficult to employ.
- *Sea water salinity*: Robust palaeosalinity proxies are still lacking. Nevertheless, palaeosalinity estimates are obtained from oxygen isotopes of palaeo-seawater which is calculated by combining SST and oxygen isotopic data extracted from planktonic foraminifera (See Rostek et al., 1997; Banakar et al., 2010 and references therein). Measurement of deuterium-hydrogen ratio (D/H) of sedimentary algal lipids is increasingly being employed to measure palaeosalinity (Sachs et al., 2009; Smittenberg et al., 2011).
- *Deep-water circulation:* Neodymium isotopes (εNd) in sedimentary Mn-oxide particulates are used to trace water-mass provenance and transport as every individual water mass has a distinct Nd isotopic composition (Kaufman et al.,

1993; Piotrowski et al., 2009). In addition, nutrient based proxies such as stable isotopes of carbon ($\delta^{13}C$) of benthic foraminifers and ratio of cadmium to calcium (Cd/Ca) are also used (Shackleton et al., 1983; Boyle and Keigwin, 1982; Ninnemann and Charles, 2002)

- *Marine productivity:* Reconstruction of marine productivity is often done by measuring C_{org}, $\delta^{13}C_{org}$, various lipid biomarkers, carbonates, opal, barium, trace metals such as cadmium, copper and scavenged radionuclides (^{230}Th). The organic molecules such as 'lipids' have been considered as most robust productivity proxies as they are largely refractory to the post depositional diagenesis (Brassell et al., 1986; Volkman, 1986; Prahl et al., 1994). The lipids also provide information about different types of photosynthetic pathways involved in synthesis of specific molecules and hence could be useful to identify marine- and terrestrial-plant biome down to their specific communities (Boon et al., 1979; Brassell, 1993; Volman et al., 1999).

1.3. Lipid biomarkers as palaeoclimate proxies

Lipids are a group of naturally occurring biological compounds that have a common property of being sparingly soluble in water, but highly soluble in organic solvents such as hexane, chloroform, acetone etc. Lipids are generally defined by their physical properties rather than by structural features as seen in other organic compounds such as carbohydrates, proteins etc. This is because lipids have diverse structures and cannot be represented by a generalized structure. Lipids are generally hydrophobic in nature but some maybe amphipathic, wherein, part of their structure is

hydrophilic. The insolubility of lipids in water is due to their long hydrocarbon chains which can be either saturated or unsaturated.

Lipids are categorised broadly into four groups following Bloor (1943) with certain modifications. These groups are: a) simple lipids, b) compound lipids, c) derived lipids, and d) miscellaneous, as depicted in Figures 2 and 3.

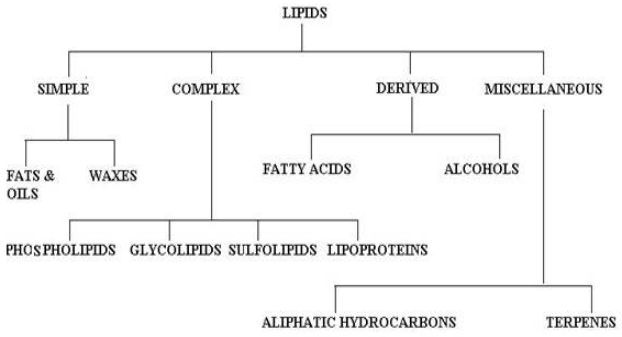

Figure 2. Classification of lipids (Bloor, 1943)

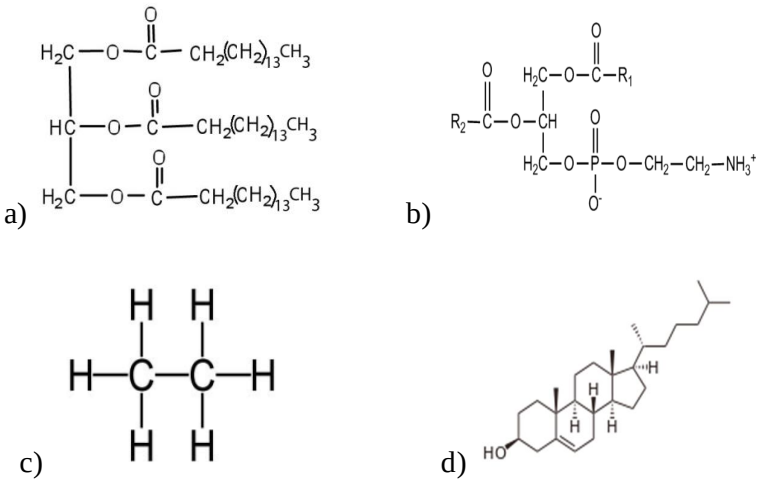

Figure 3. Structure of, a) Simple lipid (triglyceride), b) Complex lipid (phospholipids), c) Hydrocarbon (ethane) and d) Derived lipid (cholesterol). (*Source:fr.wikipedia.org catalog.flatworldknowledge.com)*

Simple lipids are those containing esters of fatty acids and various alcohols i.e., basically made up carbon, hydrogen and oxygen (fats, triglycerides, waxes etc.). The complex lipids include esters containing elements or groups besides carbon, hydrogen, oxygen, fatty acids and alcohols. These groups or elements may contain constituents such as phosphates (phospholipids), sulphur (sulpholipids), carbohydrates (glycolipids), proteins (lipoproteins) etc. Derived lipids are the hydrolysis products of simple and complex lipids, which retain the fundamental characteristics of lipids. This group includes fatty acids and alcohols. The miscellaneous group consists of all the compounds, which could not be grouped in the above three categories. It includes hydrocarbons, terpenes, carotenoids, squalene, vitamins E and K.

Besides this, there are several classifications of lipids based on different parameters. The most recent internationally accepted classification is given by the LIPID MAPS (LIPID Metabolites and Pathways Strategy) Consortium (2005), wherein, lipids have been classified into eight major groups based on well defined chemical and biochemical principles (Fahy et al., 2005). They are fatty acyls (fatty acids and eicosanoids), glycerolipids (diacyl and triacylglycerols), glycerophospho-lipids (phosphatidylcholines and phosphatidyl-ethanoamines), sphingolipids (ceramides, glycolipids and sphingomyelins), sterol lipids (cholesterol, bile acids and sterol hormones), prenol lipids (isoprenoids), saccharolipids (acylaminosugars) and polyketides (flavanoids).

Lipids are widely distributed throughout living organisms. The functions of lipids in biological entities are diverse. The most prominent function is in the formation of structural layers in cell membranes. A cell membrane is composed of a lipid bilayer consisting of glycerophospholipids. Membrane layers also provide fluidity and flexibility to the membranes. Lipids also partake in energy storage as

triglycerides in adipose tissue. Here, the triglycerols are inert and are composed of three fatty acids and a glycerol. In addition, lipids also function as 'chemical messengers' in multicellular organisms, also known as 'signal transduction' to send information between organelles and other cells. Intracellular organelles such as mitochondria of liver cells and grana of chloroplasts contain lipoproteins which contribute to their structural maintenance and functional integrity. Besides, lipids are superior to proteins and carbohydrates in providing energy to the body. (A detailed account of lipids may be obtained from 'Lipid Biochemistry: An Introduction', by M.I. Gurr, J.L. Harwood, K.N Frayn, 2008).

Lipids form a small fraction of the total organic pool in marine environment. However, they reveal important information especially on their sources when characterised at molecular level (Meyers, 2003). Lipids are comparatively resistant to bacterial degradation (Volkman, 2006), and remain in marine sediments and water column over a long period of time without undergoing diagenesis. Thus, they retain their fundamental structures, which permit them to serve as powerful biomarkers. A biomarker is defined as an organic compound with a carbon skeleton having a clear link with a known, contemporary natural product (Eglington and Calvin, 1967; Mackenzie, 1984). In a natural environment, biomarkers could be found structurally intact or as rearranged biomolecules. The concept of biomarkers (also known as molecular markers) was first introduced in the late 1960s by Eglington and Calvin (1967) wherein, these markers were originally named as "chemical fossils". Such molecular compounds or biomarkers give long time-scale information about their biological origins (Brassel et al., 1986), and also the processes, metabolism and carbon sequestration in water columns as well as sediments (Hedges et al., 1997; Meyers, 1997). Lipid are widely used in palaeoclimate studies, because, they are source

specific and their synthesis is directly connected to the ambient environment (Poynter et al., 1989).

Lipids in marine sediments are generally derived from marine and terrestrial OM (also known as soil-carbon). Besides, polycyclic aromatic hydrocarbons (PAHs) derived from crude petroleum and oil spills also contribute to the sedimentary organic pool. The lipids from these sources have distinct molecular characteristics and can be identified/quantified. Broadly, autochthonous marine sources are characterised by short chain lipids whereas, long chain lipids are characteristic of allochthonous terrestrial plants (Bray and Evans, 1961; Clark and Blumer, 1967; Eglington and Hamilton, 1967). While sources of autochthonous marine sedimentary lipids include phytoplanktons, marine bacteria, fungi, yeast, zooplanktons, eukaryotes etc, and allochthonous sources include terrestrial C3 or C4 plants.

Some lipids are diagnostic of specific group of organisms. For instance, sterols such as brassicasterols and dinosterols are specific to diatoms and dinoflagellates respectively (Boon et al., 1979; Volkman et al., 1998). Marine compounds such as phytosterols, haptophyte derived $U^{K'}_{37}$ and alkyl alkenoates are helpful in tracing surface productivity (Poynter et al., 1989; Madureira et al., 1995). The $U^{K'}_{37}$ (alkenone unsaturation) is also helpful in estimating past SST (Marlowe et al., 1984; Prahl and Wakeham, 1987; Banakar et al., 2005). Thus, the potential of lipid biomarkers is remarkable in tracing past changes in productivity patterns and their associated biogeochemical processes.

As already mentioned, the synthesis of lipids during photosynthesis of marine and land plants is largely specific to community levels and hence, a powerful tool to understand past climate variation based on their distribution in sedimentary-OM. For example, the intact polar lipids (IPL: membrane lipids) were used to provide an estimate

of ~90 Petagram (billion tones) of carbon buried in the upper 1 m sediment column of the world oceans is composed of bacterial biomass (Lipp et al., 2008). This in itself is an indicator of the importance of marine productivity in sequestering most prominent greenhouse gas, the CO_2. The variation in the lipid proxy phytol, would indicate the changes in marine productivity, while the brassicasterols are synthesized by diatoms and alkenones by cocolithophores (Brassell, 1993; Boon et al., 1979; Tolosa et al., 2003).

1.4. Marine primary production

Karl et al. (2001) demonstrated a direct relationship between climate variability and oceanic productivity and biodiversity. Marine palaeoproductivity studies give insights into the causes of biological changes and provide valuable information on biogeochemical feedbacks and interactions of the climatic system (Rao and Graffiths, 1998). The focus of palaeonutrient is to study changes in the deep-water formation and circulation (Sigman and Mathis, 2012; Ruttenberg, 1993; Sarmiento and Gruber, 2006). Studies have revealed that even in regions of high concentrations of nutrients, the availability of micronutrient such as iron can greatly affect the productivity which has direct link to atmospheric CO_2 budget (Martin et al., 1994; Boyd et al., 2000). Dezileau et al. (2004) have proposed that the paleoproductivity in upwelling systems of eastern South Pacific has been dictated by the iron input from Andes. Thus, the climate-productivity link can be understood through past nutrient-cycling.

The fixation of atmospheric CO_2 by primary producers is quite significant and changes in their production would affect the atmospheric CO_2 balance. The photosynthesis wherein, autotrophs synthesize OM (carbohydrates) from CO_2 and water in the presence of sunlight is described in the relationship given below:

$$6CO_2 + 6H_2O \xrightarrow{\text{sunlight}} C_6H_{12}O_6 + 6O_2 \uparrow$$

The microscopic phytoplanktons which play a phenomenal role in regulating the atmosphere CO_2 inhabit the euphotic zone and vary in size from <1 to >100 µ. As a result of degradation of chlorophyll- a (primary indicator of photosynthesis), it is difficult to assess the production based on this direct proxy (Gorham et al., 1974). However, successful attempts have been made to estimate the production of this pigment by measuring its alteration products such as chlorins (Chen et al., 2000; Higginson et al., 2003; Haiyan et al., 2010).

1.5. Indian monsoons

The word "monsoon" is derived from the word "*mausam*" which, in Arabic, means "season". The monsoon system is defined as a seasonal reversal of wind direction (Ramage, 1971; Gadgil, 2003). The Indian monsoon consists of two phases known as South-West monsoon (summer monsoon: June-August) and North-East monsoon (winter monsoon: November-January). Monsoons are of great importance to a country like India where rain-dependent agriculture is the backbone of the nation. This is because the summer monsoon which accounts for ~75 to 80 % of total annual rainfall (Kelkar, 2009) drives the country's agriculture. Thus, it is necessary to understand its behavior in the past to help in forecasting its variability under rapidly changing climatic conditions. It is also necessary to know clearly the natural changes in the pattern of monsoons to enable us to subtract it from the cumulative effect of natural and manmade forcing. It is noteworthy here, that, the atmospheric CO_2 rise during the post-industrial period is extremely rapid (~100 ppmv in ~200 years: i.e., 0.5

ppmv/y) as compared to that of natural rise that occurred from coldest glacial maximum to warmest interglacial optimums (~100 ppmv in ~8000 years: i.e., 0.012 ppmv/y), i.e, the human induced changes are nearly 50 times faster than the nature induced changes in the climate system.

Globally, there are six monsoon systems of which, the Indian monsoon system is one of them (Overpeck et al., 1996). The Indian monsoons are believed to have started with the uplift of Himalayas and Tibetan Plateau. This tectonic evolution brought about the required atmospheric circulations necessary to cause seasonal reversal of Indian monsoons (Kutzbach et al., 1989; Valdiya 1993; Zhiseng et al., 2001). In the 17^{th} century itself, Edmund Halley (1686) proposed that the Indian monsoon was the result of differential heating of the Asian landmass and the Indian Ocean, which till today remains as primary forcing. This is because water has higher heat capacity with respect to land. A pressure gradient develops as a result of thermal contrast between these two components inducing air to flow from high pressure area to low pressure area. Accordingly, because of the higher insolation during the summer, moisture filled air from a high pressure area (Indian Ocean) blow towards a lower pressure area (Indian sub-continent) causing summer (southwest) monsoons. A reverse process occurs during the winter and is known as the northeast (winter) monsoons. Walker (1920) recognized the role of El Nino-Southern Oscillation (ENSO) in the Indian monsoon dynamics, which has become the matter of rigorous study and debate. More recently, Gadgil (1988) proposed that the monsoons were also dictated by the latitudinal position of Inter-Tropical Convergence Zone (ITCZ). Thus, sustenance and teleconnections in the Indian monsoon system are yet to be clearly understood to provide tools for accurate prediction.

Based on the Arabian Sea sedimentary records, palaeoclimate studies have indicated that the summer monsoons strengthened during the warm interglacials, while winter monsoons intensified during the cold glacials (Prell et al., 1980; Cullen, 1981; Duplessy, 1982; Banakar et al., 2005, 2010; Chodankar et al., 2005; Sirocko and Ittekot, 1992; Clemens and Prell, 1991). The effects of variation in Indian monsoons are manifested as variation in terrestrial vegetation and productivity in the surrounding seas. The time-series of climate sensitive proxies preserved in marine sediment provide an opportunity to understand such changes in the past.

This thesis essentially addresses monsoon variability through changes in the characteristics of marine and terrestrial photosynthetic reservoirs (productivity) utilizing sedimentary lipids as proxies.

1.6. Circulation in the northern Indian Ocean

As the water circulation plays a vital role in modulating the climatology and biogeochemistry in response to reversing monsoon wind system, it is necessary to know the seasonal changes in the circulation pattern. The circulation in the northern Indian Ocean consists of currents present in the Arabian Sea, BoB and equatorial region north of 10˚S (McCreary et al., 2009). This surface circulation system is largely forced by the monsoon wind system and hence, is an important component of biogeochemical processes occurring in these basins. In general, surface currents in the Indian Ocean are stronger than those in the Pacific and Atlantic Oceans (Tomczak and Godfrey, 1994). During the winter monsoon, surface circulation is anticlockwise, while during summer monsoons it is clockwise (Shankar et al., 2002) (see Figure 4 A & B). The major currents which appear during the winter monsoons are South Equatorial Current, the Equatorial Counter Current, the North Equatorial Current and

associated currents of the summer monsoons are the Southwest Monsoon Current and the northward Somali Currents become dominant (Tomczak and Godfrey, 1994). The circulation in northern Indian Ocean is mainly driven by the seasonally reversing monsoon winds. Hence, these currents and their associated features occur rhythmically according to the seasons (Kantha et al., 2008).

Summer monsoon currents:

The southwesterly summer monsoon currents appear as an extension of Somali current system in the western Arabian Sea, flows through the southeast in the EAS, turns east and enters into the BoB (Vinaychandran et al., 1999 and reference therein). The summer monsoon currents are initially fed by the south equatorial currents and East African Coastal Current in the equatorial region of the Indian Ocean. Off the west coast of India, the West Indian Coastal Current (a southward flowing current along the western coast of India) feeds into the summer monsoon currents. This merged current then flows southeast and around the Lakshadweep Low, turns eastward south of Sri Lanka and finally into the BoB. The East Indian Coastal Current bifurcates in the BoB (Figure 4A).

Winter monsoon currents:

The northeasterly winter monsoon current is a westward flowing current which appears south of Sri Lanka around the month of November. It is initially fed by the East Indian Coastal Current (equatorward flowing current) along the eastern coast of India. The Winter Monsoon Current bifurcates into two branches in the Arabian Sea, one of which turns around the Lakshadweep High and joins the poleward West Indian Coastal Current while the other branch continues to flow westwards. This westward current becomes the Somali Current after reaching the western Arabian Sea. The

Somali Current then flows southwest and along with the northward flowing East African Coastal Current, they both turn eastward and feed into the South Equatorial Counter Current (Figure 4B).

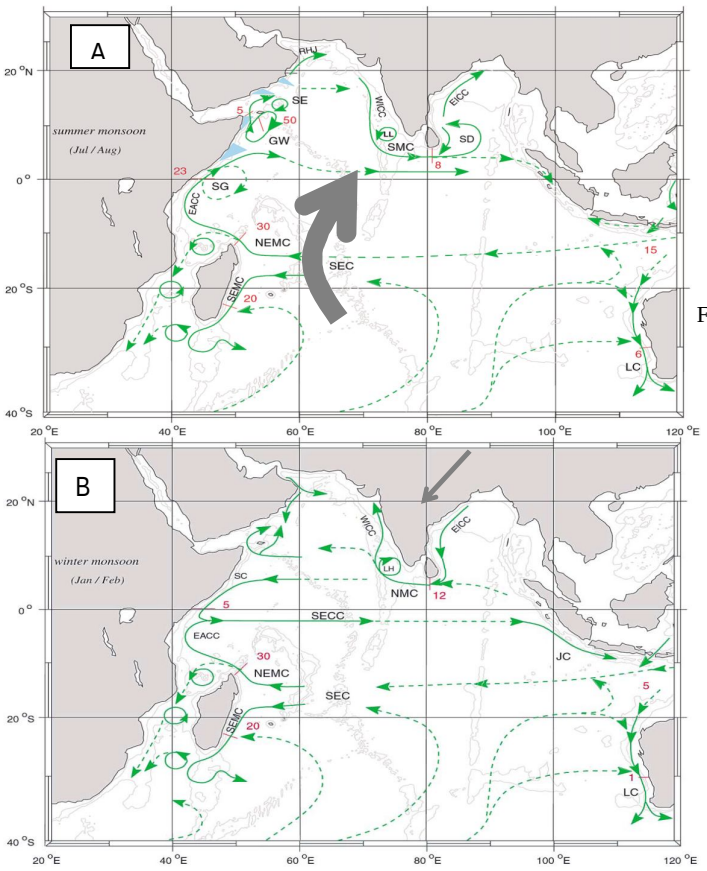

Figure 4 A & B. Circulation in the northern Indian Ocean. Figure 4A shows the southwest monsoon circulation while the Figure 4B depicts the northeast monsoon circulation (EC- Equatorial Current; SC – Somali Current; EICC – East Indian Coastal Current, WICC – West India Coastal Current, SMC – Summer Monsoon Current, WMC – Winter Monsoon Current, LL – Lakshadweep Low, LH – Lakshadweep High, EACC – East African Coastal Current, SECC – South Equatorial Counter Current, SEC – South Equatorial Current, GW – Great Whirl) (*Source: Schott and McCreary, 2001; Shankar et al., 2001*). The shaded arrows general direction of summer and winter monsoon winds respectively.

Equatorial currents:

In the EIO region, strong eastward surface jets known as Westerly Jet (WJ) (Wyrtki, 1973), which were named later as Wyrtki Jet, are dominant during the inter-monsoon periods. The appearance of the WJ during the spring and fall inter-monsoon periods makes the Indian Ocean unique from the other oceans. The surface currents are westward during winter and summer monsoons whereas, they are much intense and eastward during spring and fall inter-monsoon periods.

1.7. Objectives and working hypothesis of the present research

The seasonally reversing Indian monsoon system dictates the nutrient availability for primary production in the Arabian Sea (Wyrtki, 1973). There is a distinct change in the basin wide productivity pattern and particle flux with the reversal of monsoons, wherein, summer monsoon period records highest particle flux (~300-600 mg/m^2/day) and winter monsoons records relatively lower particle flux (~100-200 mg/m^2/day) (Haake et al., 1993), where particle flux is largely governed by the settling biogenic matter.

Further, the type of production also varies depending upon the monsoons, e.g., summer monsoon production is dominated by coccolithophores and winter monsoons with diatoms (Haake et al., 1993; Balch et al., 2000; Prahl et al., 2000). Hence, time-series of refractory lipid biomarker in a sediment core should be able to provide not only the past variation in the relative intensity of the monsoons, but also variability in the type of production and causes thereof. This hypothesis essentially forms the basis of the present thesis.

The present study area, the northern Indian Ocean comes under the direct influence of reversing Indian monsoons and hence, is well suited to accurately reconstruct the changes in biogeochemistry with the help of lipid biomarkers as tools. To the best of my knowledge, palaeoproductivity reconstructions in the northern Indian Ocean using lipid biomarkers are rare and limited to very few publications (see Rostek et al., 1997; Schubert et al., 1998; Cayre and Bard, 1999; Schulte et al., 1999; Schouten et al., 2000; Schulte and Bard, 2003; Kurian et al., 2009).

The lipid biomarkers can clearly demarcate marine and terrestrial sources of OM and also are sources specific. For example, the phytol is used to trace general productivity (Didyk et al., 1978) and brassicasterol is used to trace opal producers

such as the diatoms (Ishiwatari et al., 1999). Short chain *n*-alkanes and *n*-alkanols are characteristic molecules synthesized by marine phytoplanktons whereas, long chain *n*-alkanes and *n*-alkanols indicate terrestrial photosynthetic production (Clark and Blumer., 1967; Rieley et al., 1991). Proxies such as C/N and $\delta^{13}C_{org}$ are analyzed along with lipid biomarkers to trace the sources of OM.

In the light of this background, the objective (aim) for the present study was defined so as to enable me to understand the changes in the input of lipid biomarkers and source-specific biomarkers to the sediment through time, and its implication to monsoon variability during the preceding climate extremes unaffected by anthropogenic impact, viz., the LGM and the Holocene.

Chapter 2

STUDY AREA

2.1. Seafloor topography

The northern Indian Ocean includes Arabian Sea, BoB and the EIO, i.e., the marine regime north of equator. The total area of the Arabian Sea (between 0˚ and 23˚ N latitudes and 50˚ and 80˚ E longitudes) is ~6.2 million sq. km., while the BoB (0 and 23˚ N latitudes and 80˚ and 100˚ E longitudes) covers an area of ~4.1 million sq. km (Qasim, 1998). The maximum depth of the Arabian Sea is ~ 4700 m with an average depth of around 2700 m (Groves and Hunt, 1980). On the other hand, the BoB has a maximum depth ~5300 m with an average depth of ~2600 m (Dutt and Chatterjee, 2005). Many major rivers such as the Ganges, Brahmaputra, Godavari, Mahanadi, Irrawady etc., flow into the BoB. Hence, the annual river runoff in the bay is huge (around 2950 km^3: Dai and Trendberth, 2002; Fekete et al., 2002). The river runoff in the Arabian Sea is nearly six times lesser than that of the BoB (525 km^3: Sengupta and Qasim, 1995).

The seafloor topography of the Arabian Sea consists of major ridges (Laxmi Ridge: Chagos Laccadive Ridge and Carlsberg Ridge (Naini and Talwani, 1982). Among these, the Carlsberg Ridge is a part of mid-ocean ridge system and is seismic while the others are aseismic ridges and remnants of hotspot track. These ridges further dissect the northern Indian Ocean into different basins such as the Arabian Basin, the Laxmi Basin and the Laccadive Basin. The fracture zones in the ridges serve as connecting links between the basins and also aid in deep water circulation. The ridges in the BoB are covered by a rather thick pile of sediments of the Bengal Fan rendering the basin virtually featureless (Sarma et al., 2000).

The sediments of the northern Indian Ocean, particularly, near the mouths of rivers are mostly composed of terrigeneous deposits brought by rivers (Tchernia, 1980). In the Arabian Sea, maximum carbon preservation (~4.9 %) occurs at a depth

of around 400 m due to preservation and accumulation owing to the presence of OMZ (Levin et al., 2000). Sediments in the equatorial region of the northern Indian Ocean mostly include red clay composed of fine grained, organic poor sediments due to its oligotrophic environment (Berger, 1974; Kennett, 1982).

2.2. Water masses

There are three distinct water masses present in the Arabian Sea, viz., the Arabian Sea High Salinity Water, the Persian Gulf Water and the Red Sea Water (Rochford, 1964). The Arabian Sea High Salinity Water is found at the surface in the north and increasingly overlain by low salinity waters towards south. The depth of Arabian Sea High Salinity Water varies from 20 m to 60 m. The Persian Gulf water is formed in the Persian Gulf and flows into the Gulf of Oman through the Straits of Hormuz. From the Gulf of Oman it spreads in to the northern Arabian Sea and is found at a depth of ~300 m (Shetye et al., 1994; Tomczak and Godfrey, 1994). The high salinity Red Sea Water enters the Gulf of Aden from the Red Sea through the Straits of Bab-el-Mandeb and can be traced even up to 1000 m depth near equator (Tomczak and Godfrey, 1994). The higher salinity Persian Gulf Water and Red Sea Water form as a result of excess evaporation over precipitation. The North Indian Deep Water which originates from North Atlantic Deep Water and Circumpolar Deep Water occupies the region between 1200 m- to 3800 m (Kallel et al., 1988; You, 2000). The depth below 3800 m is occupied by the Antarctic Bottom Waters (Reid, 2003). Each of these water masses has distinct properties along with oxygenation and nutrient history.

2.3. Sea surface temperature and salinity distribution

The SST varies from 24-30 ˚C in the Arabian Sea (Rao and Graffiths, 1998). The SST in the EIO varies in a narrow range of 28-29 ˚C due to less intense seasonal effects (Fernandes et al., 2008). In the northern Indian Ocean, in general, the SST maximum occurs during the spring inter-monsoon, which instantly begins to decrease with the setting-in of summer monsoons (Tomzack and Godfrey, 1994). Significant lowering of SSTs is observed during the summer monsoon in the upwelling regions off Oman where the SST decrease to ~22 ˚C (Fieux and Stommel, 1976).

The surface salinity in the northern Indian Ocean varies from an average of 32 psu in the BoB to ~37 psu in the Arabian Sea (Rao and Graffiths, 1998). High salinity water is characteristic of the Arabian Sea as it is an evaporative basin and also receives low river-water input as compared to the river input to BoB, mainly because of draining of small and medium seasonal rivers, except Indus. On the contrary, the lower salinity in the BoB is due to very high freshwater flux to the basin by a major river system, viz., Ganga-Brahmaputra, in addition to heavy overhead precipitation (Rao and Sivakumar, 2003).

Surface salinity changes in the Arabian Sea follows the Evaporation – Precipitation (E-P) budget. The E-P, in turn, is dictated by the monsoons. During the summer monsoons, rate of precipitation exceeds evaporation whereas, during the winter monsoons, evaporation rate is high due to the dry northeasterly winds (Luis and Kawamura, 2004 and references, therein). The surface salinity in the Arabian Sea follows a north-south and west-east gradient with high salinity in the northern and western part and low salinity in the corresponding south and east Arabian Sea, respectively. During winter, the formation of the Arabian Sea high salinity water causes the salinity to reach ~ 37 psu in northern Arabian Sea which gradually

decreases towards the south. On the other hand, the Poleward Coastal Current (PCC) which flows northward along the western margin of India (Shetye et al., 1991) transport ~6 Sv of low salinity waters from the BoB (~33 psu) into the EAS (Shankar, 2000), which dramatically reduces the salinity in the EAS (Wyrtki, 1973) to ~35 psu (Figure 5). During the summer monsoons the salinity of the EAS is governed by volume of overhead precipitation.

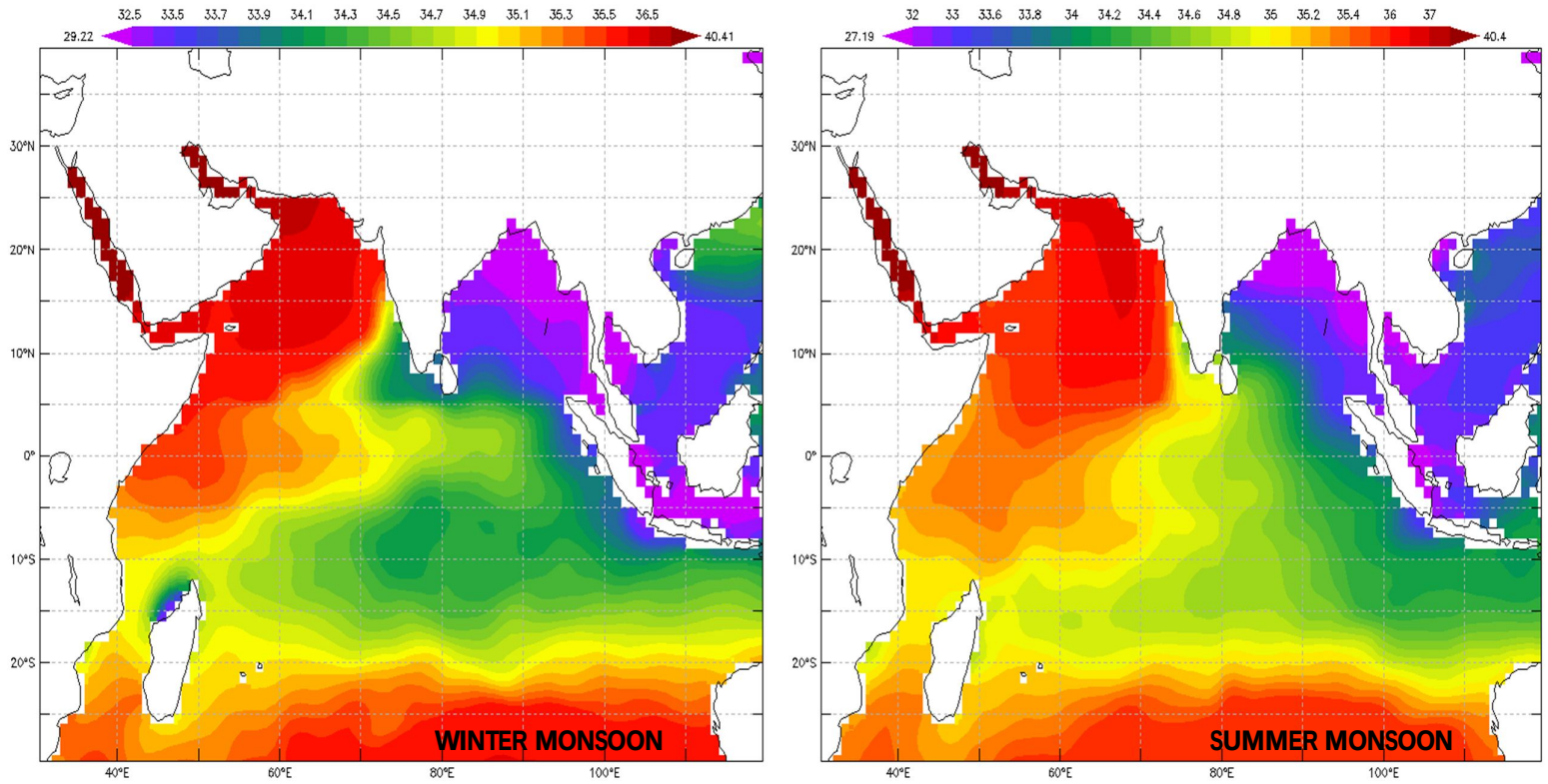

Figure 5. Surface salinity distribution during the winter monsoon and summer monsoon (*Source: http://las.northern Indian Ocean.org*)

2.4. Upwelling and primary productivity

In the Arabian Sea, two forms of upwelling viz., the open ocean upwelling and the coastal upwelling are observed. These two occur as a consequence of strong Ekman transport of surface water away from the coast during the summer monsoon (Smith and Bottero, 1977; Swallow, 1984; Brock et al., 1992). The extent of coastal upwelling includes the domain between the coast and 150 km offshore (Tudhope et al., 1996). Off the Arabian coast, open ocean upwelling associated with low level Findlater Jet is observed at about 400 km offshore (Findlater, 1974; Swallow, 1984) pumping the cold nutrient-rich subsurface waters from the thermocline in to the surface. The open ocean upwelling off the Arabian Coast (Oman) is of high significance in terms of productivity in the entire Arabian Sea because this upwelled water spreads across the basin due to vigorous clock-wise summer monsoon currents (Qasim, 1982; Nair et al., 1989). Hence, the Arabian Sea is known to be one of the most biologically productive domains of the world oceans (Ryther and Menzel, 1965; Madhupratap et al., 1996). Modern measurements of primary productivity in the northern Arabian Sea (north of 15˚N) during the summer monsoons are ~700-900 $gCm^{-2}d^{-1}$ (Qasim, 1982) and during the winter monsoons, it is ~600 $mgCm^{-2}d^{-1}$ (Madhupratap et al., 1996). The primary productivity in the Arabian Sea south of 15˚N during the summer monsoons is ~900-1700 $mgCm^{-2}d^{-1}$ (Barber et al., 2001) and during the winter monsoons it is ~200-300 $mgCm^{-2}d^{-1}$ (Bhattathiri et al., 1996; Madhupratap et al., 1996). Upwelling is observed as a result of Southwest monsoon forcing, usually, along the coastal zone of the Arabian Sea (Currie et al., 1973). Upwelling is reportedly absent in the EIO (Schott et al., 2002). Figure 6 shows the spatial distribution of chlorophyll-*a* (productivity indicator) in the northern Indian Ocean during the southwest monsoon and northeast monsoon, respectively.

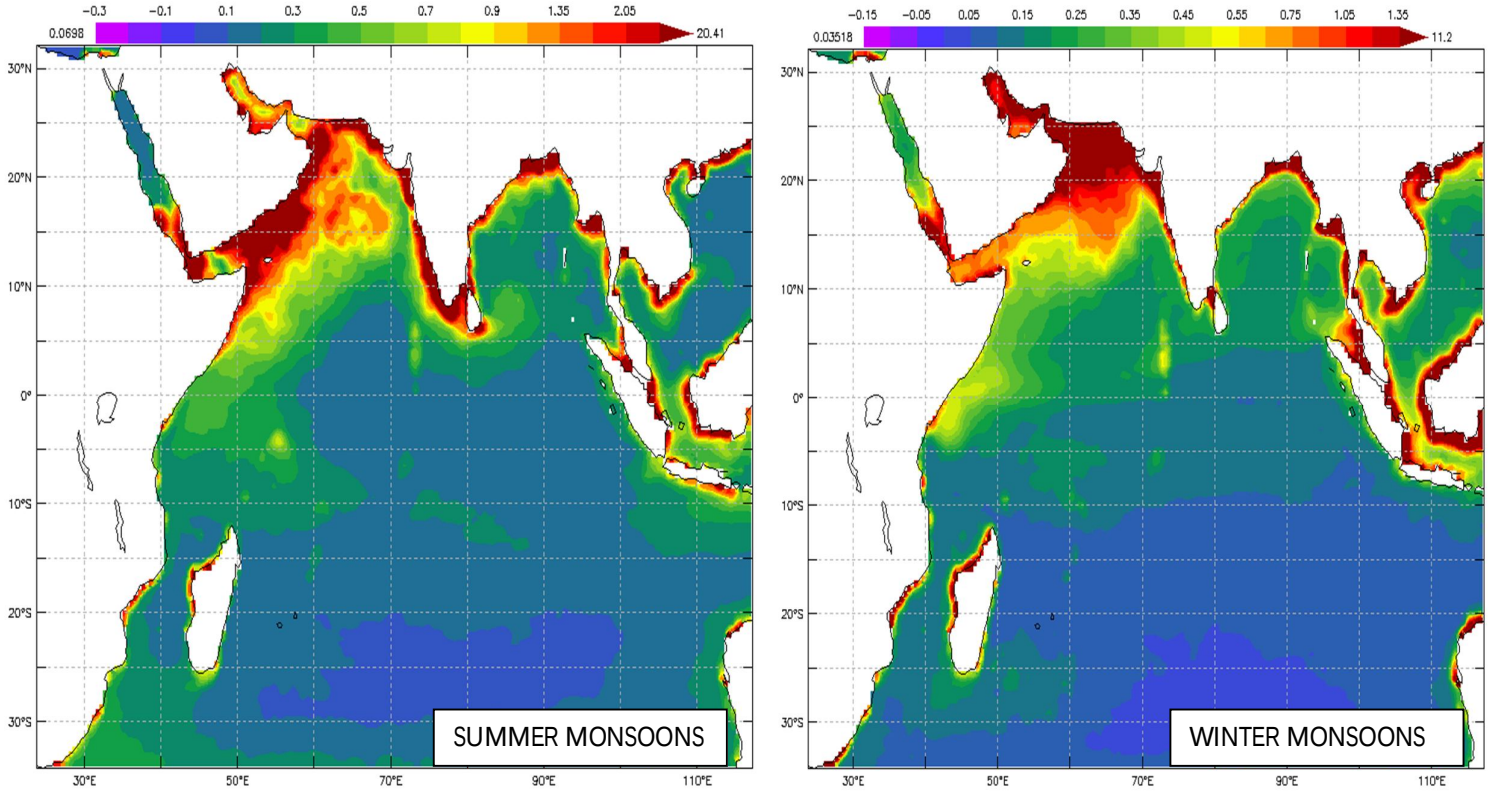

Figure 6. Modern seasonal distribution of chlorophyll-*a* (mg m^{-3}) in the northern Indian Ocean (*Source: http://las.northern Indian Ocean.org*)

2.5 Oxygen minimum zone

Oxygen minimum zone (OMZ) in the Arabian Sea occurs between depths ~100 - 1000 m where dissolved oxygen concentration level is <0.5 ml/L (Wyrtki, 1971; Rogers, 2000). The presence of OMZ across the Arabian Sea is mainly attributed to the high consumption of oxygen by large amount of settling OM resulting from high surface water productivity (Ryther and Menzel, 1965; Sarma, 2002). The reconstruction of OMZ over the last 225 kyr has shown that the OMZ strengthened whenever productivity increased and winter-mixing was shallow (Reichart et al., 1998). The sustenance of OMZ has been attributed to the moderate to low ventilation of the thermocline by low oxygenated Indian Ocean Central Water (IOCW: dissolved oxygen, ~1 ml/L) (Olson et al., 1993), the PGW (dissolved oxygen, 2.6 ml/L) (You and Tomczak, 1993) and the RSW (dissolved oxygen, 3.5 ml/L) (Olson et al., 1993). Vertical profiles of dissolved oxygen in the EAS show that the oxygen content steadily increases with depth below the OMZ and reach >3 mL L^{-1} at 3500 m depth (Paul and Ramamirtham, 1963).

2.6. Nutrient distribution

The supply and level of nutrients in the Arabian Sea are controlled by southwest and northeast monsoons (Smith and Codispoti, 1980) wherein, enriched nutrients are observed as a result of monsoon circulation (Reid et al., 1978). This is brought about by the nutrient injection into the photic zone by monsoonal winds through physical processes such as upwelling, advection and variations in mixed-layer depth (Brink et al., 1998).

In the Arabian Sea the nitrate (NO_3^-), a macronutrient is largely responsible for regulating the primary productivity. The iron (Fe), which is a micronutrient, is reported to be non-limiting as far as the primary productivity in the Arabian Sea is concerned (Smith, 2001). This is because, the surrounding land-mass and strong winds blowing from continent over the Arabian Sea provide rich source of Fe in the Arabian Sea water. In general, the sub-surface waters of the northern Indian Ocean are enriched with phosphate (PO_4^{3-}) and nitrate but below 1000 m depth, the concentration of nitrate is low (Conkright et al., 1994). The concentration of nutrients in the surface waters is low during the inter-monsoon. However, with the onset of monsoons, NO_3^- and PO_4 levels in the euphotic zone increase due to the deepening of mixed layer (Haake et al., 1993). Surface waters affected by winter convection show increased levels of NO_3^- and PO_4 wherein, the level of silicates (SiO_4^{4-}) is low (Madhupratap et al., 1996). Surface waters of the EIO are depleted in nutrients (Conkright et al., 1994).

In the northern Arabian Sea, a NO_3^- concentration of ~2 µM is observed during the winter monsoons in the surface layer, where as it falls below detection level during the inter-monsoon periods (Madhupratap et al., 1996). Studies have shown that productivity increases (~600 $mgCm^{-2}d^{-1}$) during the winter monsoons as compared to the inter-monsoons (~10 $mgCm^{-2}d^{-1}$) due to intense vertical convection resulting in the deepening of the mixed layer and injection of nutrients into the euphotic layer (Madhupratap et al., 1996).

Thus, the Arabian Sea circulation, productivity, biogeochemistry and monsoons are closely linked to each-other. If we could reconstruct the changes in past productivity through robust proxies such as lipid biomarkers, it is feasible to understand the changes in the monsoon patterns during climate extremes, which forms the basis of the present thesis.

CHAPTER 3

MATERIALS AND METHODS

3.1. Locations of the studied sediment cores

In order to get acquainted with analytical protocol for the present study, a set of samples from the Visakhapatnam Harbour were used for estimating the concentration and composition of lipid (*n*-alkanes) to evaluate their sources**.** The Visakhapatnam Harbour lies on the east coast of India and is connected to the BoB (Figure 7). The harbour serves as a repository of a large input of marine, terrestrial and anthropogenic organic matter (Ganapati and Raman, 1973; Raman, 1995). Hence, samples from the Visakhapatnam Harbour are well suited to unscramble the sources of various lipids in the sediment and to establish the analytical protocol for the proposed study.

Three deep-sea sediment cores used for the present study were collected in different cruises conducted by the National Institute of Oceanography under Cobalt-Crust Project funded by the Ministry of Earth Sciences. These cores were retrieved *en route* the sailing of the research vessels. Two sediment cores (BP3/GCR1 and BP3/GCR2) were collected onboard IB Boris Petrov Cruise-3 (March 2005) from the top of Wadia Guyot and Raman Seamount respectively in Lakshmi Basin of the EAS. One sediment core (CC2/GCEq2) was retrieved on board R. V. A. A. Sidorenko Cruise-65 (August 2003) from the EIO. The details of sediment cores are given in Table 2 and Figure 7.

Table 2. Location details of the sediment cores selected for the present study

Core Number	Latitude	Longitude	Water Depth (m)	Core Length (m)
BP3/GCR1	15°30’ N	70° 00’ E	1500	5.5
BP3/GCR2	17°10.5’ N	69° 00’ E	2400	5.2
CC2/GCEq2	02°29’ N	78° 00’ E	3788	5.6

(2 cm interval sub-samples of the above sediment cores were already available for the present study)

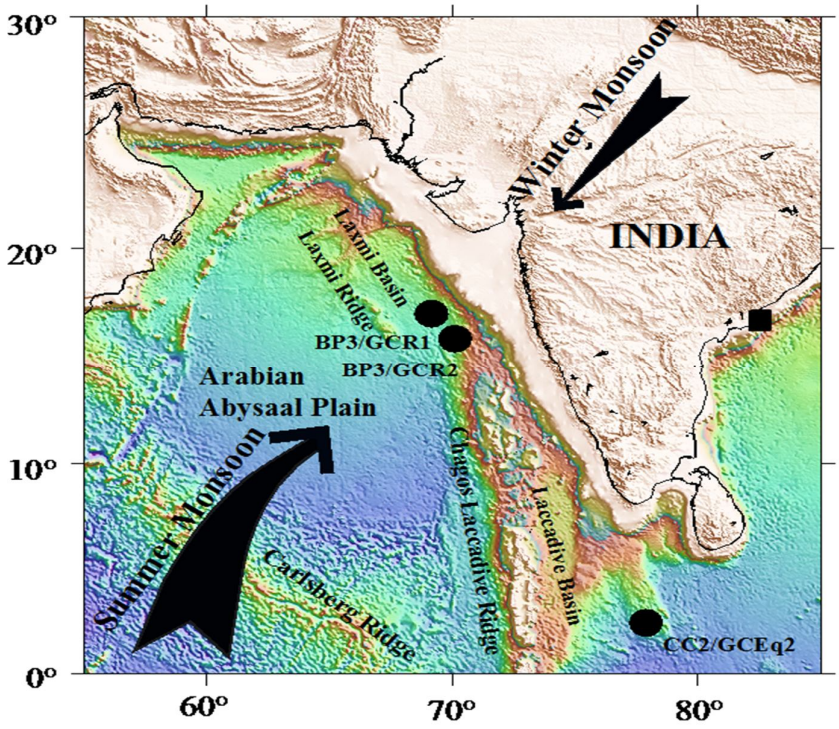

Figure7. Location map of the studies sediment cores BP3/GCR1, BP3/GCR2 and CC2/GCEq2. Arrows indicate Indian monsoon circulation where their thicknesses approximately correspond to the modern relative intensity. Filled circles are the locations of the sediment cores Filled square is the surface sediment samples off Visakhapatnam used for developing lipid extractions protocol.

3.2. Sediment processing

Around 10 gm of dried sediment was soaked overnight in RO water to which ~10 ml of 10 % sodium hexametaphosphate was added to disperse the clay lumps. The dispersed sediment samples were subjected to wet sieving using 63 μ standard sieve under a soft jet of tap water until all the -63 μ particles (silt + clay) were removed. The coarse fraction (+63 μ) was dried and stored in labelled vials. Around 20 tests of *Globigerinoides sacculifer* (*G. sacculifer*) without terminal-sacs were hand-picked under the binocular microscopes from coarse fraction of 250 to 355 μ size-range for $\delta^{18}O$ measurements. While around 1000 tests of *G. sacculifer* and *G.*

ruber species together in nearly equal proportions from the same size-range were picked for radiocarbon dating.

3.3. Oxygen isotope analysis

The visibly clean tests of *G. sacculifer* from forty five sub-sections from upper 1 m of each of the sediment cores were used for the oxygen-isotope measurements. The $\delta^{18}O$ measurement for EAS sediment cores was carried out at the Godwin Institute for Paleoclimate Research, Cambridge University, UK, while the EIO sediment core was analyzed using in-house Micromass IR-MS facility.

The tests were first crushed in sample vials, soaked in 3 % H_2O_2 for about 15 minutes to remove organic coatings and then ultrasonically agitated in presence of acetone to detach any contaminant clay particles and chamber filling nanoplanktons. The supernatant was removed with the help of a tissue paper string and the sample was cleaned twice in DI-water and dried at 50^{o}C before measurement. The CO_2 generated by reaction of clean test fragments with 100% ultra high purity phosphoric acid was used for measuring the isotopic ratios on a VG Siera-Prism IRMS with respect reference standard Pee Dee Belemnite (PDB) in permil (‰) unit. The precision of six replicate measurements was 0.008 ‰.

3.4. Radiocarbon dating

The radiocarbon (AMS-^{14}C) measurements were done at National Science Foundation's Accelerator Mass Spectrometry facility at the University of Arizona (USA). The selection of intervals for radiocarbon dating was based on the $\delta^{18}O$ depth profiles so as to cover critical intervals such as LGM, Holocene Optimum and deglacial transition. The AMS-^{14}C dates were corrected for uniform reservoir age of

600 y defined for the Northern Idian Ocean (http://calib.qub.ac.uk/marine) before converting in to calendar age using the CalPal2007-HULU Calibration (Danzeglocke et al., 2007). The upper ~100 cm radiocarbon dated sections of GCR1, GCR2 and GCEq2 correspond to maximum ages of ~35 ky BP, ~33 ky BP and ~32 ky BP, respectively. The core-top sections of respective cores recorded ages of 5841 ± 86 ky BP, 5863 ± 73 ky BP and 5204 ± 105 ky BP, suggesting that the Late Holocene record of ~5 ky was missing from all three sediment cores. However, the recorded temporal loss does not prevent us to understand the biogeochemical variation occurred in the Northern Idian Ocean at two extreme climate conditions (LGM and Holocene) as a significant part of the Holocene Optimum is well preserved.

3.5. Organic matter chemical and isotopic analysis

Finely ground and dried carbonate-free samples were used for C_{org}, N_{Total} and $\delta^{13}C_{org}$ measurements. The decarbonisation was done by repeatedly treating ground sediment with 1N HCl followed by rinsing with DI-water until the evolution of CO_2 ceased completely. The dried decarbonised samples were analyzed using an in-house Thermo Flash-1112 elemental analyzer coupled with Delta-V^+ IR MS Facility. The 2, 5-Bis-(5-tetrabutyl-benzoxazol-2-yl) thiopen (BBOT) was used as a standard for calibration. The $\delta^{13}C$ is expressed relative to Pee Dee Belemnite (PDB) standard in per mil (‰) unit.

$$\delta^{13}C_{org} = \{(^{13}C/^{12}C)_{sample} / (^{13}C/^{12}C)_{PDB} - 1\} \text{ X } 1000$$

The accuracy of C_{org} and N_{Total} measurement is within ±3 % and the precision of $\delta^{13}C_{org,}$ measurements based on 5 replicates is 0.1 ‰.

3.6. Extraction of lipids

A portion of the sediment samples from each interval (2 cm) was preserved at –20ºC in onboard deep-freezer immediately after sub-sampling. They were transported to on-land laboratory in Goa in frozen condition and subjected to freeze drying. The freeze-dried sub-samples were powdered and homogenized in an agate mortar. The powdered samples were transferred to sterilized glass vials and stored at ~ –25°C until taken for lipid extraction.

All glasswares used for lipid extraction were washed with chromic acid and distilled water, heated at 450°C and rinsed with methanol and dichloromethane. All solvents were double distilled before use. Sodium sulphate was ashed at 450°C. Silicic acid was washed with methanol and chloroform. Similarly, silica and alumina were washed with methanol, dichloromenthane and *n*- hexane. These pre-treatment of solvents and reagents are routinely done to free the reagents from traces of contaminants.

Total lipids (hereafter 'TL') were extracted from lyophilized sediments following the method of Bligh and Dyer (1959), and estimated following Harji *et al (*2008). In brief, aliquots were shaken vigorously with a mixture of chloroform + methanol + phosphate buffer (in 1 : 2 : 0.8 V/V/V ratio) and allowed to stand for 24 h. For separating the organic phase from above mixture, the concentration ratio of the mixture was adjusted to 1:1:0.9 in a separating funnel by the addition of equal amount (volume) of chloroform and phosphate buffer considering the volume of original components of the mixture. After the addition of solvents, there will be two distinct phases (layers), in which the lower layer in the separating funnel contains lipids.

The lipid phase was collected in sterilized conical flasks. This is called as lipid extract. The required amount of anhydrous sodium sulphate was added to the flasks and stirred continuously to remove water molecules, which is attained as soon as the extract becomes clear. The clear water-free lipid extract was filtered through Whatman No.1 filter paper. The filtrate was concentrated using a rotary evaporator under reduced pressure and made to a known volume (1 ml). The TL was further subjected to column chromatography as described in the following sections.

3.7. Silicic acid chromatography

The activated silicic acid was packed on a glass column (length 10 cm and diameter 0.5 cm). The silicic acid column was conditioned by passing the chloroform before loading the lipid extract. The extract was loaded on the preconditioned silicic acid column and eluted with 10 ml of chloroform to remove the neutral lipids. This fraction was evaporated to near dryness at 30°C in a rotary evaporator.This fraction was then used to proceed to the next step for separating different lipid compounds using silica-alumina chromatography.

3.8. Silica-alumina chromatography

Activated silica and alumina at 110 °C overnight followed by deactivated with distilled water were used for fractionation of lipid extract. The glass column was filled with silica and alumina mixed with hexane and topped with activated copper powder. The neutral lipid extract was loaded onto the column to separate two fractions viz., Fraction-1 (F1) consisting of *n*-alkanes and Fraction-2 (F2) consisting of sterols and *n*-alkanols. The F1 and F2 were eluted using *n*-hexane and

dichloromethane, respectively. The elutes were evaporated under reduced pressure. The F1 fraction was adjusted to a final volume after adding methyl nonadecanoate as the internal standard. A suitable aliquot of this fraction was analysed using the GC-MS. The F2 fraction was further derivatized to identify and quantify the *n*-alkanols and sterols from GC-MS spectra, as they cannot be measured directly from the F2.

3.9. Derivatization

The derivatization is a technique to transform a less volatile chemical compound into a more reactive product (derivate) of similar chemical structure (www.wikipedia). The relatively non-volatile polar O-H groups with hydrogen bonding in lipid compounds may be converted into relatively more reactive non-polar groups by replacing the O-H group with tri-methyl silyl (TMS) group. The resulting derivative shall be more volatile thus, allowing analysis by gas chromatography. Bulky, non-polar silyl groups are often used for this purpose.

The F2 was evaporated and the residue was dissolved in 400 µl of a mixture of bistrimethyl-silyl-trifluoroacetamide (BSTFA) and pyridine in the ratio 1:3 (V/V) and silylated at 50 ˚C for 1 h in the oven. This was evaporated to dryness under a stream of nitrogen and the final volume was adjusted by adding hexane and BSTFA (4:1 V/V). The 5α-cholestane was added as the internal standard before dissolving the residue. A suitable aliquot was then analysed using the Gas Chromatography Mass Spectrometer (GC-MS).

3.10. GC-MS Analysis

The analyses were carried out on a Shimadzu QP-2010 GC-MS equipped with RTX-5MS capillary column (30 m x 0.32 mm i.d. x 0.25 µm film thickness). One µl of the sample was injected into an on-column injector when the injector and ion source housing temperatures were maintained at 60 °C and 250 °C, respectively. Helium was used as a carrier gas and flow rate was maintained at 1.5 ml min^{-1}. For *n*-alkanes, the oven temperature was programmed at 80 °C to 120 °C at a ramped rate of 30 ° C min^{-1}, then from 120 °C to 320 °C at a ramped temperature of 4 °C min^{-1} and maintained at this temperature for 15 min. For sterols and *n*-alkanols, oven temperature was programmed at 80 °C to 140 °C at a ramped rate of 30 ° C min^{-1}, and then from 140 °C to 320 °C at a ramped temperature of 6 °C min^{-1} and maintained at this temperature for 18 min. The MS instrument was operated in full scan mode scanning from range of 50 to 500 m/z under electron impact ionization with ionization energy of 70 eV. The lipid compounds were identified from mass spectra and retention times obtained from commercial standards of Supelco, USA. The base peak for *n*-alkanes is at m/z 57. The base peak ions for the TMS derivatized *n*-alkanols and sterols are at m/z 75 and m/z 129, respectively. Concentrations of lipid compounds are expressed in ng/g on dry weight basis. The carbon preference index (CPI) for *n*-alkanes was obtained by the ratio of the sum of odd carbon number homologues in the range of C_{23-33} to the sum of even carbon number in the same range; and CPI for *n*-alkanols is the ratio of sum of even carbon numbers in the range of C_{22-32} to the sum of odd carbon numbers in the given range (Eglinton and Hamilton, 1967; Cranwell, 1973; Rieley et al., 1991).

$$CPI_{n\text{-alkanes}} = \frac{C_{23}+C_{25}+C_{27}+C_{29}+C_{31}+C_{33}}{C_{22}+C_{24}+C_{26}+C_{28}+C_{30}+C_{32}}$$

$$CPI_{n\text{-alkanols}} = \frac{C_{22}+C_{24}+C_{26}+C_{28}+C_{30}+C_{32}}{C_{23}+C_{25}+C_{27}+C_{29}+C_{31}+C_{33}}$$

The ACL for *n*- alkanes and *n*-alkanols was calculated using Poynter et al. (1989) equation.

$$ACL_{n\text{-alkanes}} = \frac{23xC_{23}+25xC_{25}+27xC_{27}+29xC_{29}+31xC_{31}+33xC_{33}}{(C_{23}+C_{25}+C_{27}+C_{29}+C_{31}+C_{33})}$$

$$ACL_{n\text{-alkanols}} = \frac{22xC_{22}+24xC_{24}+26xC_{26}+28xC_{28}+30xC_{30}+32xC_{32}}{(C_{22}+C_{24}+C_{26}+C_{28}+C_{30}+C_{32})}$$

The recovery based on the internal standards for *n*-alkanes (C_{20} to C_{29}) and *n*-alkanols ($C_{24\ to}$ C_{30}) + phytol + brassicasterol was >91 % and >87 %, respectively. The quantification of various lipids was done in comparison with peak area of internal standard against its quantity added to aliquots before extraction process. Thus, any deviations in lipid recovery are taken care by the instrument software so as to obtain their concentration quantitatively in the sediment irrespective of recovery efficiency. Solvents were passed through the entire analytical procedure and used as blank samples to check for probable contamination while carrying out the analytical perocedure. Sample values were blank corrected before conversion to concentration units. The sum of all the identified individual *n*-alkanes or *n*-alkanols or sterols is defined as the total *n*-alkanes, total *n*-alkanols and sterols, respectively.

CHAPTER 4

RESULTS

4.1. Lipids in surface sediments of Visakhapatnam harbour: Standardizing the analytical protocol

A suite of 19 surface sediment samples from Visakhapatanam Harbour, which are rich in organic components were selected for standardization of analytical protocol. The organic components are added to this harbour sediments through both natural (estuarine) processes and anthropogenic activities. Therefore, these harbour sediments provide excellent material for standardizing the analytical procedures required for subsequent analysis of sediment core samples to fulfill the palaeoclimatic objectives of my thesis.

4.2. C_{org} , $\delta^{13}C_{org}$ and TL

The distributions of C_{org}, $\delta^{13}C_{org}$ and TL are presented in Table 2. The C_{org} ranges from 0.6 % (Station 4) to 7.6 % (Station 5). The $\delta^{13}C_{org}$ in the Visakhapatnam harbour varied from -29.3 ‰ to -23.8 ‰. Highly depleted $\delta^{13}C_{org}$ (-29.3‰) is recorded for Station 17, while relative enrichment (-23.8‰) is evident at Station 19. On dry weight basis, the TL ranges from 300 μg g^{-1} (Stations 14 and 17) to 14,948 μg g^{-1} (Station 5). The TL variation also is comparable to earlier reported range for coastal sediments (Harji *et al* 2008).

The distribution of the total hydrocarbons (T_{HC}), total *n*-alkanes (T_{Alk}) and unresolved complex mixture (UCM) also exhibit considerable spatial variability (see Table 3). The T_{HC} contents range from 0.2 μg g^{-1} (Station 17) to 2277 μg g^{-1} (Station 6) and are comparable to other coastal areas (Mille *et al* 2007; Harji et al 2008). The T_{Alk} in these sediments varies from 0.2 μg g^{-1} (Station 17) to 31 μg g^{-1} (Station 5) (Table 3). The T_{Alk} are relatively higher at stations 2, 3, 5, 6 and 10 compared to

other remaining stations and are comparable to those reported earlier for other coastal regions. (Marmugao Harbour: 1.6 μg g^{-1} - 10.7 μg g^{-1}, Harji *et al.,* 2008; Guanabara Bay: 7.66 μg g^{-1} to 57.22 μg g^{-1}, Wagener *et al.,* 2012).The concentrations of the UCM range from 157 μg g^{-1} (Station 4) to 2244 μg g^{-1} (Station 6). The presence of UCM is observed at stations 1, 2, 3, 4, 5, 6, 7, 8, 9, 10, 12, 13 and 19.

Table 3. Organic components in surface sediments of Visakhapatnam Harbour, East Coast of India (all values are on dry weight basis)

Station No.	C_{org}	$\delta^{13}C_{org}$	TL	T_{Alk}	T_{HC}	UCM
	%	‰	(μg g^{-1})			
1	1	-25.4	4200	11	344	332
2	-	-	4050	23	550	519
3	6.7	-26.1	1528	19	847	822
4	0.6	-26.1	1575	8	166	157
5	7.6	-26.3	14948	31	327	295
6	7.4	-29.2	6900	18	2277	2244
7	4	-24.6	4083	16	860	843
8	1.9	-27.4	5400	7	457	446
9	2.4	-28.1	900	9	386	372
10	-	-	2724	23	318	291
11	2.7	-26.8	600	13	13	-
12	4.4	-27	1575	8	195	185
13	4.1	-24.4	2550	6	258	252
14	1.3	-25.1	300	2	2	-
15	-	-26.9	2600	10	11	-
16	3	-25.8	2250	5	5	-
17	0.7	-29.3	300	0.2	0.2	-
18	1.2	-24.9	1718	0.4	1	-
19	1.3	-23.8	3825	11	948	933

C_{org} - Organic carbon, TL - Total lipid, T_{Alk} - Total *n*-alkane, T_{HC} - Total hydrocarbon, UCM - Unresolved Complex Mixture. (- = not determined)

In addition, pentacyclic triterpanes/hopanes (8 to 1602 ng g^{-1}: Stations 17 and 3, respectively) and steranes (0 – 554 ng g^{-1}: Stations 17 and 3, respectively) are detected at the study site (Figure 8). Of these, the presence of 17α (H), 21β (H)

configuration and 18 (H)-22, 29, 30-trisnorneohopane is observed at stations 2, 3, 5, 6, 7, 9, 12, 13 and 19. Minor concentrations of tricyclic (1–180 ng g^{-1}: Stations 1 and 11, respectively) and tetracyclic terpanes (0.3 – 102 ng g^{-1}: Stations 18 and 3, respectively) are also detected. Elevated concentration of steranes was observed at stations 2, 3, 5, 6, 7, 9, 12, and 19.

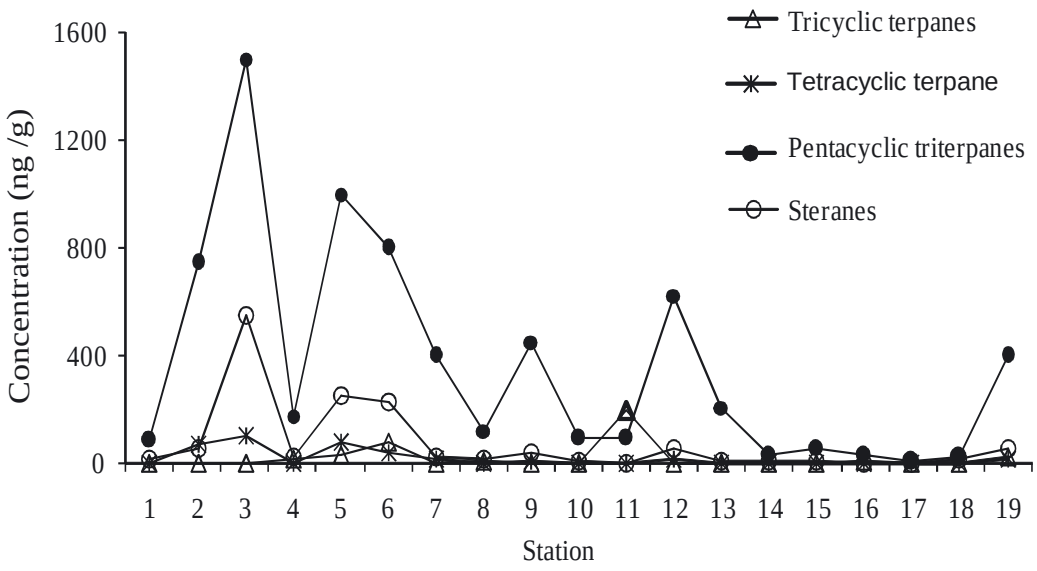

Figure 8. Distribution of tricyclic terpanes, tetracyclic terpanes, pentacyclic triterpanes and steranes in the Visakhapatnam Harbour

4.3. Radiocarbon ages and sedimentation rate

The details of measured and reservoir corrected radiocarbon ages of various sections of the three sediment cores are given in Table 4. The ages >5 ky BP for core-top sections of all three sediment cores suggest that the Late Holocene records have been erased from the studied cores either due to core-top losses while retrieving the cores or due to erosion of surface sediment due to bottom water activity (see Banakar et al., 1991). However, the major portion of Holocene period is intact and hence the core-top loss does not prevent comparison between two extreme climatic conditions i.e., LGM and Holocene.

Table 4. Details of AMS ^{14}C dates obtained for selected sections from three sediment cores

Sediment core	Laboratory[@] Reference No.	Depth in Core (cm)	^{14}C Measured Age (yr BP)	Error (±y)	Calendar Age[#] (yr BP)	Error ±y
BP3/GCR1	91095	2.5	5381	42	5481	86
	91097	19.5	8617	49	8867	97
	91098	30.5	17360	93	19750	307
	91099	39.5	17062	120	19970	305
	91100	50.5	19490	120	22730	276
	91101	60.5	19650	120	22883	303
	91102	69.5	22390	160	26031	54
	91103	79.5	23820	180	27806	372
	91104	99.5	31620	480	35119	483
BP3/GCR2	91111	2.5	5762	42	5863	73
	91112	19.5	8012	48	8239	63
	91113	29.5	11625	59	12917	61
	91114	39.5	12992	65	14574	108
	91115	59.5	18850	130	21930	326
	91116	81.5	21250	140	24604	333
	91117	101	28980	320	32796	140
CC2GCEq2	X10253	2	5159	43	5204	105
	X10254A	11	6644	46	6892	64
	X10255A	21	10659	58	11605	180

	X10256	31	12309	99	13591	156
	X10257	43	15628	84	18262	240
	X10258	62	19070	140	22079	334
	X10259	91	28500	380	32467	395
	X10260	121	29960	350	33717	388

@ - NSF AMS Facility at the Arizona University, USA; # - calculated after correcting measured dates for reservoir age of 600 y.

4.4. Oxygen isotopes

The oxygen isotopes of *G. ruber* and *G. sacculifer* (without terminal-sac) extracted from the sediment cores are presented in Tables 5, 6 and 7.

Table 5. Time-series of oxygen-isotopes with depth in sediment core BP3/GCR1(Bold fonts indicate the radiocarbon dated sections)

Depth (cm)	Calendar Age (Ky BP)	$\delta^{18}O_{G.sacculifer}$ ‰ (vs PDB)
2.5	**5.5**	-1.19
6.5	6.3	-1.20
9	6.8	-0.98
11	7.2	-1.27
13	7.6	-0.63
15	8.0	-1.28
17	8.4	-1.31
19	8.8	-0.87
19.5	**8.87**	NA
21	10.4	-1.17
25	12.3	-0.28
27	16.3	-0.11
29	18.3	0.25
30.5	**19.75**	NA
31	19.8	0.35
37	19.9	-0.11
39	19.96	0.02
39.5	**19.97**	NA
41	20.4	0.00
45	21.4	0.12
47	21.9	-0.16
49	22.4	0.13

50.5	**22.73**	NA
51	22.74	0.21
55	22.8	0.03
59	22.86	0.04
60.5	**22.88**	NA
61	23.1	0.03
63	23.8	0.12
65	24.5	0.02
67	25.2	0.13
69.5	**26.03**	NA
70	26.08	0.05
74	26.8	0.02
78	27.5	-0.16
79.5	**27.8**	NA
82	28.8	-0.22
86	30.3	-0.27
90	31.8	-0.30
94	33.4	-0.28
98	34.8	-0.41
99.5	**35.1**	NA

NA=Not Analyzed

From Table 5 it is evident that the lightest $\delta^{18}O_{G.\ sacculifer}$ (-1.31‰) is recorded at 17 cm depth (8.4 ky BP), while the heaviest $\delta^{18}O_{G.sacculifer}$ (0.35 ‰) occurs at 31 cm (19.8 ky BP). The $\delta^{18}O_{G.sacculifer}$ rapidly decreases from 0.25 ‰ to -1.17 ‰ between 29 cm (18.3 ky BP) and 21 cm (10.4 ky BP) (Figure 9). A distinct range of heavy $\delta^{18}O_{G.sacculifer}$ is observed between 74 cm (26.8 ky BP) to 31 cm (19.8 ky BP) (Table 5; Figure 9).

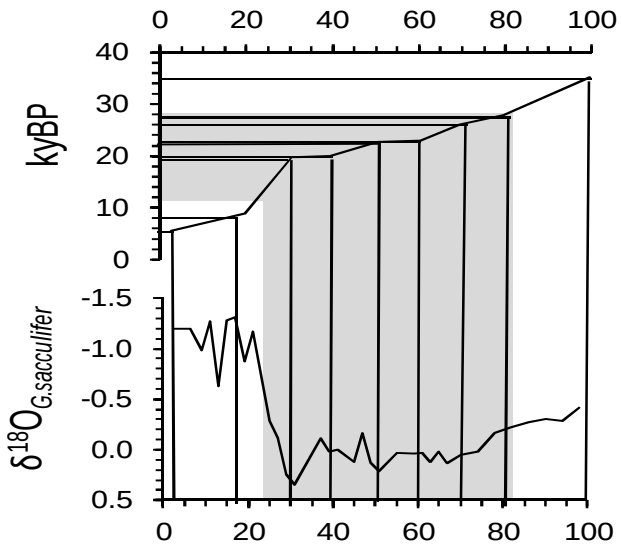

Figure 9. Depth-profile of $\delta^{18}O_{G.sacculifer}$ in BP3/GCR1. The age model (upper panel) is derived from tuning the depth-in-core to AMS ^{14}C dates. The horizontal and vertical solid lines indicate age-depth relationship. The shaded part represents MIS 2.

The $\delta^{18}O_{G.\ sacculifer}$ for GCR2 is presented in Table 6 and the age model in Figure 10.

Table 6. Time-series of oxygen-isotopes in sediment core BP3/GCR2 (Bold fonts indicate the radiocarbon dated sections)

Depth (cm)	Calendar Age (Ky BP)	$\delta^{18}O_{G.sacculifer}$ ‰ (vs PDB)
2.5	5.9	-0.91
7	6.4	-0.98
9	6.8	-0.93
11	7.1	-1.14
13	7.3	-0.96
15	7.6	-1.07
17	7.9	-1.12
19	8.17	-1.17
19.5	**8.20**	NA
21	8.9	-1.20
23	9.9	-0.96
25	10.8	-0.73
27	11.7	-0.58
29	12.7	-0.72
29.5	**12.9**	NA
31	13.2	-0.68
33	13.5	-0.56
35	13.8	0.09

37	14.2	-0.05
39	14.5	-0.20
39.5	**14.6**	NA
41	15.1	0.15
43	15.9	-0.04
45	16.6	0.32
47	17.3	0.27
49	18.1	0.46
51	18.8	0.50
53	19.5	0.38
55	20.3	0.42
57	21.0	0.45
59	21.7	0.36
59.5	**21.9**	NA
61	22.1	0.47
63	22.4	0.60
65	22.6	0.31
67	22.8	0.45
70	23.2	0.31
74	23.7	0.37
78	24.2	0.28
81.5	**24.6**	NA
82	24.9	0.21
86	26.5	0.04
90	28.3	0.24
94	30.0	0.05
98	31.9	0.03
101	**32.8**	NA

NA = Not Analyzed

The lightest $\delta^{18}O_{G.\ sacculifer}$ (0.60 ‰) is observed at 63 cm depth (22.4 ky BP). The heaviest $\delta^{18}O_{G.\ sacculifer}$ (-1.20 ‰) is recorded at 21 cm (8.9 kyBP). Rapid decrease in $\delta^{18}O_{G.\ sacculifer}$ is observed from 0.46 ‰ at 49 cm (18.1 ky BP) to -0.72 ‰ at 29 cm (12.7 ky BP). The heavy $\delta^{18}O_{G.\ sacculifer}$ (0.31‰ to 0.60 ‰) are observed between 74 cm (23.7 ky BP) and 51 cm (18.8 ky BP) (Table 6, Figure 10).

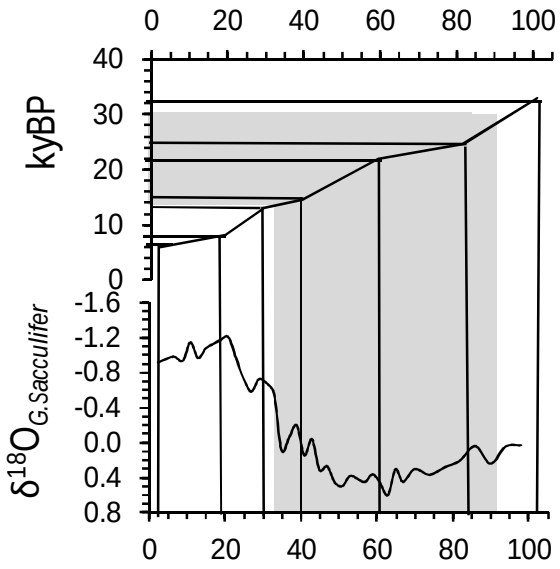

Figure 10. Depth-profile of $\delta^{18}O_{G.sacculifer}$ BP3/GCR2. The age model (upper panel) is derived from tuning the depth-in-core to AMS ^{14}C ages. The horizontal and vertical solid lines indicate age-depth relationship. The shaded part represents LGM.

The $\delta^{18}O_{G.\ ruber}$ for GCEq2 is presented in Table 7 and the age model in Figure 11.

Table 7. Time-series of oxygen-isotopes with depth in sediment core CC2/GCEQ2
(Bold fonts indicate the radiocarbon dated sections)

Depth (cm)	Calendar Age (Ky BP)	$\delta^{18}O_{G.ruber}$ ‰ (vs PDB)
2	**5.2**	-1.75
5	5.8	-2.18
7	6.1	-2.13
9	6.5	-2.14
11	**6.9**	-2.15
13	7.8	-2.37
15	8.8	-2.26
17	9.7	-2.34
19	10.7	-2.27
21	**11.6**	-1.97
24	12.2	-1.66
28	13.0	-1.60
31	**13.6**	NA
32	14.1	-1.07
36	15.7	-0.99

40	17.1	-0.92
43	**18.3**	NA
44	18.5	-0.83
48	19.2	-1.02
54	20.7	-0.93
60	21.4	-0.96
63	**22.1**	NA
64	22.5	-1.14
68	23.9	-1.13
72	25.4	-1.08
76	26.9	-1.31
80	28.4	-1.40
84	30.0	-1.45
88	31.4	-1.34
91	**32.5**	-1.28
96	32.7	-1.46
100	32.8	-1.47
121	**33.7**	NA

NA=Not Analyzed

From Table 4 it is evident that the actual top section of the core corresponding to last 5.2 Ky BP is lost, which is the case with other two cores also. The $\delta^{18}O_{G.ruber}$ in the apparent core-top corresponding to 5.2 Ky BP is -1.75 ‰. The lightest $\delta^{18}O_{G.ruber}$ (-2.37 ‰) is recorded at 13 cm depth, which corresponds to 7.8 ky BP. Heaviest $\delta^{18}O_{G.\ ruber}$ (-0.83 ‰) is recorded at 44 cm corresponding to 18.5 ky BP. The $\delta^{18}O_{G.\ ruber}$ shows a rapid decrease from -0.83 ‰ at 18.5 ky BP to -2.27 ‰ at 10.7 ky BP, i.e., within a time-span of ~8 Ky BP. The heaviest $\delta^{18}O_{G.\ ruber}$ (-1.02 to 0.83 ‰) are observed from 60 cm (21.4 ky BP) to 40 cm (17.1 ky BP) (Table 7, Figure 11).

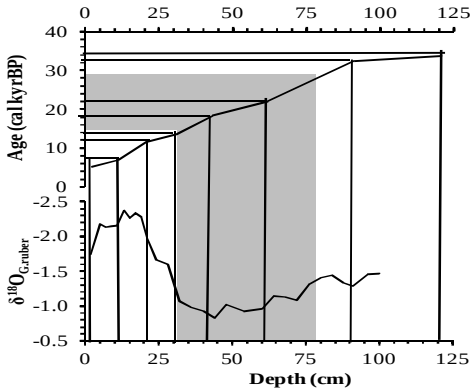

Figure 11. Depth-profile of $\delta\,^{18}O_{G.ruber}$ in CC2/GCEq2. The age model (upper panel) is derived from tuning the core-depth to AMS ^{14}C ages. The horizontal and vertical solid lines indicate age-depth relationship. The shaded part represents MIS 2.

Although, the lightest and heaviest $\delta^{18}O$ recorded by *G. sacculifer and G. ruber* are significantly different (Lightest: *G. ruber*: -2.37 ‰; *G. sacculifer*: -1.31 ‰ & -1.2 ‰ and corresponding Heaviest: -0.83‰ and 0.35 ‰ & 0.60 ‰, see Tables 4-6), the difference between lightest and heaviest in each of these sediment cores irrespective of the species is nearly similar (1.67 ± 0.13 ‰). The differing maximum and minmum $\delta^{18}O$ is due to species difference which is a natural phenomenon. When $\delta^{18}O$ in all three sediment cores are compared with each other, the timing offset of lightest $\delta^{18}O$ is within 0.5 Ky BP around a mean of 8.4 ky BP; while there is a significant offset of ~2 Ky BP around a mean of 20.2 ky BP in heaviest $\delta^{18}O$ events. However, the periods of isotopically lighter values occur after 12 ky BP and the heavier isotopic values occur between 30 and 20 ky BP in all the sediment cores indicating a robust behaviour of oxygen-isotopes.

4.5. Sedimentary C_{org}, N_{Tot} and $\delta^{13}C_{org}$

The C_{org}, N_{Tot} and $\delta^{13}C_{org}$ in GCR1 are presented in Table 8. The C_{org} and N_{Tot} vary between 0.7 and 2.0 %, and 0.1 and 0.2 %, respectively. The C/N ratios range from 7.2 to 12.4. The $\delta^{13}C_{org}$ vary from -21 ‰ to -19 ‰.

Table 8. Time-series of organic carbon (C_{org}), total nitrogen (N_{Tot}), $\delta^{13}C_{org}$ in BP3/GCR1
(all data is on carbonate-free basis and applicable to Table 9 & 10 also)

Age (ky BP)	C_{org} (%)	N_{Tot} (%)	C/N (mol/mol)	$\delta^{13}C_{org}$ ‰ vs PDB
5.5	1.4	0.2	9.3	-20.8
6.3	1.1	0.2	8.1	-20.5
6.8	1.1	0.2	8.4	-20.4
7.2	0.8	0.1	8.1	-20.4
7.6	1.1	0.2	8.7	-20.2
8.0	0.9	0.1	7.2	-20.3
8.4	1.1	0.2	8.5	-20.8
8.8	1.1	0.1	9.0	-20.4
10.4	1.2	0.2	8.8	-20.4
12.3	1.1	0.2	8.4	-20.5
16.3	0.8	0.1	7.5	-21.0
18.3	1.4	0.2	10.6	-21.0
19.8	1.5	0.1	12.2	-19.6
19.9	1.7	0.2	10.8	-20.0
20.0	1.5	0.2	11.2	-19.3
20.3	2.0	0.2	12.1	-20.1
21.4	1.9	0.2	11.9	-20.1
21.9	1.5	0.2	10.7	-19.6
22.4	1.4	0.2	11.1	-19.0
22.7	1.4	0.2	10.5	-19.6
22.8	1.6	0.2	10.4	-19.6
22.9	1.9	0.2	11.3	-19.7
23.1	1.4	0.1	11.1	-19.2
23.8	1.3	0.1	12.4	-19.5
24.5	1.6	0.2	10.4	-20.0
25.2	1.4	0.1	12.1	-19.2
26.1	1.5	0.2	10.9	-19.6
26.8	1.3	0.1	10.3	-20.1
27.5	1.9	0.2	11.7	-20.3

28.8	0.7	0.1	10.2	-19.7
30.3	0.8	0.1	9.2	-19.9
31.8	1.1	0.1	10.7	-20.3
33.4	0.7	0.1	9.8	-19.8
34.8	0.7	0.1	9.6	-19.5

The C_{org}, N_{Tot} and $\delta^{13}C_{org}$ in GCR2 are given in Table 9. The C_{org} and N_{Tot} vary between 0.4 and 1.7 %, and 0.1 and 0.2 %, respectively. The C/N ranges from 5.6 to 11.4. The $\delta^{13}C_{org}$ vary from -20.9 ‰ to -19.2 ‰.

Table 9. Time-series of organic carbon (C_{org}), total nitrogen (N_{Tot}) and $\delta^{13}C_{org}$ in BP3/GCR2

Age (ky BP)	C_{org} (%)	N_{Tot} (%)	C/N (mol/mol)	$\delta^{13}C_{org}$ ‰ vs PDB
5.9	0.9	0.1	7.7	-20.3
6.4	0.7	0.1	9.2	-20.2
6.8	0.7	0.1	6.2	-20.3
7.1	0.9	0.1	7.6	-20.6
7.3	1.0	0.1	8.9	-20.3
7.6	0.9	0.1	7.5	-20.3
7.9	0.8	0.1	7.8	-20.5
8.2	0.8	0.1	8.1	-20.6
8.9	0.7	0.1	7.9	-20.4
9.9	0.8	0.1	9.8	-21.0
10.8	0.6	0.1	7.0	-20.6
11.7	0.5	0.1	7.7	-20.9
12.7	0.4	0.1	6.9	-20.9
13.2	0.6	0.1	8.2	-20.5
13.5	0.4	0.1	6.7	-20.8
13.8	0.5	0.1	7.9	-20.6
14.2	0.4	0.1	7.3	-20.6
14.5	0.5	0.1	6.8	-20.7
15.1	0.7	0.1	9.0	-20.2
15.9	0.9	0.1	10.5	-20.7
16.6	0.7	0.1	9.6	-20.1

17.3	0.6	0.1	11.0	-19.5
18.1	0.9	0.1	10.7	-19.3
18.8	1.5	0.2	11.2	-19.6
19.5	1.6	0.2	10.4	-19.5
20.3	1.4	0.1	11.4	-20.0
21.0	1.5	0.2	8.7	-19.3
21.7	1.7	0.2	11.2	-20.1
22.1	1.3	0.2	9.3	-19.4
22.4	1.0	0.1	9.5	-19.6
22.6	1.6	0.2	8.9	-19.2
22.8	1.5	0.2	10.0	-20.2
23.2	1.6	0.2	9.8	-19.3
23.7	1.4	0.2	9.1	-20.1
24.2	1.1	0.1	9.3	-19.3
24.9	1.3	0.2	7.5	-19.5
26.5	0.8	0.2	5.6	-20.5
28.3	0.9	0.1	7.7	-20.2
30.0	0.7	0.1	6.4	-20.4
31.9	0.9	0.1	8.3	-20.1

The values of C_{org}, N_{Tot} and $\delta^{13}C_{org}$ of sediment core GCEq2 are given in Table 10. The C_{org} and N_{Tot} vary between 0.4 and 1.3 %, and 0.1 and 0.2 %, respectively. The C/N range from 5.1 to 8.2 whereas, the $\delta^{13}C_{org}$ vary from -22.8 ‰ to -19.0 ‰.

Table 10. Time-series of organic carbon (C_{org}), total nitrogen (N_{Tot}), $\delta^{13}C_{org}$ in CC2/GCEq2

Age (ky BP)	C_{org} (%)	N_{Tot} (%)	C/N (mol/mol)	$\delta^{13}C_{org}$ ‰ vs PDB
5.2	0.5	0.1	6.1	-21.4
5.8	0.5	0.1	6.5	-20.1
6.1	0.7	0.1	6.7	-22.4
6.5	0.5	0.1	5.2	-19.9
6.9	0.6	0.1	5.7	-20.7
7.8	0.7	0.1	6.5	-22.1
8.8	0.5	0.1	5.1	-20.8
9.7	0.6	0.1	6.4	-21.7
10.7	0.8	0.1	7.2	-22.5
11.6	0.6	0.1	7.0	-21.0

12.2	0.4	0.1	6.5	-22.1
13.0	0.5	0.1	7.1	-21.3
14.1	0.6	0.1	6.6	-22.8
15.7	0.8	0.1	6.9	-22.0
17.1	1.1	0.2	8.0	-19.8
18.5	1.2	0.2	7.7	-19.3
19.2	1.1	0.2	8.0	-20.2
20.7	1.0	0.1	7.7	-20.5
21.4	1.2	0.2	8.2	-19.3
22.5	1.0	0.2	7.4	-20.6
23.9	0.9	0.1	7.6	-19.3
25.4	0.8	0.1	7.9	-19.0
26.9	0.9	0.1	7.3	-21.4
28.4	1.1	0.2	7.7	-19.7
30.0	1.3	0.2	7.4	-20.5
31.4	1.2	0.2	7.2	-20.0
32.5	1.2	0.2	7.3	-19.8
32.7	0.9	0.2	6.3	-19.7
32.8	1.0	0.2	6.9	-19.8

Among the three sediment cores, the C_{org} values in GCR1 and GCR2 are comparatively higher than that of GCEq2 (see Tables 8, 9 and 10). The highest C_{org} values in GCR1 and GCR2 are 2 % and 1.7 %, respectively, while in GCEq2, it is 1.3 %. The range of N_{Tot} is similar (0.1-0.2 %) in all the three sediment cores. The highest C/N value in GCR1 and GCR2 is 11.4 and 12.4, respectively whereas, in GCEq2 it is 8.2. The maximum values of $\delta^{13}C_{org}$ in GCR1 and GCR2 are -21.4 ‰ and 20.9 ‰, respectively, which is comparatively heavier than GCEq2 which has a maximum value of -22.8 ‰.

4.6. Lipid distribution

The results of lipid analysis for the present sediment cores are presented in Tables 11, 12 and 13 and the highlights of variations observed are briefly described in this section.

4.6.1. Sediment core BP3/GCR1

The downcore distribution of total *n*-alkanes, C_{23-33} *n*-alkanes, total *n*-alkanols, C_{22-32} n-alkanols, phytol, total sterols and brassicasterol for GCR1 is given in Table 11.

Table 11. Time-series of various lipids analyzed in Arabian Sea sediment core BP3/GCR1

Calendar Age	Total *n*-alkanes	C_{23-33} *n*-alkanes	Total *n*-alkanols	C_{22-32} *n*-alkanols	Phytol	Total sterols	Brassicasterol
(Ky BP)	(ng/g)						
5.5	1010	257	494	85	38	52	20
6.2	1476	311	426	69	27	61	15
6.7	885	203	349	62	ND	24	11
7.2	941	249	354	87	33	110	40
7.6	1141	259	349	57	ND	25	10
8.0	1516	419	375	65	42	62	40
8.4	1630	539	328	75	24	92	30
8.8	1541	536	390	86	46	80	55
10.4	1174	360	333	69	45	77	30
14.3	973	236	428	83	57	95	40
16.3	1420	497	405	67	36	55	19
18.3	2005	610	380	76	34	85	41
19.8	1844	398	494	142	26	70	32
19.9	2009	727	597	111	70	101	58
20.0	1577	635	529	146	53	90	40
20.3	1506	405	445	118	110	145	83
21.4	2119	721	459	125	50	82	46
21.9	1717	616	484	123	65	141	58
22.4	2155	373	447	132	87	134	83
22.7	2162	760	472	108	61	115	60
22.8	1920	665	600	144	93	154	88
22.9	1879	418	412	97	96	96	77
23.1	1641	446	522	148	48	128	59
23.8	1887	655	514	119	92	130	90
24.5	1875	773	413	118	66	71	41
25.2	944	309	541	144	58	85	58
26.1	1186	354	451	119	52	80	43
26.8	839	318	481	111	69	91	60
27.5	932	206	375	115	42	97	30
28.8	1084	327	287	83	39	69	35
30.3	602	170	286	70	32	49	24
31.8	822	251	331	92	18	43	ND
33.4	802	304	344	70	54	17	27
34.8	594	173	410	90	74	6	20

ND: Not Detected

The total *n*-alkanes, total *n*-alkanols and total sterols range from 594 to 2162 ng/g, 286 to 600 ng/g and 6 to 154 ng/g, respectively. The concentrations of C_{23-33} *n*-alkanes and C_{22-32} *n*-alkanols range from 170 to 773 ng/g and 57 to 146 ng/g, respectively. Concentration of phytol ranges from 18 to 110 ng/g while brassicasterol range from 10 to 90 ng/g.

4.6.2. Sediment core BP3/GCR2

The downcore distribution of total *n*-alkanes, C_{23-33} *n*-alkanes, total *n*-alkanols, C_{22-32} *n*-alkanols, phytol, total sterols and brassicasterol for GCR2 is given in Table 12.

Table 12. Time-series of various lipids analyzed in Arabian Sea sediment core BP3/GCR2

Calendar Age	Total *n*-alkanes	C_{23-33} *n*-alkanes	Total *n*-alkanols	C_{22-32} *n*-alkanols	Phytol	Total sterols	Brassicasterol
(Ky BP)	(ng/g)						
5.9	940	263	157	40	39	41	15
6.4	1189	296	205	51	28	37	12
6.8	963	247	163	37	20	17	12
7.1	850	255	212	52	25	15	13
7.3	761	167	178	38	22	17	18
7.6	896	269	129	37	40	41	16
7.9	833	236	211	59	18	60	18
8.2	690	210	218	55	41	51	20
8.9	484	151	174	52	47	45	22
9.9	856	266	184	45	47	59	33
10.8	831	224	181	55	20	65	23
11.7	654	212	193	59	11	62	13
12.7	609	189	137	38	7	40	11
13.2	994	261	186	53	35	66	17
13.5	683	241	129	34	29	63	9
13.8	825	255	211	62	54	52	28
14.2	1134	327	200	60	32	40	18
14.5	863	292	226	67	51	70	23
15.1	1045	293	236	61	50	84	27
15.9	854	280	221	43	82	68	38
16.6	647	204	234	52	91	33	45
17.3	865	265	385	122	96	68	48
18.1	1238	421	253	63	104	45	36
18.8	1072	322	286	86	65	60	19
19.5	883	305	290	78	97	64	52
20.3	1068	336	261	88	56	70	25
21.0	875	261	290	90	82	99	32
21.7	846	337	413	116	99	77	35
22.1	1002	355	290	86	108	64	56
22.4	879	275	256	81	42	89	17
22.6	1538	502	439	143	113	63	52
22.8	880	281	315	89	71	53	34
23.2	821	287	237	71	28	55	16
23.7	786	300	212	66	41	72	28
24.2	916	303	208	62	26	36	14
24.9	873	198	276	59	100	55	28
26.5	858	260	277	69	42	82	ND

28.3	836	230	265	70	35	51	ND
30.0	934	286	271	64	47	67	ND
31.9	934	286	255	71	19	42	ND

ND: Not Detected

The total *n*-alkanes, total *n*-alkanols and total sterols range from 609 to 1538 ng/g, 129 to 439 ng/g and 15 to 99 ng/g, respectively. The concentrations of C_{23-33} *n*-alkanes and C_{22-32} *n*-alkanols range from 151 to 502 ng/g and 37 to 143 ng/g, respectively. Concentration of phytol ranges from 7 to 113 ng/g while brassicasterol range from 9 to 56 ng/g.

4.6.3. CC2/GCEq2

The downcore distribution of total *n*-alkanes, C_{23-33} *n*-alkanes, total *n*-alkanols, C_{22-32} n-alkanols, phytol, total sterols and brassicasterol for GCEq2 is given in Table 13.

Table 13. Time-series of various lipids analyzed in Equatorial sediment core (CC2/GCEq2)

Calendar Age (Ky BP)	Total *n*-alkanes	C_{23-33} *n*-alkanes	Total *n*-alkanols	C_{22-32} *n*-alkanols	Phytol	Total sterols	Brassica sterol
	(ng/g)						
5.2	762	58	153	14	1.6	1	1.4
5.8	235	86	138	30	1.3	3	1.1
6.1	481	47	140	9	1.3	5	0.8
6.5	209	71	109	20	1.6	2	1.2
6.9	360	77	191	22	2.3	7	2.5
7.8	381	142	170	30	1.8	5	0.7
8.8	337	72	137	28	1.3	4	1.3
9.7	260	49	155	20	2.0	5	3.3
10.7	412	107	81	31	2.5	7	1.4
11.6	753	72	140	15	1.8	9	0.5
12.2	565	28	150	21	1.1	7	1.4
13.0	696	62	141	51	1.5	11	3.6
14.1	635	145	124	48	3.0	9	2.9
15.7	553	193	202	92	4.0	12	4.0
17.1	688	227	253	83	5.6	20	7.3
18.5	433	147	149	97	7.8	19	5.9
19.2	570	205	286	148	6.6	21	3.9
20.7	491	179	347	59	5.8	16	5.9
21.4	412	139	207	73	6.1	19	4.1
22.5	511	183	312	93	5.2	17	6.6
23.9	690	236	259	57	4.6	9	2.8
25.4	224	76	250	68	5.1	12	2.3
26.9	145	38	112	34	1.9	7	1.2
28.4	587	117	140	60	1.9	6	3.3
30.0	586	113	139	77	3.4	5	ND
31.4	652	124	191	81	1.5	3	ND
32.5	621	103	104	51	1.5	1	ND
32.7	473	60	147	76	1.5	1	ND
32.8	336	87	90	51	1.2	4	1.2

ND: Not Detected

The total *n*-alkanes, total *n*-alkanols and total sterols range from 145 to 762 ng/g, 81 to 347 ng/g and 1 to 21 ng/g, respectively. The concentrations of C_{23-33} *n*-alkanes and C_{22-32} *n*-alkanols range from 28 to 236 ng/g and 9 to 148 ng/g,

respectively. The phytol varies from 1.1 to 7.8 ng/g while brassicasterol ranges from 0.5 to 7.3 ng/g.

The total lipid content is found to be higher in GCR1 than in GCR2 than in GCEq2 (see Tables 11-13). Amongst various lipids, the concentration of the total *n*-alkanes is highest, followed by total *n*-alkanols and then sterols.

CHAPTER 5

DISCUSSION

In this chapter, the EIO sediment core (GCEq2) is treated separately from that of EAS sediment cores (GCR1 and GCR2), because, there are significant differences in regional oceanographic set-up between these two areas. For instance, winds over the EIO are maximum speeds during inter-monsoon periods (Spring: April to May and Fall: October to December), unlike that of the Arabian Sea, where strongest winds occur during summer monsoon (June-July) and winter monsoon (December-January) periods. In terms of productivity, the EIO is a low productive region (Fernandes et al., 2008; Schulte et al., 1999), whereas, the Arabian Sea is known to be highly productive region (Ryther et al., 1966; Kabanova, 1968; Qasim, 1977; Madhupratap et al., 1996). The high productivity in the Arabian Sea is one of the main reasons for the existence of an intense OMZ between ~100 and 1500 m water depth (Schultz et al., 1996; Gooday et al., 2009). On the other hand, the EIO is not characterised by such an intense OMZ.

The role of the OMZ in burial (preservation) of OM is well known (Schulte et al., 2000; Sarma, 2002; Resplandy et al., 2012). The seafloor swept by an intense OMZ of the Arabian Sea receives large amount of export production leading to organic-rich laminated sediments (Reichert et al., 1998). Further, Schulte et al. (2000) have observed that the sediments within OMZ are rich in extractable lipids such as *n*-alkanols, *n*-alkanes, sterols, and phytol, suggesting well preserved OM in the sediment. This is evident in decreasing lipid contents with increasing water depth of OM burial, i.e., in general, the lipid contents show a decreasing trend from shallow water depth sediment core towards deeper water depth sediment core (lipid contents in GCR1- 1500 m water depth > GCR2- 2400 m water depth > GCEq2- 3788 m water depth) (See Table 2 and Tables 11 through 13). Thus, the sediment

cores retrieved from water depths within or close to the OMZ are expected to preserve past record of productivity with considerable fidelity.

It is already described that EAS sediment cores GCR1 is from the base of intense OMZ (1500 m water depth) and GCR-2 well below the OMZ (2400 m water depth). The GCEq2 is from deep-waters underlying the OMZ-free region of the EIO. Although, these three sediment cores are from distinctly different depositional environments, they are expected to record more or less similar climatic forcing on the productivity regimes of the northern Indian Ocean, because, the effect of past climate variability on biogeochemical processes must have been nearly uniform in the entire study region irrespective of site-specific differences in the primary production.

Previously published sedimentary lipid-based studies from Arabian Sea have indicated that the lipids specific to marine primary productivity such as phytol and brassicasterol exhibit variations in response to changes in the surface productivity (Schubert et al., 1998; Schulte et al., 2000). An enhanced concentration of brassicaseterol during the glacial periods was interpreted as an indication of enhanced diatom production (Schulte et al., 1999; Schulte and Bard, 2003). Schubert et al. (1998) suggested nearly unchanged phytoplankton community during the last 200 kyr based on nearly constant concentration of brassicasterols in a sediment core from the Arabian Sea. Kurian et al. (2009) related variation of sedimentary-phytol from EAS to the changes in total solar irradiance during the last ~700 y. These few previous studies demonstrate the potential of sedimentary lipids in reconstructing the changes in productivity of the northern Indian Ocean in response to past climate variability. In the following sections, for convenience, the data is discussed with

respect to two regions (viz., EAS and EIO) before presenting a synthesis of all data together in terms of climate forcing.

5.1. Arabian Sea palaeoproductivity paradox

Modern productivity in the Arabian Sea varies geographically in response to seasons. Significant increase in productivity occurs during two monsoon periods viz, summer mnsoon and winter monsoon as compared to inter-monsoon periods (Banse, 1987; Sawant and Madhupratap, 1996; Barber et al., 2001). The geographically averaged seasonal primary productivity for the Central and Eastern Arabian Sea has two distinct productivity peaks of ~1000 $mgC/m^2.d^{-1}$ during summer monsoon period and ~500 $mgC/m^2.d^{-1}$ (Prasannakumar et al., 2000). Where as, during inter-monsoon periods the productivity drops to a lowest of ~200 $mgC/m^2.d^{-1}$ (Prasannakumar et al., 2000). In general the highest productivity is evident during summer monsoons along the coasts of Oman, Somalia and India (Figure 12) due to upwelling of sub-surface nutrient-rich cold water to the photic zone. On the other hand, during winter monsoons high productivity is recorded in the northern Arabian Sea due nutrient entrainment caused by deep winter-convection. (Findlater, 1971; Wyrtki et al., 1973, Banse and McClain, 1986; Bhattathiri et al., 1996; Wiggert et al., 2005)

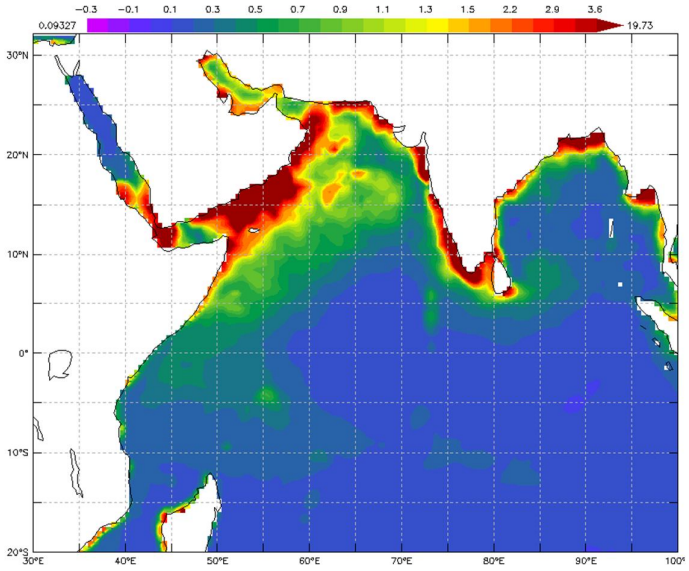

Figure 12. Distribution of chlorophyll-a during the southwest monsoon in the northern Indian Ocean. High chlorophyll-a is seen along the coasts of Somalia, Oman and India. (*Source*: SeaWiFS image, http://las.northern Indian Ocean.org)

Previous palaeoproductivity reconstructions suggested that the productivity in Arabian Sea has varied on glacial-interglacial time-scales. However, there are opposing views. According to few studies based on palaeo-upwelling reconstructed from foraminiferal assemblages, the productivity was higher during the interglacial periods and decreased significantly during glacial periods (Naidu and Malmgren, 1995; Rai and Das, 2011; Emeis et al., 1995). On the other hand, the geochemical proxies indicated higher productivity during the glacial period than during interglacial period (Almogi-Labin et al., 2000; Tamburini et al., 2003; Pourmand et al., 2007). On one hand, the interglacial high-productivity in general was attributed to summer monsoon winds driven upwelling, while on the other hand, the glacial high-productivity was attributed to intensified winter monsoons driven nutrient injection in to photic waters (Rostek et al 1997; Pourmand et al., 2007) in accordance with modern observations.

Palaeoproductivity reconstructions for the EAS are also not free from such controversy. Based on variable contents of sedimentary organic carbon (C_{org}) and alkenone Banakar et al. (2005) suggested increased productivity during the glacial period. The transfer functions of planktonic foraminifera and alkenones have also indicated increased glacial productivity (Rostek et al., 1994; 1997; Beaufort et al., 1997; Schulte et al., 1999; Cayre and Bard, 1999; Ivanova et al., 2003; Prabhu and Shankar, 2005). In all these studies, high productivity during the cold and dry glacial period was attributed to intensification of winter monsoons, which strengthened the deep convective mixing enhancing nutrient injection. Pattan et al., (2003) and Thamban et al., (1997) observed low glacial and high interglacial productivity based on proxies such as calcium carbonate, biogenic opal, barium and C_{org} contents in a sediment core from the southern EAS region. These contrasting views have thrown open the past productivity variation for further investigation.

In this chapter, a suite of organic-geochemical proxies such as lipids, C_{org} and N_{Tot} contents and their isotopes have been examined to address the above paradox and resolve. Further, the probable ocean-atmosphere coupled dynamics which might have been responsible for the observed changes in past productivity are also presented.

5.2. Radiocarbon age

As already presented in material and method section, the radiocarbon dated upper 1 m length of all the three sediment cores cover a time period of last ~32-35 kyr. The age of core-top sections in all the three sediment cores indicate a loss of latest Holocene sedimentation record of ~5 kyr (Table 3). Such core-top losses are common while collecting sediment core using gravity corer. However, in sediment

cores from regions affected by strong bottom currents such loss may also be due to erosion of younger sediment from the site of deposition (Banakar et al., 1993). As a significant part of sediment deposited during the early Holocene and entire LGM is intact, it is feasible to understand the productivity shifts that have occurred during cold to warm climate transition in the immediate past.

The sedimentation rate provides general information regarding the overall climate dynamics of a specific region along with associated biogeochemical history. Marine sediments in general are composed of a mixture of biogenous, terrigenous and authigenic components. The biogenic material in marine sediment is derived primarily by marine life. A small but considerable amount of biogenic material also comes from soil-OM via fluvial or eolian transport. The transport of terrigenous materials through the rivers is controlled by prevailing regional climate. Melting glaciers and increased precipitation during interglacial warm periods render the rivers mostly perennial and turbulent thus enhance the transport of terrigenous material that normally composed of weathering products of silicates and plant humus of soil. Similarly, intense dry winds of the cold glacial periods have potential to deliver significant amount of terrigenous material to the adjacent seas. Therefore, the sedimentary organic components contain valuable information about the past climatic conditions.

Climate variability is known to modulate productivity of the oceans through processes such as nutrient upwelling and injection from light-starved intermediate waters in to light-abundant mixed layer. These nutrients are the ultimate trigger of productivity in the upper few-hundred meters thick photic layer. Therefore, the biogenic fraction, may be hard skeletal inorganic material (calcium carbonate or

opaline silica) or the soft tissue (organic matter or OM) preserved in the sediment hold clues about the climatic conditions prevailed during the time of their production by various microscopic planktonic organisms. Thus when all preservation conditions are satisfactory, then higher the biogenic material deposition on seafloor, higher shall be the productivity in overlying photic zone.

The sedimentation rates from the age-depth relationships in the studied sediment cores are given in Table 14. In the EAS (represented by GCR1 and GCR2), the sedimentation rate varies from 2 to 4 cm/kyr with higher rate during the LGM. In the EIO (represented by GCEq2), the rate varies marginally ~3.5 cm/kyr Table-14). Thus, the sedimentation in EAS is distinctly higher during the LGM, but in the EIO it remained nearly constant irrespective of similar climate forcing in both the regions. Such difference in sedimentation rates in two distinctly different oceanic regimes in spite of being under the similar climatic set-up is rather expected. In that, the EAS, a highly productive continental marginal environment, is expected to show high amplitude biogeochemical responses. Whereas, the EIO, an open ocean oligtrophic region such responses are normally weak. This could result in highly variable sedimentation rates in the marginal seas as compared to the open ocean environments.

Higher sedimentation rate during dry and cold LGM in the EAS either could be due to an increased transport of dust (terrigenous matter) from the land or due to increased export production or both. To examine the contribution of each of these two sedimentary components in controlling the sedimentation rates, a set of geochemical and lipid biomarker have been utilized in the present study.

Table 14. Climate period averaged sedimentation rates, elemental and isotopic composition in BP3/GCR1, BP3/GCR2 and CC2/GCEq2 sediment cores

Sediment Core	Period	Sedimentation rate (cm/kyr)	C_{org} (%)	C/N (mol/mol)	$\delta^{13}C_{org}$ ‰ PDB
BP3/GCR1	Holocene	2.03	1.1	8.4	-20.5
	LGM	3.67	1.6	11.2	-19.6
BP3/GCR2	Holocene	2.17	0.8	8	-20.5
	LGM	4	1.5	10	-19.7
CC2/GCEq2	Holocene	3.18	0.6	6.2	-21.3
	LGM	3.66	1.0	7.8	-19.8

Apart from higher sedimentation rates during the LGM, the C_{org}, C/N and $\delta^{13}C_{org}$ also exhibit distinctly higher values. This observation at the outset suggests that the sedimentary components deposited during the LGM were in fact different than those deposited during the Holocene. To unscramble the fundamental nature of these sedimentary components from mixed product, i.e., the sediment, lipid biomarkers are used extensively in the present study.

5.4. Oxygen isotopes

Oxygen has three isotopes, viz., ^{16}O, ^{17}O and ^{18}O of which ^{16}O is most abundant (99.8 %) followed by ^{18}O (0.2 %) ^{17}O (0.04 %) (Hoefs, 1996). The fractionation of isotopes occurs during processes such as melting, evaporation, precipitation, etc. The ratio of ^{18}O to ^{16}O normalized to a reference standard (here PeeDee Bellemnite) ($\delta^{18}O$) is expressed in per mil (‰, parts per thousand), which is obtained as: $\boldsymbol{\delta^{18}O\ ‰ = [(^{18}O/^{16}O)_{Sample}/(^{18}O/^{16}O)_{Standard} - 1] \times 1000}$

As per the Rayleigh's fractionation, during evaporation the light-water molecules ($H_2{}^{16}O$) are preferentially removed from the oceanic reservoir to the vapour as compared to heavy-molecules ($H_2{}^{18}O$). This fractionation leaves the

reservoir relatively enriched with heavy-water molecules (i.e., higher $\delta^{18}O$). The reverse happens when there is precipitation. If the evaporated water does not return back to the oceanic reservoir due to its deposition as ice in high-latitude and high altitude regions (as in the case of glacial climates), the oceanic reservoir becomes relatively depleted in light-water molecules. This depletion of light water molecules leads to long-term enrichment of $\delta^{18}O$ in oceanic reservoir. Conversely, if the evaporated water returns back to the reservoir in the form of precipitation/rains (as in the case of inter-glacial climate) the reservoir would retain its $\delta^{18}O$ mostly unaffected. At certain times if melting of ice is enhanced due to intense warming then increased amount of lighter-water molecules are delivered to the ocean leading to recognisable depletion of $\delta^{18}O$ ($\delta^{18}O$ depleted reservior). These signatures are well-preserved in planktonic foraminiferal calcite that is secreted in equilibrium with ambient seawater. Therefore, the $\delta^{18}O$ of planktonic foraminifera is a measure of the seawater-$\delta^{18}O$, in turn, evaporation-precipitation balance, i.e., the monsoon intensity.

5.4.1. Temporal changes in $\delta^{18}O$ of planktonic foraminifera

The $\delta^{18}O_{G.sacculifer}$ varies between -1.31 and 0.35 ‰ and -1.20 and 0.60 ‰, respectively in GCR1, GCR2 (Tables 5 and 6). In GCEq2, the $\delta^{18}O_{G.ruber}$ variation is between -2.37 and -0.83 ‰ (Table 7). The temporal variation of $\delta^{18}O$ is given in Figure 13a. The glacial-interglacial gradients in GCR1, GCR2 and GCEq2 are ~1.7 ‰, 1.8 ‰ and 1.6 ‰, respectively. The global ice-volume contribution to this glacial-interglacial $\delta^{18}O$ gradient is 1 ‰ (Shackleton, 2000). Hence, the remainder $\delta^{18}O$ gradient of 0.7 ‰ in GCR1 and 0.8 ‰ in GCR2 (i.e, in EAS) and 0.6 ‰ in GCEq2 (i.e., in EIO) must have been resulted from changes in the net evaporation – precipitation (E-P) budget in the respective regions. These residual $\delta^{18}O$ gradients

between the cold-LGM and warm-Holocene also suggest that the climatological changes in the EIO are relatively less intense than in the EAS (0.6 ‰ v/s 0.8 ‰).

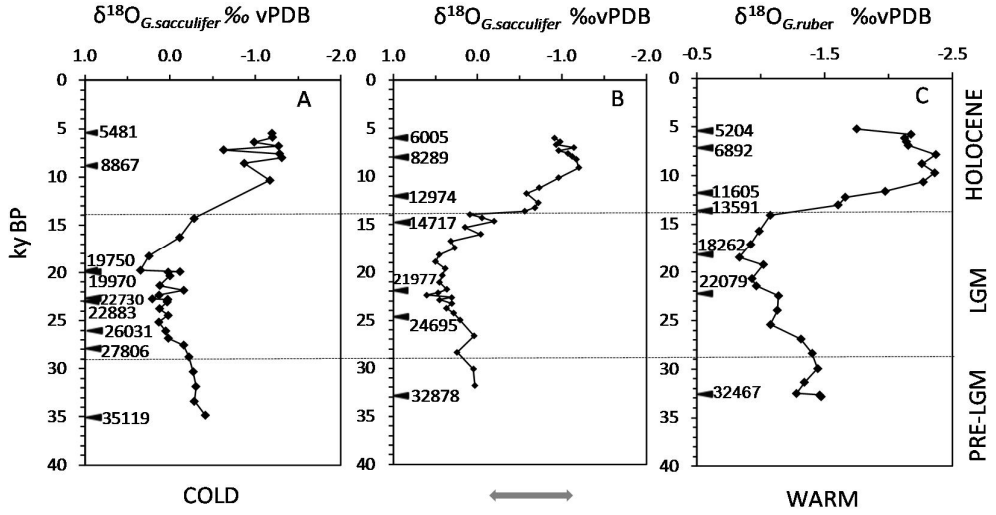

Figure 13a. Composite of time-series of $\delta^{18}O_{G.sacculifer}$ in sediment cores (A) BP3/GCR1, (B) BP3/GCR2 and (C) $\delta^{18}O_{G.ruber}$ in CC2/GCEq2. The filled arrow heads on vertical axis denote the radiocarbon dated sections along with their corresponding calendar age in ky BP. The broken horizontal lines running across all the panels denote the marine oxygen isotope boundaries labeled on right vertical boarder of the right panel. The double headed filled arrow below the diagram suggests that $\delta^{18}O$ depletion indicate that the climate shifting towards warmer conditions and $\delta^{18}O$-enrichment indicates shifting towards colder conditions.

The MIS 1/2 (Holocene-LGM Boundary) occurs at ~13.8 Ky BP in all the three sediment cores. These indicate offsets of 0.2 Ky BP when compared with the Holocene-LGM Boundary (MIS1/2) in the reference curve of global benthic oxygen isotope stack LR-04 (MIS 1/2 is at 14 Ky BP: Lisiecki and Raymo, 2005). This difference is rather negligible and hence, the observed Holocene-LGM boundary in the studied sediment cores is in accordance with the global climate system. However, a comparison with the SPECMAP which is based on planktonic foraminifera oxygen isotope stack (MIS 1/2 is at 11 Ky BP: Imbrie et al., 1984) yields an age offset of ~3 kyr indicating the effect of local climatology in modulating the timing of global climate events. It should be noted that the LR-04 represents the global deep-sea

cooling that is insulated from local surface climatological effect and hence is a robust indicator of global climate or global ice-volume or global sea level unlike the SPECMAP. Therefore, the LR-04 time-scale is preferred to define the MIS 2/3 boundary at 29 Ky BP in the studied sediment cores, because, in these the MIS-3 is not complete to identify the actual MIS2/MIS3 boundary. Therefore, the part of the MIS-3 is denoted as Pre-LGM.

The LGM is characterised by heaviest $\delta^{18}O_{G.sacculifer}$ which occurs between 26.8 - 19.8 Ky BP and 23.7 -18.8 Ky BP in GCR1 and GCR2 respectively. In GCEq2, the heaviest $\delta^{18}O_{G.ruber}$ (representing LGM) occurs between 21.4 -17.1 Ky BP. The Holocene optimum conditions appear to have reached at ~8.5 Ky BP in EAS and ~11 Ky BP in the EIO. The deglacial transition begins as a rapid depletion of $\delta^{18}O_{foraminifera}$ uniformly *at* ~18.5 Ky BP in the study region irrespective of the local climatological differences.

The time-series of $\delta^{18}O_{foraminifera}$ for the EAS and EIO sediment cores in general, are closely comparable with those of global planktic and benthic foraminiferal $\delta^{18}O$ stacks (Imbrie et al., 1984; Lisiecki and Raymo, 2005). They also are closely comparable to Antarctic climate records such as atmospheric-CO_2 and -Temperatures and tropical planktic foraminiferal $\delta^{18}O$ stack of Bassinot et al. (1994) (Figure 13b). The LGM, transition and the Holocene in the present sedimentary records are also comparable to the Vostok (Antarctic)-CO_2 and -atmospheric temperatures (Barnola et al., 1987; Petit et al., 1999) (Figure 13b) both in timings and the structure. These observations clearly suggest that the EAS and EIO climatology has varied in concert with the global climate variability. The local climatology forced by the regional monsoon system therefore, is superimposed on

the global climate pattern to enhance the global signal of $\delta^{18}O_{foraminifera}$ by ~0.7 ‰ in the studied sediment cores. Thus, the oxygen-isotope variation recorded in the planktonic foraminifera of the present sediment cores (Figure 13a) is mainly forced by the changes in the global ice-volume (or Glacial-Interglacial Climate variability), wherein, the local effect of monsoon variability acts as an additional signal over the global climate background.

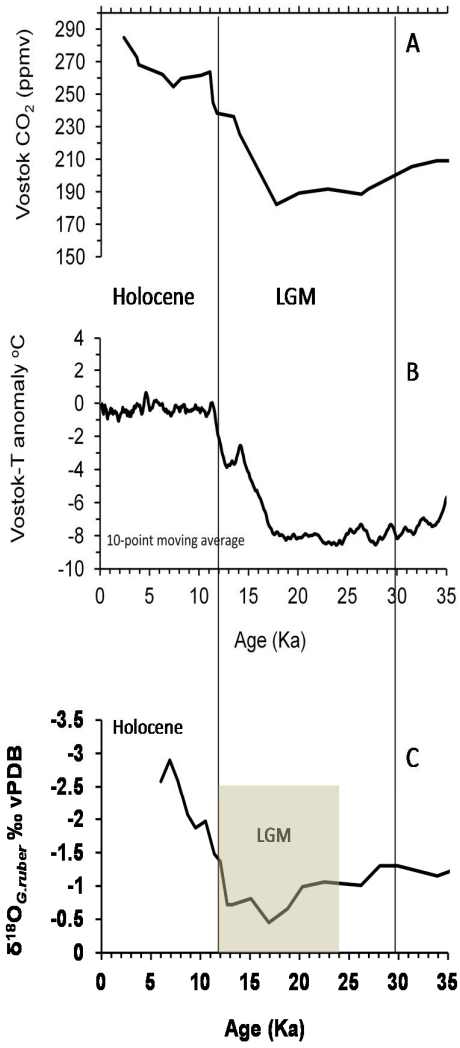

Figure 13b. Time-series of climate proxies representing the global climatic features for the last 35 Ky BP retrieved from polar-ice (A & B) and tropical sediments (C). A: Atmospheric carbon-dioxide variation constructed from the Antarctic Ice-Core (Barnola et al., 1987); B) Atmosphperic temperature anomaly constructed from Deuterium Gas in the Antarctic Ice-Core (Petit et al., 1999); C) Planktonic foraminiferal oxygen-isotope stack of tropical Indian Ocean sediment (Bassinot et al., 1994). Vertical lines indicate MIS-Boundaries based on LR-4 global ocean benthic oxygen isotope stack (Leisiecki and Raymo, 2005), while the shaded part in panel C is the LGM based on planktic oxygen-isotope stack (Imbrie et al., 1984). Note highly consistent patterns of Glacial and Interglacial conditions along with transition in different climate repositories. Similar patterns are evident in the studied sediment cores from the EAS and EIO (Figure 13a).

5.5. C_{org}: productivity versus preservation

In marine sediments, the concentration of C_{org} depends on various factors such as surface productivity, preservation on burial within the sediments or combination of both (Canfield, 1994; Hedges et al., 1995). The average C_{org} in the EAS sediment deposited during the LGM is ~1.5 % as compared to ~1 % in

Holocene sediment, whereas, it is 1% during the LGM as compared to 0.6 % during the Holocene in EIO sediment (Table 13). The temporal variation of C_{org} is shown in Figure 14.

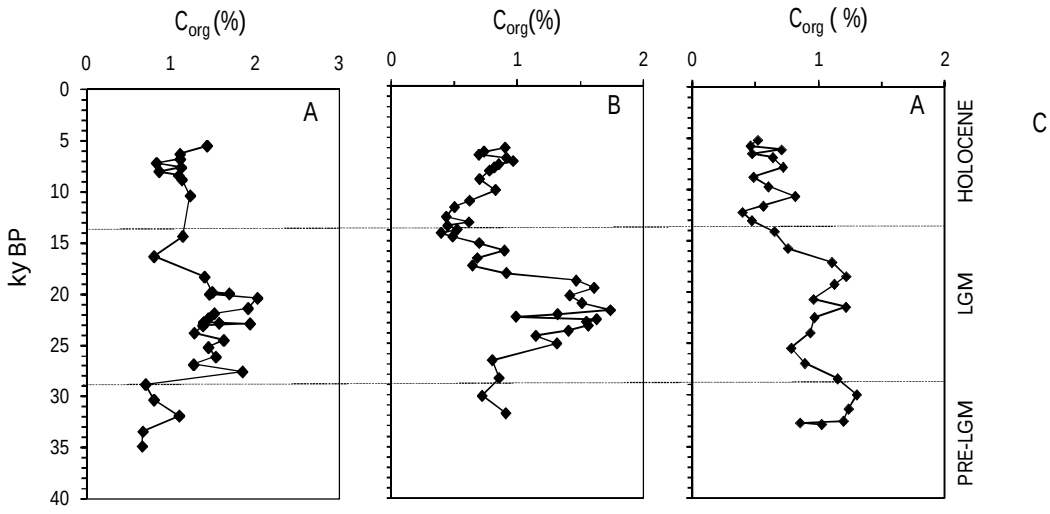

Figure 14. Composite of time-series of organic carbon (C_{org}) in sediment cores (A) BP3/GCR1, (B) BP3/GCR2 and (C) CC2/GCEq$_2$. The broken horizontal lines running across all the panels denote the marine oxygen isotope boundaries

Previous studies on past productivity of the EAS have suggested different reasons for C_{org} enhancement in the sediments. Some studies have suggested productivity as a factor causing higher C_{org} concentration (Thamban et al., 1997; Prakash Babu et a., 1999; Prabhu and Shankar, 2005, Banakar et al., 2005). On the other hand, few studies attribute high C_{org} concentration to preservation as a result of anoxic condition created by the OMZ (Paropkari et al., 1993). Agnihotri et al., (2003) attributed the glacial C_{org} enhancement in the EAS to the preservation of C_{org} due to increased sedimentation rate as a result of erosion and deposition of shelf sediments. In other studies, the increase of C_{org} in glacial periods is attributed to the increased contribution of terrestrial C_{org} (Pattan et al., 2003).

The EAS is located in the region that falls under the influence of modern winter convection and associated enhanced productivity (Banse, 1987; Madhupratap et al., 1996). Therefore, distinctly higher C_{org} content during the LGM in the EAS reflects increased surface productivity (export production). In addition, the C_{org} input derived from the adjacent landmass (soil carbon) to the EAS might have also increased due to intensified winter winds during the LGM (Banakar et al., 2005, 2010; Punyu et al., 2014; Mahesh and Banakar, 2014) as the winter winds (northeasterlies) blow over the Indian Subcontinent towards the surrounding marginal seas and the open ocean. A similar increase in the C_{org} in the EIO during the LGM (Rostek et al., 1997; Schulte et al., 1999; Pailler et al., 2002) further confirms that the increased LGM productivity is rather regional than a local feature. This interpretation has a direct relevance to the climate cooling feedback during the LGM. It is quite possible that the increased surface production and enhanced soil-carbon transfer to the northern Indian Ocean probably have, to some extent, contributed to the drawdown of atmospheric CO_2.

However, the bottom waters in this region have remained largely oxygenated throughout the study period based on both lipid proxies (Schulte et al., 1999) and redox sensitive metal variations (Pailler et al., 2002). In such a scenario, it is extremely difficult to assess the variation in the preservation of OM to interpret the observed variations in C_{org} only in terms of surface productivity. The higher sedimentation rates of the order of few cm/ky in the northern Indian Ocean (Table 14) (also see Tiwari et al., 2006) as compared to few ~2 mm/ky in further south (Central Indian Ocean: Banakar et al., 1991) might have assisted in better preservation of OM in the study region in spite of bottom waters were not oxygen-

depleted. Therefore, at the outset, one can assume that the sedimentary carbon in the northern Indian Ocean is mainly controlled by the export production. This interpretation still cannot be considered as unequivocal. Therefore, more robust and refractory organic proxies are required to address this uncertainty.

In the subsequent section a suite of lipid biomarkers which are considerably refractory for post-depositional alteration (oxidation/diagenesis) are examined in detail to know whether the productivity was actually responsible for the observed increases in the LGM-C_{org}. At least the location of GCEq2 sediment core might have not witnessed a great deal of bottom water oxygen variability in the past because its location is in deep water regime (>3500 m) without an overlying OMZ.

5.6. C/N and $\delta^{13}C_{org}$: Marine versus terrestrial organic matter

In order to find out the contribution of marine- and terrestrial-OM to the sedimentary OM-pool in the northern Indian Ocean, the C/N and $\delta^{13}C_{org}$ are used. The C/N and $\delta^{13}C_{org}$ are used to broadly classify the sources of OM in the sediments. Further, the $\delta^{13}C_{org}$ is used to find out the contribution of terrestrial-C3 and -C4 plant derived OM or soil organic matter. The C3 and C4 terrestrial plants are classified according to the photosynthetic pathway they follow (Figures 15 and 16). The C3 and C4 pathways operate in different environmental conditions depending on climatic parameters such as atmospheric CO_2 and temperature (Ehleringer and Cerling, 2002; Boom et al., 2002). Therefore, in palaeoclimatic studies, these plants provide us with the information about the prevailing climatic conditions. The C4 plants grow in dry and cold conditions with limited availability of soil-moisture and CO_2, while the C3 plants flourish during wet and warm conditions with ample of soil

moisture and elevated CO_2 in the atmosphere. The former is the characteristic of glacial climate and the latter is typical of inter-glacial climate.

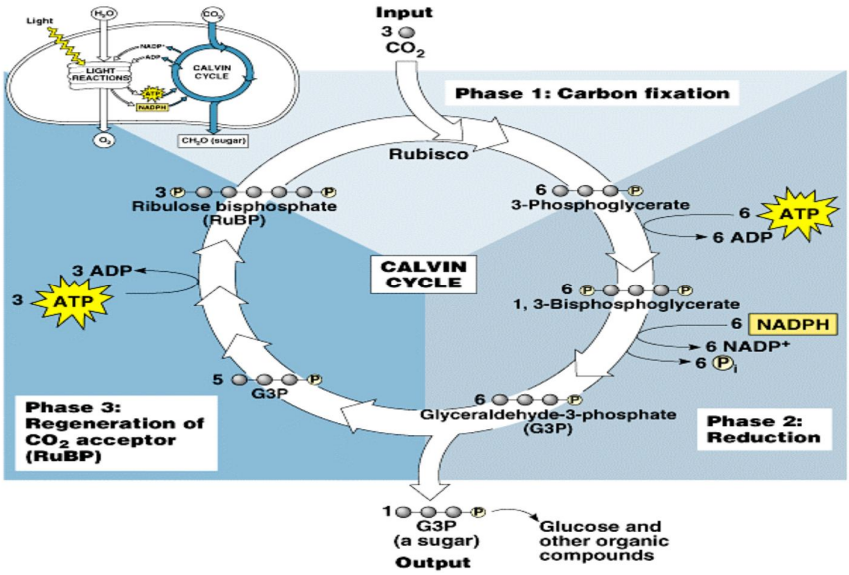

Figure 15. C3 (Calvin Cycle) photosynthetic pathway; ATP-Adenosine triphosphate, NADPH-Nicotinamide adenine dinucleotide phosphate (*image source*: http://tnau.ac.in/)

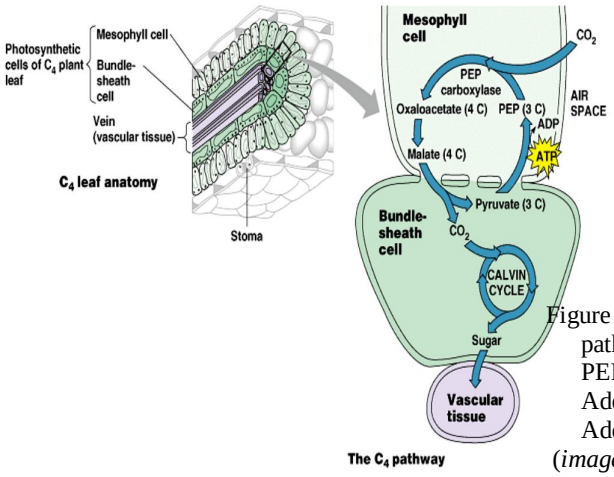

Figure 16. C4 (Hatch and Slack pathway) photosynthetic pathway; PEP- phosphoenol pyruvate, ADP-Adenosine diphosphate, ATP-Adenosine triphosphate (*image source*: http://tnau.ac.in/)

The C/N of marine OM is generally ~6 (Redfield et al., 1963; Sardans et al., 2012) while that of terrestrial is ~30 (Walsh et al., 1981). Therefore, any C/N ratios between these two end-members represent mixture of terrestrial- and marine-OM. Similarly, the $\delta^{13}C_{org}$ for different sources of OM has distinct values. The $\delta^{13}C_{org}$ for marine OM is ~ –23 ‰ (Laws et al., 1995), terrestrial C3 is –27 ‰ (Hoefs, 1996) and that of terrestrial C4 is –11 ‰ (Cotton et al., 2012). On the other hand, most of the $\delta^{13}C_{org}$ in the present sediment cores are ~ –20 ‰. This value could be obtained not only by mixing marine-OM and terrestrial-C4, but also by mixing only terrestrial C3 & C4 biomass. To resolve these complications first, the binary mixing based on C/N ratios and $\delta^{13}C_{org}$ with marine and terrestrial end-members are prepared to know marine and terrestrial proportions of OM (Figure 17). The ternary mixing diagrams using both the C/N and $\delta^{13}C_{org}$ end-members were prepared to know proportions of marine, terrestrial-C3 and –C4 OM (Figure 18).

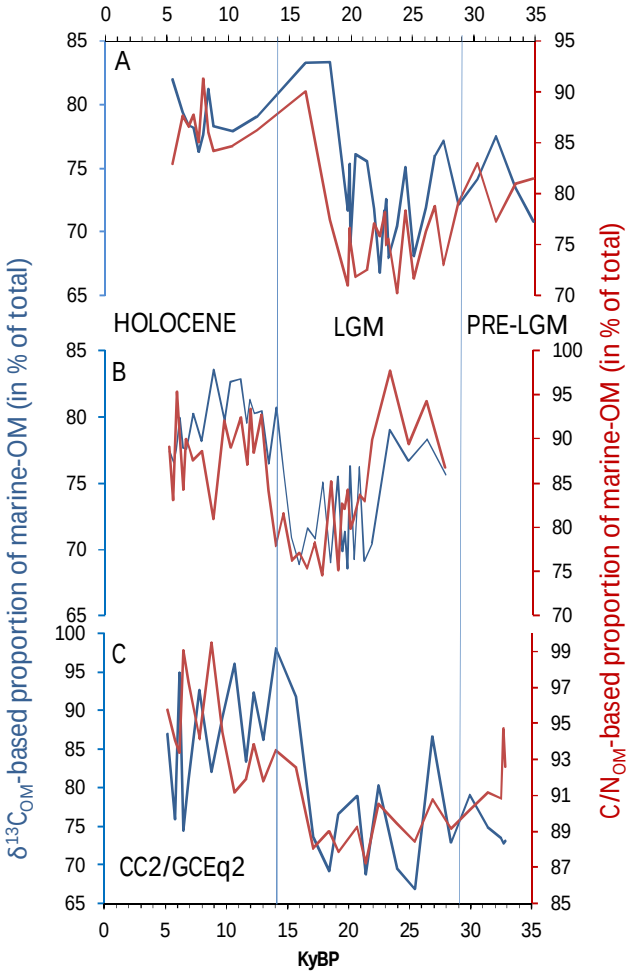

Figure 17. Proportion of marine-organic matter in the total-organic matter calculated using binary mixing model (Bindler et al., 2008) with $\delta^{13}C$ phytoplankton end-member as -23 ‰ (Laws et al., 1995), terrestrial C4 end-member as -11 ‰ (Cotton et al., 2012) and C/N end members as 30 for terrestrial plant biomass and 5 for marine phytoplankton biomass (Sardans et al., 2012).

[Note: Although the Redfield ratio of C/N for marine phytoplankton is 6.6, a value of 5 as end-member is chosen to accommodate the lowest C/N obtained in this study. The lower than ideal Redfield C/N are common in natural systems due to several variable environmental forcing on metabolism of the organism in space and time (see Sardans et al., 2012). A relative increase in the terrestrial-organic matter causing decreased proportion of marine-organic matter is evident in all three sediment cores. The decreased proportion of marine-OM however does not indicate reduced marine production as the mixing diagrams depict relative abundance but not the absolute concentration (see text)].

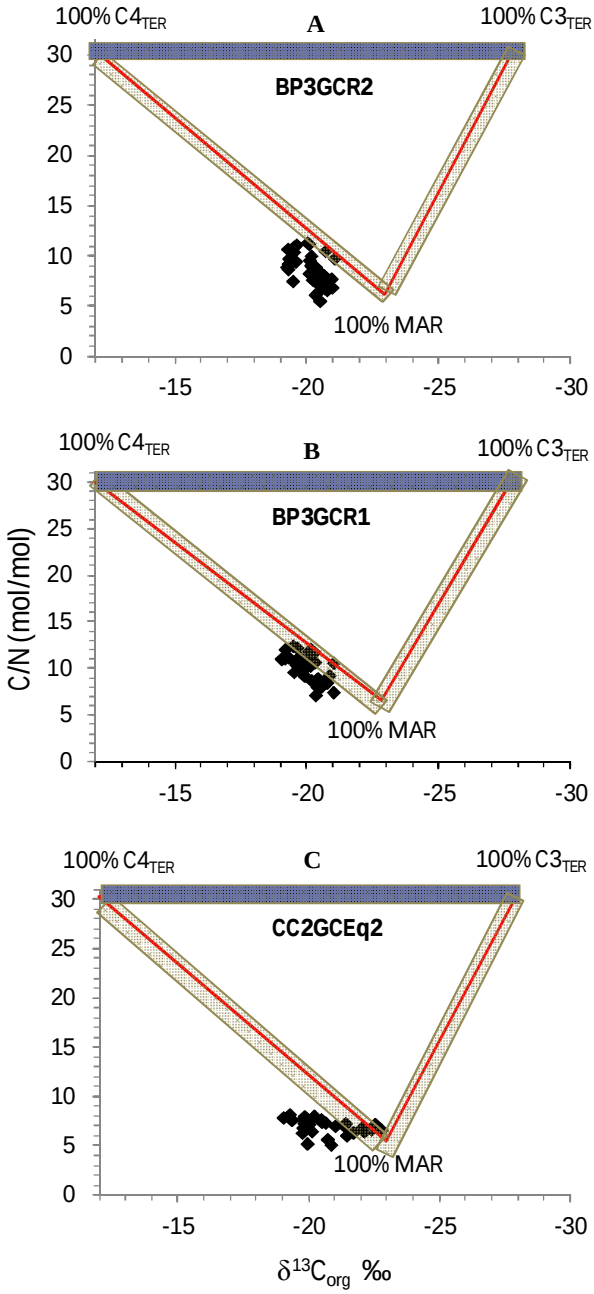

Figure 18. Ternary mixing diagram to show mixing of organic matter (OM) from three different sources in the studied sediment cores. Three end-members defined for the ternary mixing based on $\delta^{13}C_{org}$ and C/N are: Terrestrial-C3 (-27 & 30) and –C4 (-11 & 30) and marine phytoplankton (-23 & 5). Note the clustering of data overwhelmingly near the marine-OM end-member in all the three sediment cores indicating dominance of marine carbon. The data-points mostly fall on the marine and C4-Terrestrial mixing line suggesting most of the sedimentary carbon could be defined by these two end-members, which supports the basis for relative proportion calculation for binary mixing model (Figure 17). Shaded vertices are indicative of probable uncertainties associated in calculating the mixing ratios.

The binary mixing model of Bindler et al. (2008) was used to calculate the relative proportions of marine- and terrestrial-OM. These proportions were estimated independently based on: 1) C/N ratio of the OM (marine phytoplankton C/N = 5; terrestrial plant C/N = 30 as end-members) (Sardans et al., 2012; Walsh et al, 1981) and 2) $\delta^{13}C_{org}$ of the OM (marine phytoplankton $\delta^{13}C_{org}$ = –23 ‰; terrestrial-C4 plants $\delta^{13}C_{org}$ = –11 ‰ as end-members) (Laws et al., 1995; Cotton et al., 2012). The equations for calculating the marine OM proportion based on C/N and $\delta^{13}C_{org}$ are as follows:

$$C/N_{Marine\ OM} = \frac{C/N_{Sample} - C/N_{Terrestrial}}{C/N_{Marine} - C/N_{Terrestrial}} \times 1000$$

$$\delta^{13}C_{org\ Marine\ OM} = \frac{\delta^{13}C_{org\ Sample} - \delta^{13}C_{org\ Terrestrial}}{\delta^{13}C_{org\ Marine} - \delta^{13}C_{org\ Terrestrial}} \times 1000$$

The binary mixing model shows that the marine-OM in the sediments of EAS and EIO varies from ~70 % to 99 % (Figure 17). This figure further suggests that the proportion of marine-OM in the total-OM decreased during the LGM indicating that the relative proportion of terrestrial-OM increased during that time. The decrease in proportion of marine-OM in total-OM (C_{org}) however, does not reflect a decrease in primary production, but simply suggests relative increase of terrestrial soil-carbon input to the EAS and EIO. The ternary mixing diagrams were constructed based on both C/N and $\delta^{13}C_{org}$ together as end-members of three distinctly different OM, viz., marine phytoplankton ($\delta^{13}C_{org}$ = –23 & C/N = 5), terrestrial-C3 plants ($\delta^{13}C_{org}$ = –27 & C/N: 30), and terrestrial–C4 plants ($\delta^{13}C_{org}$ = –11 & C/N = 30). The edges of the ternary diagram represent 100 % of each of these three types of OMs (Figure 18).

If the data-points of C/N and $\delta^{13}C_{org}$ pair fall along the vertices of the ternary diagram, it indicates mostly two component dominant mixing; if the data-points fall within the area of the ternary diagram, then it indicates mixing of three components.

In the present study most of the C/N and $\delta^{13}C_{org}$ pairs are located around the marine end-member. This clustering indicate that the marine (primary productivity) derived OM is the dominant component. However, the data-distribution does not exhibit 100% marine-OM, but shows a minor loading on the terrestrial-C3 and -C4 OM (Figure 18) in line with binary mixing model (Figure 17), where the soil-carbon (terrestrial C3 + C4) content is < 30 %. This observation suggests presence of minor amount of both types of soil-carbon. Interestingly, in the Figure 18C representing EIO, some of the data points fall marginally outside the ternary region, which cannot be defined by any of the three end-members considered here.

The temporal variation of the C/N and $\delta^{13}C_{org}$ is given in Figures 19 and 20 and the average values are given in Table 14.

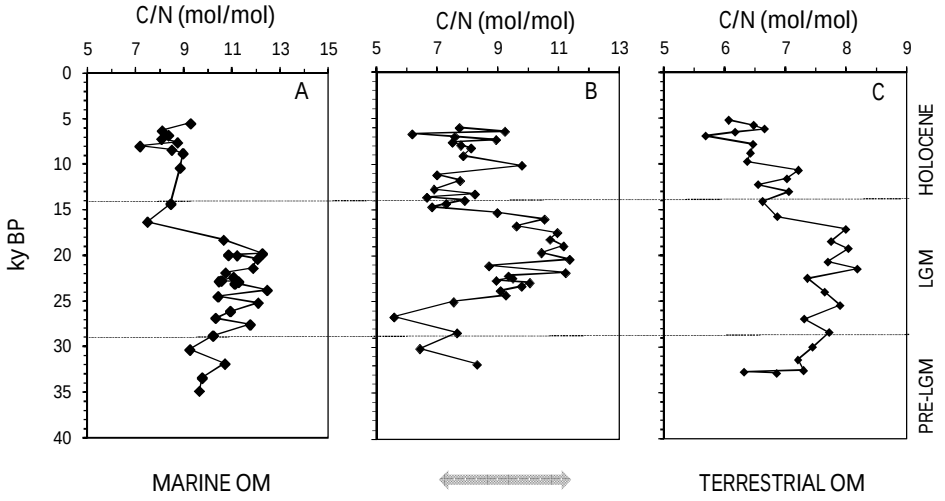

Figure 19. Composite of time-series of C/N in sediment cores (A) BP3/GCR1, (B) BP3/GCR2 and (C) CC2/GCEq2. Dotted lines running across the panels denote marine oxygen isotope boundaries. Shaded arrow common for all three panels shows that higher the C/N means increasing amount of Terrestrial-OM and vice-versa

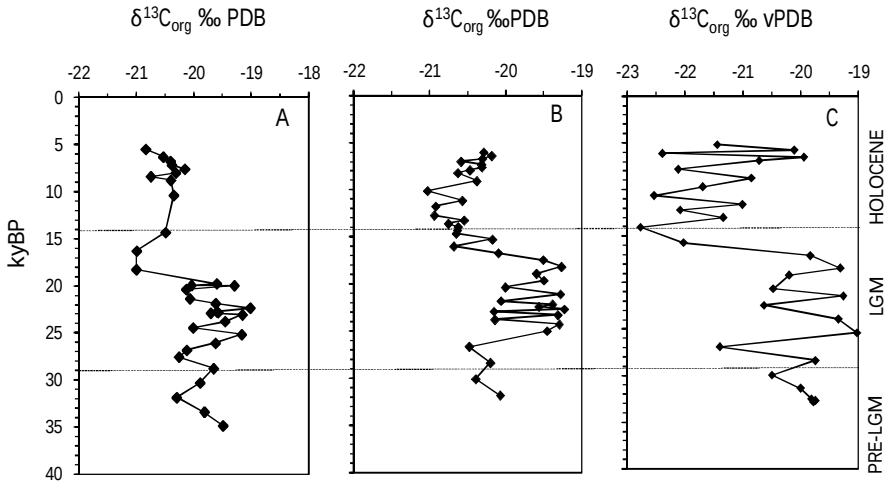

Figure 20. Composite of time-series of isotopic carbon ($\delta^{13}C_{org}$) in sediment cores (A) BP3/GCR1, (B) BP3/GCR2 and(C) CC2/GCEq2. Dotted horizontal lines running across all the panels denote the marine oxygen isotope boundaries

The C/N and $\delta^{13}C_{org}$ are higher than the pure marine-OM values (C/N = 5 and $\delta^{13}C_{org}$ −23 ‰). Further, they are relatively higher during the LGM than during the Holocene. This observation suggests that, a) the OM in both EAS and EIO is of mixed type as also depicted in mixing models, and b) the terrestrial-OM input during the LGM was higher than during the Holocene. Before interpreting the variations in C/N, it is necessary to rule-out the effect of denitrification process. The denitrification in sub-oxic environment within the sediments may enhance the C/N ratios of the sedimentary-OM (Walsh et al., 1981; Mùller, 1997; Mejanelle and Laureillard, 2008) due to nitrate reduction to elemental nitrogen. The X-Y scatter plot of C_{org} vs N_{tot} help to assess this process, wherein, the linear positive correlation between both these parameters is indicative of no denitrification effect. The X-Y scatter diagrams for all three sediment cores exhibit a strong positive linear variation with high R^2 (> 0.7) (Figure 21), suggesting the OM has not been influenced by denitrification or any diagenetic change after its burial.

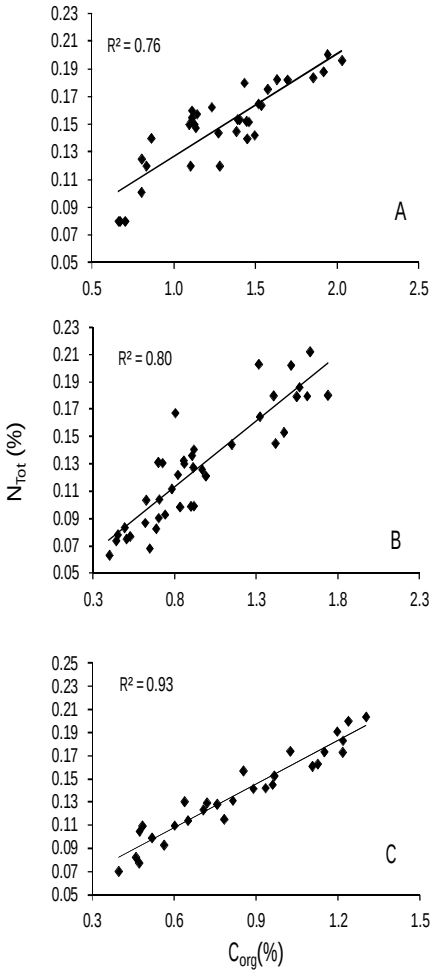

Figure 21. X-Y Scatter plots of C_{org} vs N_{Tot} in sedimentary OM of the three in sediment cores (A) BP3/GCR1, (B) BP3/GCR2 and (C) CC2/GCEq2. A strong linear co-variation of these two components indicates well-preserved OM with some amount of remineralization (diagenesis). The non-zero intercept of the best-fit line on positive side of the Y-axis at ~0.05 % of N suggests preferential loss of C during the diagenesis. This loss however has not affected intact linear relationship between these two components dictated by constant C:N ratios during the synthesis of OM

Therefore, C/N ratios in the present sediment cores retain the original signals of the source material. The observed higher C/N during the LGM suggests enhanced input of terrestrial-OM. In addition, a relatively heavier $\delta^{13}C_{org}$ during the LGM indicates that the increased terrestrial-OM input was dominated by C4- OM. This interpretation is in accordance with the type of vegetation that flourished in dry and cold conditions with low atmospheric CO_2 (C4-vegetation), which is characteristic of the LGM. The atmosphere contained nearly 100 ppmv less CO_2 during the glacial stages compared to interglacial stages (Barnola et al., 1987) and explains the dominance of C4 over C3 OM during the LGM in EAS and EIO.

5.7. Long-chain lipids and terrestrial organic matter

To unscramble the proportion of terrestrial plant biomass in the sediments of the EAS and EIO, distinct terrestrial lipid biomarkers are analysed. The long-chain (higher molecular weight: HMW) *n*-alkanes and *n*-alkanols lipid are commonly used as indicators of terrestrial-OM sources because of their characteristic association with terrestrial higher plants (Clark and Blumer., 1967; Eglington and Hamilton, 1967; Rieley et al., 1991). Representative GC-MS profiles of *n*-alkanes and *n*-alkanols in the EAS and EIO sediment corers are given in Figures 22 and 23.

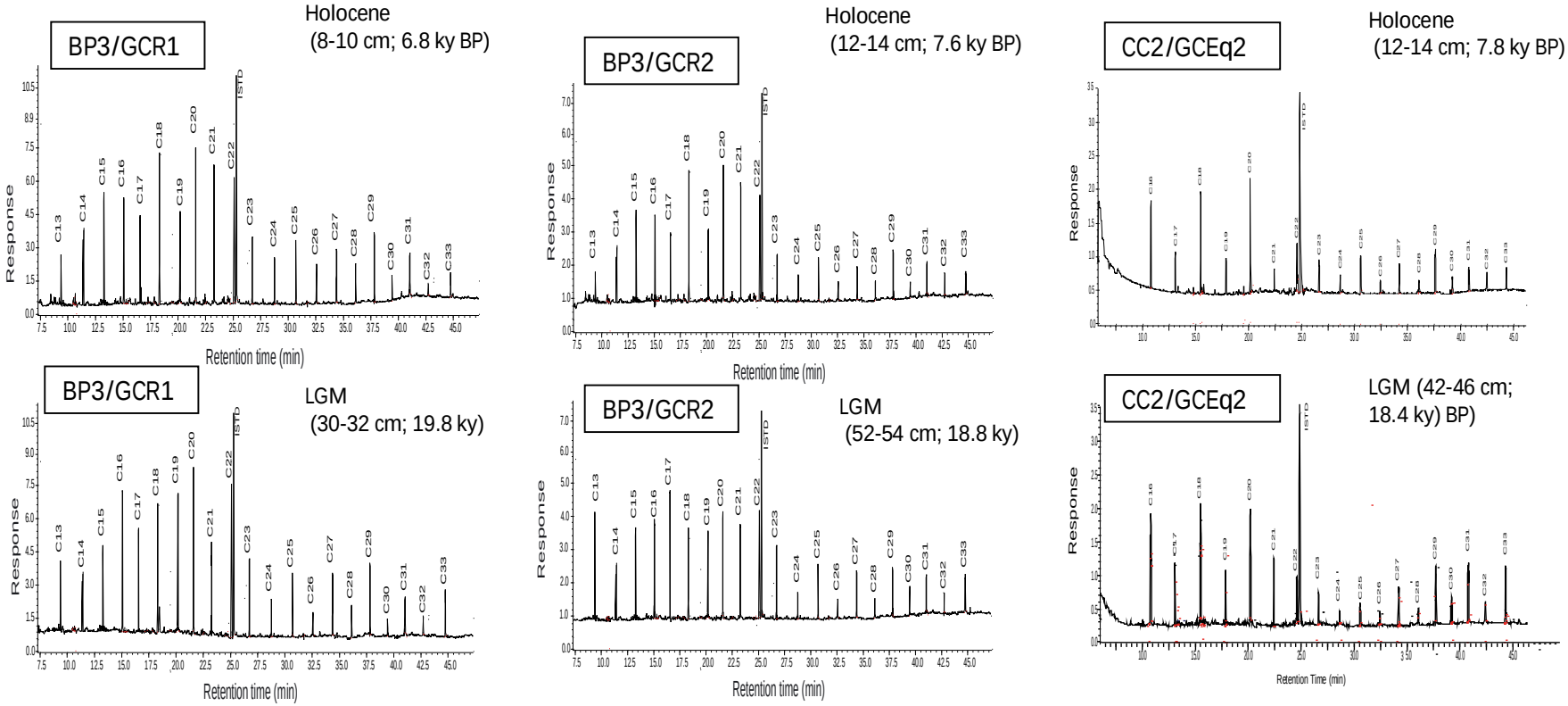

Figure 22. Representative GC-MS profiles of *n*-alkanes obtained at different sections from the sediment cores GCR1, GCR2 and CC2/GCEq2 (LGM-Last Glacial Maximum; ISTD-Internal Standard)

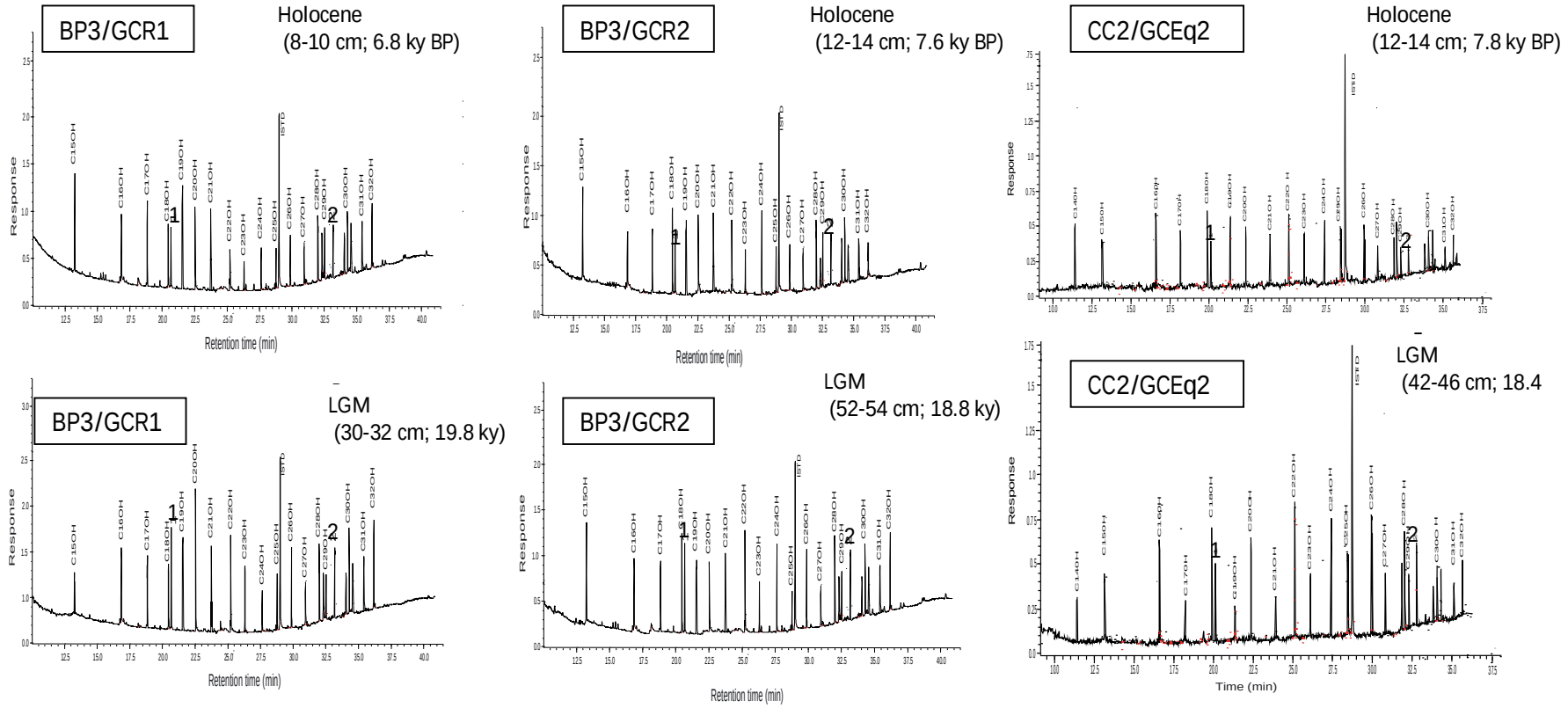

Figure 23. Representative GC-MS profiles of *n*-alkanols and sterols obtained at different sections from the sediment cores GCR1, GCR2 and CC2/GCEq2. (LGM-Last Glacial Maximum; ISTD-Internal Standard; 1-Phytol peak, 2-Brassicasterol peak)

The *n*-alkane with carbon-numbers C_{13-33} and *n*-alkanol with carbon numbers C_{15-32} were detected in the sediments. However, only the HMW *n*-alkanes (C_{23-33}) and HMW *n*-alkanols (C_{22-32}) have been considered here because they are characteristic of terrestrial sources of OM and their concentrations are given in Tables 11, 12 and 13 in Chapter 4. Their percentages in total *n*-alkanes and *n*-alkenols, their CPI and ACL in the sediments of EAS and EIO are given in Tables 15, 16 and 17 below.

Table 15. Distribution of terrestrial lipid biomarker indices in sediment core BP3/GCR1

n-alkanes				*n*-alkanols		
Age ky BP	C_{23-33} %	CPI	ACL	C_{22-32} %	CPI	ACL
5.5	25	3.2	27.4	22	3.4	27.8
6.3	21	4.1	27.7	18	3.9	27.4
6.8	23	3.5	27.2	24	3.9	28.1
7.2	26	3.9	28.1	26	3.6	27.4
7.6	23	3.4	27.3	19	4.3	27.9
8	28	2.7	27.4	22	3.5	27.4
8.4	33	4.7	27.6	36	3.8	28.2
8.8	35	4.1	27.1	25	4.6	27.1
10.4	31	2.3	27.3	34	4.3	27.5
14.3	24	4.1	28.2	19	4.6	27.9
16.3	35	4.6	27.5	27	3.4	27.9
18.3	30	3.2	28.1	22	3.6	28.6
19.8	22	4	28	20	4.7	27.8
19.9	36	5.5	29.2	31	4.6	29.2
20	40	4.8	28.4	34	5.1	28.9
20.3	27	5.1	29.5	28	4	29
21.4	34	5.8	28.6	33	5.4	28.4
21.9	36	5.1	28.1	31	4.3	29.4
22.4	17	3.7	29.7	24	5.6	28.7
22.7	35	5.3	28.6	34	4.3	29.5
22.8	35	4	28.4	29	5.4	29.1
22.9	22	5.1	29.2	25	4.5	29.2
23.1	27	4.5	29.3	25	5.4	29.3

23.8	35	5	28.7	30	4.6	28.7
24.5	41	3.8	29.6	35	5.4	29.2
25.2	33	3.1	28.1	30	4.2	28.2
26.1	30	4.1	28.4	29	4.9	29
26.8	38	4.6	28.9	29	5.3	28.5
27.5	22	2.5	28.6	20	3.6	29
28.8	30	3.2	27.6	29	4.5	27.6
30.3	28	2.3	27.9	16	3.5	27.7
31.8	31	3.7	27.9	25	3.9	27.8
33.4	38	2.1	27.7	33	4.2	27.7
34.8	29	3.2	27.8	19	3.3	27.8

CPI: Carbon Preference Index; ACL: Average Chain Length

Table 16. Distribution of terrestrial lipid biomarker indices in sediment core BP3/GCR2

n-alkanes				*n*-alkanols		
Age ky BP	C_{23-33} %	CPI	ACL	C_{22-32} %	CPI	ACL
5.9	28	3.6	27.2	25	3.1	27.2
6.4	25	3.9	27.4	25	2.6	27.5
6.8	26	2.7	27.3	23	3.6	27.1
7.1	30	3	27.1	25	2.2	27.4
7.3	22	4.3	27.5	21	3	27.7
7.6	30	3.5	27.2	29	2.8	27.3
7.9	28	2.8	27.7	28	2.2	27.2
8.2	30	3.6	27.4	25	3.2	27.2
8.9	31	2.7	27.3	30	2.7	27.9
9.9	31	3.9	27.8	24	2.9	27.4
10.8	27	3.4	27.1	30	2.1	27.2
11.7	32	4.6	27.7	31	3.5	27.5
12.7	31	2.9	27.2	28	3	27.8
13.2	26	3.5	27.81	28	2.3	27.3
13.5	35	2.6	27.5	26	2	27.6
13.8	31	4.4	27.6	29	2.9	27.2
14.2	29	2.8	27.3	30	2.6	27.7
14.5	34	3.9	27.5	30	1.9	27.5
15.1	28	3.5	28.3	26	3.6	27.4
15.9	33	3.1	27.8	19	3.9	28.2

16.6	32	5	27.9	22	3.5	27.8
17.3	31	3.7	28.09	32	3.1	28.4
18.1	34	5.5	28.4	25	4.2	28.3
18.8	30	4.3	28	30	3.8	28.6
19.5	35	5.3	28.3	27	4.5	28.5
20.3	31	4.8	28.5	34	3.9	28.3
21	30	5.6	27.9	31	4.2	28.5
21.7	40	4.3	28.4	28	3.2	28.2
22.1	35	5.1	27.68	30	3.9	28.5
22.4	31	4.6	28.3	32	4.3	28
22.6	33	5.3	28.1	33	4.4	28.2
22.8	32	4	28.5	28	3.6	28.6
23.2	35	4.9	28.3	30	4.1	28.7
23.7	38	3.9	27.59	31	3.6	27.9
24.2	33	5.1	28.2	29.8	2.8	28.4
24.9	23	3.3	27.8	21.4	2	28.3
26.5	30	4	27.3	24.9	3.2	27.8
28.3	28	3.6	27.8	26.4	2.9	28
30	31	3.7	27.4	23.6	1.9	27.5
31.9	31	2.9	28	27.8	2.2	28.1

CPI: Carbon Preference Index; ACL: Average Chain Length

Table 17. Distribution of terrestrial lipid biomarker indices in sediment core CC2/GCEq2

n-alkanes				*n*-alkanols		
Age ky BP	C_{23-33} %	CPI	ACL	C_{22-32} %	CPI	ACL
5.2	8	1.4	29	9	4.3	25.4
5.8	37	1.6	29.3	21	5.1	25.3
6.1	10	2.2	29.3	7	4.5	25.7
6.5	34	1.9	29.6	18	4.9	25.1
6.9	21	2.4	29.7	12	5.3	25.7
7.8	37	2.1	29.5	18	4.6	25.5
8.8	21	2.4	29.6	21	5.2	25
9.7	19	2	29.4	13	4.9	25.1
10.7	26	2.3	29.5	38	3.6	25
11.6	10	2.8	29.4	11	4.7	25.3
12.2	5	2	29.4	14	4.9	25.5
13	9	2.2	29.6	36	4.3	25.3
14.1	23	2.9	29.5	39	5.4	25.3
15.7	35	3.4	29.9	46	5.5	26.2
17.1	33	3.8	30	33	6.1	26.1
18.4	34	3.6	30	65	5.7	26
19.2	36	4.3	30.2	52	5.1	25.7
20.7	36	4	30.1	17	5.9	26.2
21.4	34	3.7	29.9	35	5.7	25.4
22.5	36	3.9	30	30	6	25.9
23.9	34	3.1	29.8	22	5.4	25.8
25.4	34	3.4	30	27	5.6	25.5
26.9	26	2.5	29.6	30	4.4	25
28.4	20	3.2	29.7	43	4.8	25.4
30	19	3.1	29.6	55	5.2	25.5
31.4	19	3.6	29.8	43	4.7	25.3
32.5	17	3.3	29.6	49	5	25.1
32.7	13	3.2	29.7	52	5.2	25
32.8	26	2.9	29.7	57	5	25.2

CPI: Carbon Preference Index; ACL: Average Chain Length

The climate period averaged content of lipids characteristic of terrestrial plant detritus are given in Table 18 to assess the influence of terrestrial carbon on the sedimentary OM.

Table 18. Climate period averaged indices of terrestrial lipid biomarkers in the studied sediment cores

Sediment Core	Period	*n*-alkanes				*n*-alkanols			
		C_{23-33} ng/g	C_{23-33} %	CPI	ACL	C_{22-32} ng/g	C_{22-32} %	CPI	ACL
BP3/GCR1	Holocene	348	27	3.7	27.5	139	24	3.9	27.7
	LGM	536	32	4.6	28.8	216	29	4.9	28.9
BP3/GCR2	Holocene	230	28	3.5	27.4	48	26	2.8	27.4
	LGM	324	34	4.7	28.1	90	30	4.0	28.4
CC2/GCEq2	Holocene	88	21	2	29.4	22	22	4.9	25.4
	LGM	174	35	3.7	30	75	35	5.7	25.8

From the two EAS sediment cores (i.e., GCR1 and GCR2), it is evident that the climate-optimum (peak-LGM and peak-Holocene represented by heaviest and lightest $\delta^{18}O \pm 0.1$ ‰), the averaged HMW *n*-alkanes (C_{23-33}) and HMW *n*-alkanols (C_{22-32}) are lower during the Holocene (277 ng/g and 69 ng/g respectively) than during the LGM (442 ng/g and 177ng/g respectively) (Table 18). In the EIO sediment core (GCEq2), the climate-period averaged HMW *n*-alkanes and *n*-alkanols are 88 ng/g and 22 ng/g respectively during the Holocene and 174 ng/g and 74 ng/g, respectively during the LGM. These observations imply that the terrestrial-OM input to both the EAS and EIO in general was higher during the LGM than during the Holocene.

When compared to the averaged ∑lipids (*n*-alkanes C_{13-33} + *n*-alkanols C_{15-32}) at LGM-optimum (1847 ng/g) and Holocene-optimum (1416 ng/g), the terrestrial lipid component (i.e., HMW: 309 ng/g during the LGM and 173 ng/g during Holocene) forms a proportion of ~17 % during the LGM and ~12 % during Holocene. In EIO sediment, this proportion is ~33% during the LGM and ~21 % during Holocene. Thus the HMW-lipid enrichment factors for LGM is 1.4 for EAS and 1.6 for EIO, suggesting nearly 50 % increase in the terrestrial carbon input to these regions during the cold-glacial climate (see Figure 24).

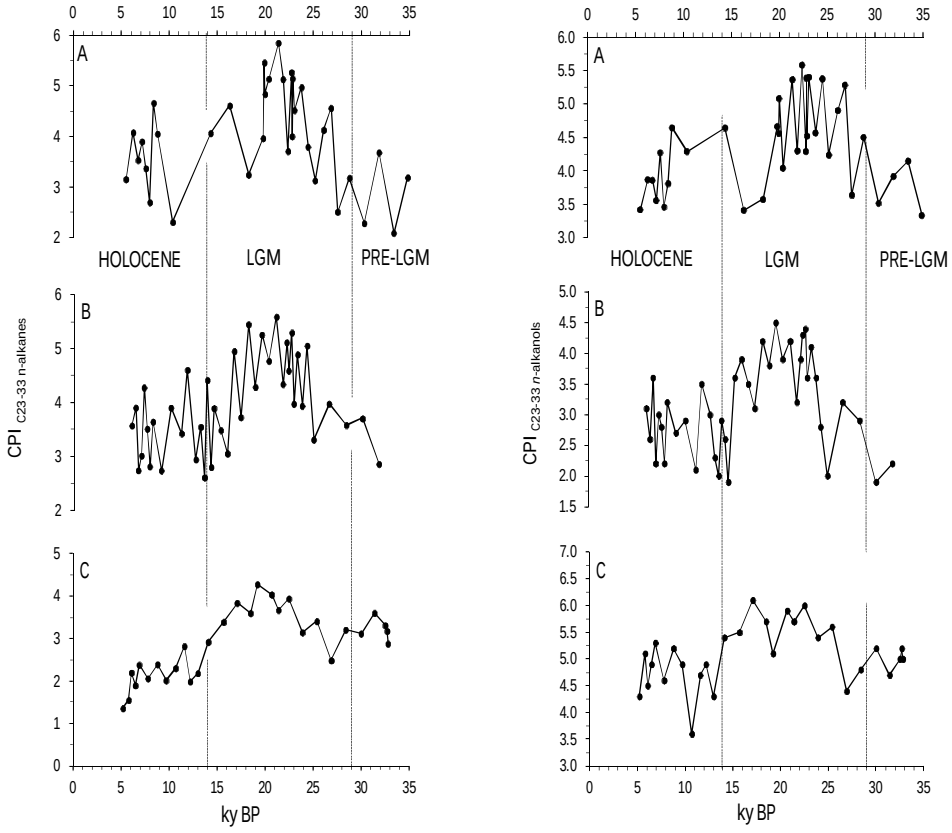

Figure 24. Time-series of Carbon Preference Index (CPI) of C_{23-33} *n*-alkanes and C_{22-32} *n*-alkanols in the sediment cores (A) BP3/GCR1, (B) BP3/GCR2 and (C) CC2/GCEq2. The area within the vertical lines indicate the Last Glacial Maximum (LGM)

As both these regions come under nearly similar seasonally reversing monsoon climate forcing, a similar enrichment of terrestrial-OM is rather expected during the LGM due to intensified and prolonged winter monsoons blowing over Indian Subcontinent towards surrounding marine environment delivering soil-carbon.

To further substantiate this, the carbon preference index (CPI) was calculated. The CPI is a well established proxy for determining the sources of OM. The calculation of CPI is given in Chapter 3, Section 3.7. The basis of CPI is that different sources of lipids exhibit different patterns of carbon predominance either toward even carbon number molecules or odd carbon number molecules, hence, exhibit distinct CPI values. In case of terrestrial plants (terrestrial-OM), the characteristic pattern of HMW *n*-alkanes is the strong odd carbon number predominance (C_{23}, C_{25}, C_{27}, C_{29}, C_{31} and C_{33}) and for n-alkanols, it is even carbon number predominance (C_{22}, C_{24}, C_{26}, C_{28}, C_{30} and C_{32}) (Brassell et al., 1978; Clark and Blumer., 1967; Cranwell and Volkman, 1981; Baker, 1982; Rieley et al., 1991; Bianchi, 1995;Pearson and Eglington, 2000). The CPI of marine lipids is close to 1 (Simoneit, 1984, Hayakawa et al., 1996) and that of terrestrial plant lipids can be up to 20 (Xie et al., 2003; Duan, 2000). The temporal variation of CPI of $C_{23\text{-}33}$ *n*-alkanes and $C_{22\text{-}32}$ *n*-alkanols is given in Figure 25.

In the EAS, the average CPI of *n*-alkanes and *n*-alkanols are ~4.7 during the LGM and ~3.8 during Holocene (Table 17, Figure 22). Similarly, in EIO, the average CPI of *n*-alkanes and *n*-alkanols is ~3.7 during the LGM and ~2.0 during the Holocene (Table 17, Figure 22). The CPI of purely marine lipids is close to 1 (Simoneit, 1984, Hayakawa et al., 1996) and that of terrestrial plant lipids can be up

to 20 (Xie et al., 2003; Duan, 2000). At the outset, the obtained CPI of ~2 during the Holocene suggests that the marine-carbon dominates the total sedimentary carbon in the study region. The higher CPI of ~4 in both EAS and EIO during the LGM as compared to the Holocene (Table 18; Figure 25) clearly indicates that the terrestrial-carbon input to the study region was relatively higher during the former period than during the Holocene. Based on CPI, the approximate portion of the terrestrial carbon during the LGM was ~25 % of the total, while it was 10-15 % during the Holocene.

The only feasible source for terrestrial (or soil) carbon to the Northern Indian Ocean is the Indian Subcontinent. If there is any increase in this soil-carbon input to the EAS or EIO, it must have been the result of intensification of winter monsoon winds which blow from continent towards surrounding seas (Van Campo et al., 1982; Rostek et al., 1997; Banakar et al., 2005, 2010). The higher CPI during the LGM, therefore, clearly suggests that the LGM winters were intense and prolonged than during the Holocene, in line with the behaviour of other sedimentary organic components in the studied region.

5.7. Average chain length (ACL) of lipids: indicator of C3- and C4-terrestrial organic matter

The dominance of either terrestrial C3-Type or C4-Type plant biomass in marine sediment indicate distinct climatic condition as described in section 5.6. (i.e, C4-Type flourishes during dry and cold environment and C3-Type during wet and warm environment). Studies have shown that the changes in ACL occur mainly depending on the humidity in the atmosphere. The cold glacial condition atmosphere was dry, whereas, the warm interglacial atmosphere was with very high humidity. Therefore, the ACL of sedimentary lipids holds the clue about the local climatic conditions that prevailed on the land (Gagosian et al., 1986; Poynter et al., 1989;

Rommerskirchen et al., 2006). The calculation of ACL is provided in Chapter 3, Section 3.10. It is evident from the equation that the variation in ACL is caused by the dominance of C_{29} and C_{31} in C3-Type and by C_{31} and C_{33} in C4-Type. Similarly, the variation in ACL of *n*-alkanols is caused by the dominance of C_{28} and C_{30} in C3 plants and by C_{30} and C_{32} in C4 plants.

The *n*-alkanes and *n*–alkanols of C3-type vegetation exhibits shorter ACL, whereas, in C4-type vegetation with longer-ACL (Rommerskirchen et al., 2006; Horikawa et al., 2010; Zhou et al., 2010; Andersson et al., 2011; Vogts et al., 2009). Although the difference is small, the variation in ACL at decimal level can provide information about the type of photosynthetic pathway the respective plant has followed. High ACL is essentially due to the prominence of C_{31} and C_{33} *n*-alkanes, which are commonly produced by C4- plants and the lower ACL values are due to the prominence of C_{29} and C_{31} commonly produced by the C3- plants (Cranwell, 1973; Rommerskirchen et al., 2006; Vogts et al., 2009) as mentioned in the above paragraph.

In the present study, the average ACL of *n*-alkanes and *n*-alkanols in the EAS and EIO are ~28 during the LGM as compared to ~27 during the Holocene (Table 18). The temporal variation of ACL in the EAS and EIO is given in Figure 25.

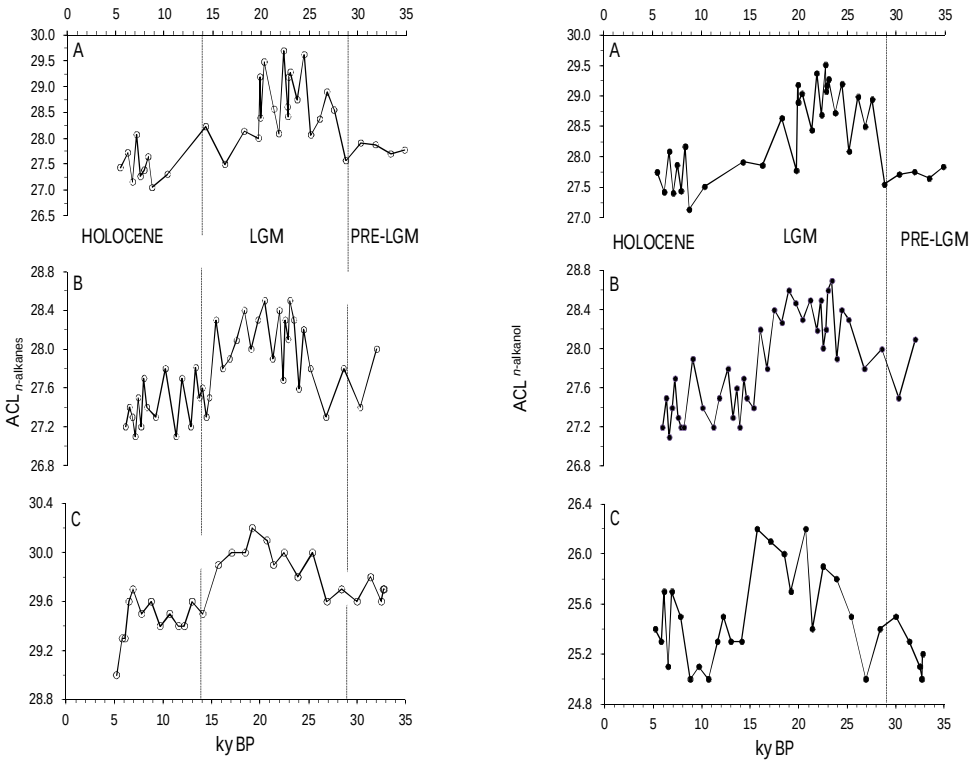

Figure 25. Time-series of Average Chain Length of C_{23-33} *n*-alkanes and C_{22-32} *n*-alkanols in the sediment cores (A) BP3/GCR1, (B) BP3/GCR2 and (C) CC2/GCEq2. Vertical lines indicate the oxygen isotope boundaries

The dominance of longer ACL during the LGM thus, indicates the dry and cold conditions than during the Holocene. This observation is in contrast with the suggestion of Poynter et al. (1989) that plants produce longer chain compounds in warmer climates, but is consistent with the results of ODP Leg 175 sediments retrieved from Eastern Atlantic (Schefuss et al., 2001) www.odp.tamu.edu/publications), wherein, the longer ACL is recorded in sediments of colder southern region as compared to warmer northern region. The southern Atlantic receives mostly C4 dominant terrestrial lipids as compared to the northern Atlantic. This further explains that the cold and dry conditions favour C4 type photosynthetic pathway.

The distinctly longer ACL (~28) during the LGM as compared to shorter ACL (~27) (Table 18; Figure 26) suggests that the Indian subcontinent was dominated by C4- type vegetation during the cold and dry LGM climate that subsequently switched over to C3 Type during the Holocene. The dominance of C4-type vegetation during the LGM as suggested by the ACL supplements the observation from $\delta^{13}C_{org}$, and binary- and ternary mixing diagrams for all the three sediment cores. Thus, it is clear that, the soil-carbon input to the northern Indian Ocean was considerably higher during the LGM, that too dominated by the carbon produced by the C4 vegetation characteristic of dry and cold climate. An independent study (Galy et al., 2008) demonstrated the dominance of C4 plant derived carbon in Bengal Fan sediment during the LGM, which was replaced by C3 type terrestrial plant carbon during the Holocene in Indo-Gangetic flood plains. The dominance of C4 during the LGM and and C3 during the Holocene in peats of Niligiri Hills (Southern India) (Sukumar et al., 1995; Rajagopalan et al., 1997) are the clear indication for the climate dependent photosynthetic pathway shift. The soil-carbon input dominated by the C4-type carbon during the LGM sediment of EAS and EIO indicate that the winter monsoons (Northeasterly Wind Regime) were stronger than the Holocene Period. As the summer monsoons of the LGM might have rendered the associated rains and rivers to weaken. This LGM drainage scenario leaves the winds from Land-towards-Sea as the most likely agent to transport soil-carbon to the northern Indian Ocean.

5.9. Marine lipid biomarkers: Productivity variation

Certain lipid biomarkers are organism specific. The phytol and brassicasterol are two such compounds, which are specific to total marine primary productivity (total marine carbon production) and diatom production (carbon produced only by diatoms), respectively (Harris et al., 1996; Ishiwatari et al., 1999; Tolosa et al., 2003). The major sources of phytol in marine sediments are enzymatic hydrolysis of chlorophyll-a during zooplankton grazing, phytoplanktonic senescence and early degradation of chlorophyll-*a* in marine sediments (Didyk et al., 1978; Wakeham et al., 2002; Rontani and Volkman, 2003). Therefore, the sedimentary-phytol in essence represents the chlorophyll-a (primary production). The brassicasterol, on the other hand, constitutes about 90% of the total sterols present in diatoms. Therefore, it is synonymous as a biomarker for diatoms (Volkman, 1986, Schubert et al., 1998; Volkman et al., 1998; Ishiwatari et al., 2005). The phytol and brassicasterol have been used in many palaeoproductivity studies and these studies have shown that these two compounds faithfully reflect the total primary productivity and diatom production respectively, over glacial-interglacial timescales (Schubert et al., 1998; Schulte et al., 1999; Ternois et al., 2001; Ishiwatari et al., 2005; Knies, 2005; Kurian et al., 2009). The temporal variation of surface productivity and diatoms in the Sea of Okhostk (Northwast Pacific) through the last 27 Ky BP based on phytol and brasicasterol respectively (Ternois et al., 2001) is given in Figure 26.

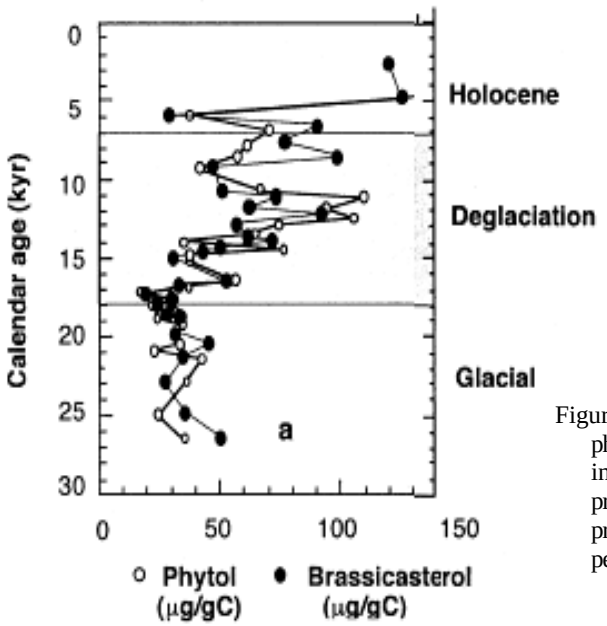

Figure 27. Time-series of phytol and brassicasterol indicating total primary productivity and diatom production respectively as per Ternois et al., 2001.

The climate averaged concentrations of phytol and brassicasterol in LGM- and Holocene-sediments of the EAS (GCR1 and GCR2) and EIO (GCEq2) are given in Table 19.

Table 19. Climate averaged distribution of marine lipid biomarkers in studied sediment cores

Sediment Core	Period KyBP	Phytol ng/g	Brassicasterol ng/g
BP3/GCR1	Holocene	30	28
	LGM	73	61
BP3/GCR2	Holocene	26	18
	LGM	69	33
CC2/GCEq2	Holocene	1.9	1.9
	LGM	5.8	4.9

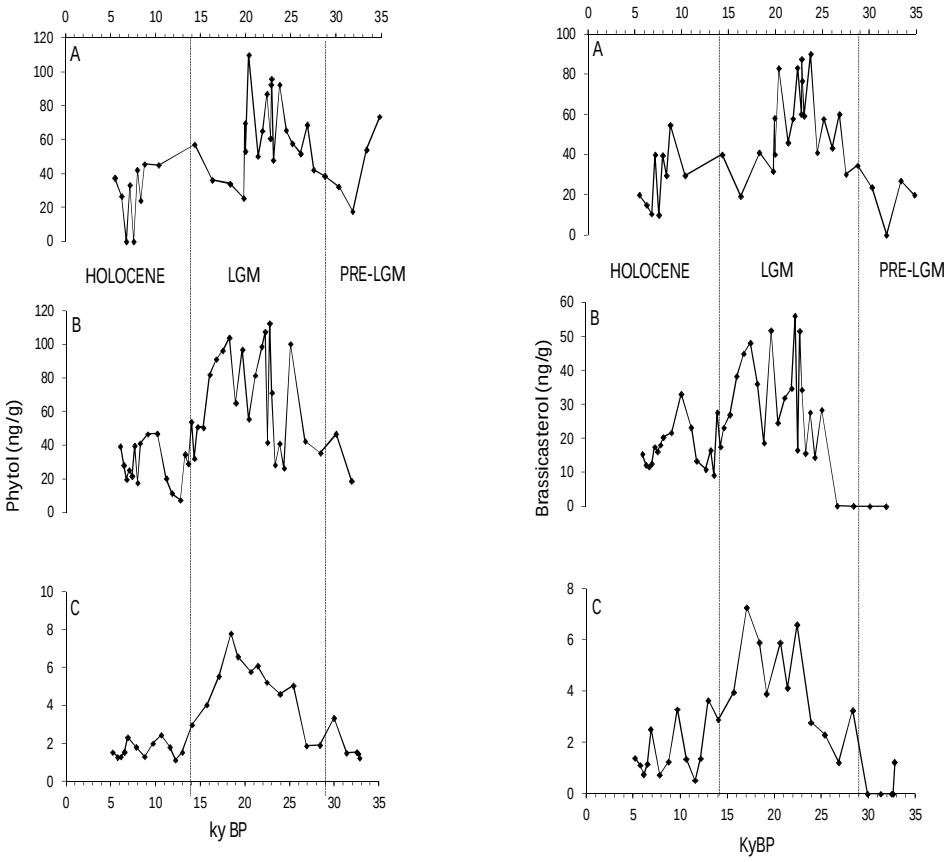

Figure 27. Time-series of phytol and brassicasterol in sediment core (A) BP3/GCR1, (B) BP3/GCR2 and (C) CC2/GCEq2. The area within the vertical lines indicate the Last Glacial Maximum (LGM)

In the EAS, the average concentrations of phytol and brassicasterol during the LGM are higher (~70 ng/g and 47 ng/g, respectively) than the Holocene (~28 ng/g and 23 ng/g, respectively). In the EIO also, the average concentrations of these compounds are higher (~ 6 and 5 ng/g, respectively) as compared to the Holocene (~ 2 ng/g). It means that the phytol and brasicasterol input to the LGM sediments was higher by a factor of two as compared to the Holocene (Figure 28). Further, distinctly higher concentration of these compounds in the EAS as compared to the

EIO in both climate extremes suggests that the former region is perennially productive, while the latter has remained oligotrophic as found in the present. The enhanced input of phytol and brasicasterol in the northern Indian Ocean (EAS and EIO) during the LGM indicates that primary productivity in general, and diatom production in particular, was higher when the climatic conditions were cold and dry, which gradually reduced during the wet and warm conditions of the Holocene. It is noteworthy here that, the winter monsoon season in the Arabian Sea recorded higher opal production than during the summer monsoons as recorded by the sediment traps (Haake et al., 1993). This modern observation suggests that the LGM winters might have been very intense and prolonged so that the diatom (brasicasterol) production had reached optimal levels and that the major portion of sedimentary phytol must have been derived from diatoms.

5.10. Factors influencing the past productivity variation

Modern studies in the Arabian Sea have indicated that a decrease of 1˚C in SST can cause enhanced convection and vertical mixing which results in significantly higher biological productivity (Shetye et al., 1991). Palaeoclimate studies from the tropical Indian Ocean suggested, based on Mg/Ca and $U^{k'}_{37}$ SST reconstructions, that the LGM SSTs were colder by about 1.5 - 2.5˚C than the Holocene (Sonzogni et al., 1998; Saraswat et al., 2005; Banakar et al., 2010). A 1ºC SST cooling in the northern Arabian Sea during the winter monsoons would result in deepening of convective mixing causing the entrainment of nutrient in the upper thermocline to reach the surface layer (Madhuparatap et al., 1996). This process instantly enhances the productivity in the Arabian Sea. This scenario might have

been expressed much stronger during the LGM, because LGM winters have been shown to be intense and longer than the winters of the Holocene (or Present Day). Therefore, the intensified deep convective winter mixing during the LGM, most likely, is the cause of increased productivity in the EAS.

The sea surface salinity in the Arabian Sea is influenced by the E-P budget. The modern measurements have shown that E-P is negative during summer monsoons indicating higher precipitation, while during winter monsoons, it is positive (Lius and Kawamura, 2004 and references therein). Several studies utilizing different proxies have suggested weakened summer monsoons and intensified winter monsoons during the LGM (Prell et al., 1980; Cullen, 1981; Duplessy, 1982; Van Campo, 1986; Banakar et al., 2005) resulting in enhanced salinity in the Arabian Sea by ~1.5 psu as compared to the Holocene. Palaeoclimate studies have further suggested that there was a reduction in the inflow of low salinity waters from the BoB into the EAS during the LGM (Cayre and Bard, 1999; Banakar et al., 2005). This reduction in BoB water inflow can be attributed to the weakening of LGM summer monsoons, because, surface salinity of the BoB is totally dependent on the summer monsoon related freshening of the bay. Another factor that affects E-P is the process of evaporation. The low humidity during winter monsoons enhances surface evaporation in the Arabian Sea, which eventually increases surface salinity (Wiggert et al., 2000 and references therein). The intensification of dry and cold winter monsoons during the LGM thus would have enhanced surface evaporation, and in turn, the surface salinity. These factors together might have caused a significant increase in the surface salinity in the Arabian Sea and enhanced the convective mixing which, in turn, increased the productivity during the LGM.

The above climatological set up however, cannot explain the increased productivity during LGM in the EIO. A study has attributed the high productivity during the glacial period to nutrient injection into the photic layer caused by deepening of mixed layer due to intensified winter monsoon winds (Rostek et al., 1997). This glacial high productivity in the EIO exhibited precession cycle (~23 ky) (Beaufort et al., 1997; Rostek et al., 1997; Cayre et al., 1999; Pailler et al., 2002).

Whether, intensified winter winds alone could have driven the recorded increased productivity in the otherwise oligotrophic EIO during the glacial times is an open question, because, presently the maximum wind speed in the EIO is evident during the inter-monsoon periods (spring and fall) unlike the rest of the northern Indian Ocean. These intense wind bursts are wellknown as Wyrtki Jets (Westerly Jets: WJ). The WJs are expected to be more intense during the cold and dry glacial times as the Inter Tropical Convergence Zone (ITCZ) is normally limited to just north of the equator, unlike its further northward migration (up to 30^{o}N latitude) during warm and wet inter-glacial time. When this ITCZ is located around the equator during the spring and fall (inter-monsoon periods), strong WJs are generated (Senan et al., 2003), causing intense divergence along the equator. The WJs are active between 2˚N and 2˚S latitudes and 65 and 85˚E longitudes (Wyrtki, 1973, Joesph et al., 2012). The WJs cause the thermocline to shoal up on either side of the equator in the western-EIO and deepen the thermocline in the eastern-EIO (Figure 28).

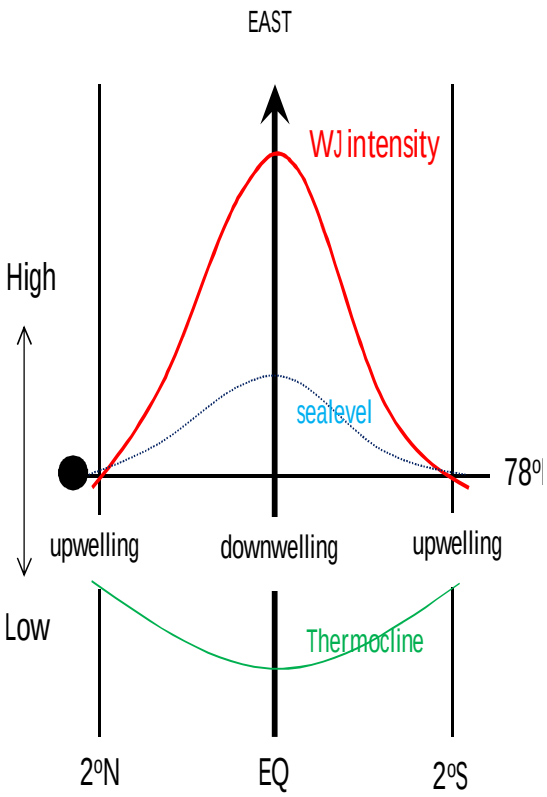

Figure 28. Highly simplified schematic sketch showing the dynamics of the Wyrtki Jets (WJ) between 2 ˚N and S in the in the Equatorial Indian Ocean (EIO). The filled circle along 78˚E is the location of the sediment core CC2/GCEq2. The arrow along the equator represents the eastward propagating WJ. The red curve represents the WJ intensity. The dotted blue curve represents the sea level rise in the along the equator. The green curve represents the lowering of thermocline along the equator. The eastward propagating WJ have their highest energy along the equator and decay outwards. This should result in convergence (thermocline deepening; downwelling) and high sea level along its propagation (Equator), while divergence (thermocline shoaling; upwelling) and lowering of sea level along its periphery.

This is because the WJs transport surface waters from west towards east resulting in a rise in sea-level in the eastern-EIO and drop in sea-level in the western-EIO (Schott and McCreary Jr., 2001). Further, due to the divergence of surface waters at the periphery of the equator at ~2˚ N and S, intense upwelling occurs and the upwelled nutrients advect all along the equator resulting in productivity increase. This is clearly depicted by the modern seasonal distribution of chlorophyll-a in the EIO, wherein, enhanced productivity is evident during WJ activity (Figure 29).

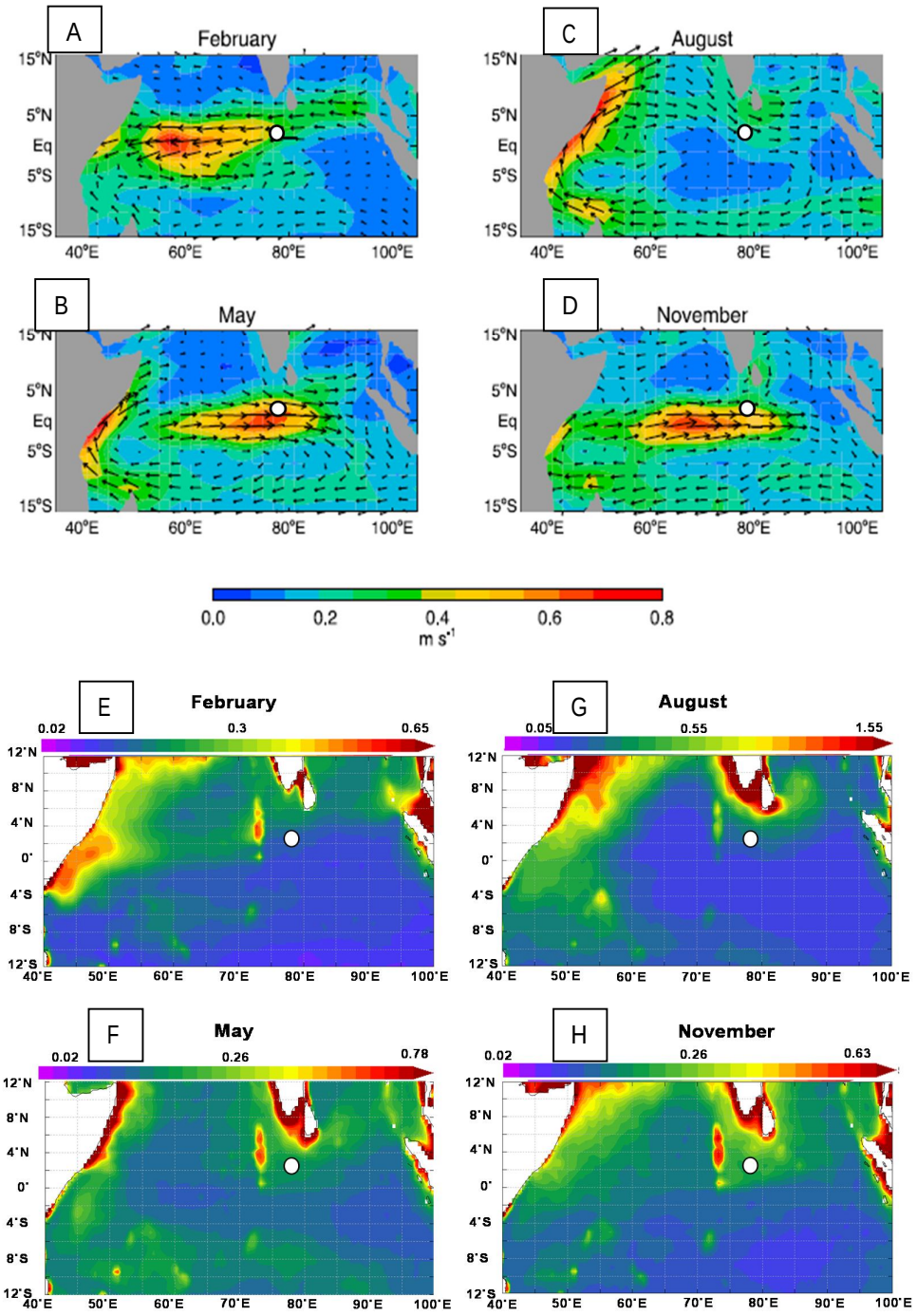

Figure 29. Climatology of the Equatorial Indian Ocean: A (February; winter monsoon); B (May; spring inter-monsoon), C (August; summer monsoon) and D (November; fall inter-monsoon). The Wyrtki Jet activity is seen during May (B) and November (D) (*source*: Nagura and McPhaden, 2010). The chlorophyll-a distribution of the corresponding months is given in E, F, G and H. Higher chlorophyll-a concentration is seen during the inter-monsoon months of May (F) and November (H) (*source*: SeaWiFS image, http://las.northern_Indian_Ocean.org). The white circle is the location of CC2/GCEq2 sediment core

Therefore, in addition to the winter wind driven nutrient injection, the WJ driven equatorial upwelling might have been a major cause of significantly increased productivity in the EIO during the LGM (Punyu et al., 2014). Beaufort et al., (1997) and Cayre et al., (1999) also suggested the possibility of intensification of equatorial westerly wind regime forcing the increased equatorial productivity during the last few glacial cycles. A recent modelling study (Liu et al., 2007) has shown intensification of equatorial westerly winds during the LGM causing shoaling of thermocline in central-western Indian Ocean forcing a negative IOD events having ~15% enhanced amplitude and increased frequency than the Present.

Thus, the increased LGM productivity in the EIO might have been caused by a combination of internally connected a) intense shoaling of thermocline in the central-western Indian Ocean due to intensified WJs along with enhanced negative IOD events and b) intensification of winter monsoons as evident from the increased input of terrestrial OM (Punyu et al., 2014).

5.11. Glacial-interglacial variation of lipids vis-a-vis atmospheric CO_2

Ice core studies have shown that atmospheric CO_2 concentrations have varied in accordance with the glacial-interglacial climates (Barnola et al., 1987; Petit et al., 1999). The Holocene atmospheric CO_2 concentration is ~ 280 ppmv, while it was ~190 ppmv during the LGM (Barnola et al., 1987; Sigman and Boyle, 2000). It is estimated that deep oceans hold nearly 37000 Gt of C (≈137000 Gt of CO_2), which potentially is 50 times more than that stored in the atmosphere 800 Gt of C (≈2960 Gt of CO_2); as much as ~20 times the C stored as humic substance in terrestrial soils 2300 Gt C (≈8500 Gt CO_2 as soil-carbon) and ~40 times the C stored in surface

ocean 1000 Gt C (≈3700 Gt of CO_2) (Ittekot, 1993; Falkowski et al., 2000; Sigman and Haug, 2003). The reactive sediments of the seafloor contain ~6000 Gt of buried C (≈22000 Gt of CO_2) which is not available for the exchange in C-cycle on long-term basis. Rest of the the reservoirs keep exchanging the C between themselves. Therefore, the amount of C (C_{org} and $C_{inorganic}$ or biogenic $CaCO_3$) that is transported to the seafloor and ultimately gets buried actually determines the long-term climatic condition of the planet Earth. That is, if the burial of C is more, it means the C removed from the atmosphere is more. In turn, this leads to reduction in the amount of greenhouse gas in the atmosphere resulting in cooling. Thus, the export production plays a vital role in regulating the glacial-interglacial climatic conditions. Several studies have shown that nearly 200 Gt (~740 Gt CO_2) of atmospheric-C per year is removed through photosynthesis (both terrestrial and marine in mostly equal proportion). But, a major portion of this returns back to the atmosphere due to respiration and dissolution of carbonate skeletons. Only a small fraction of the photosynthetic-C actually becomes part of the marine sediment or the soil, which must have resulted in nearly 100 ppmv of CO_2 reduction of atomospheric-CO_2 during the Glacial Climate: (see Falkowski et al., 2000; Sigman and Boyle, 2003). In other words, the glacial marine productivity must have been higher than the interglacial productivity on a global scale. Interestingly, the phytol (a robust marine productivity indicator) in the present study shows coherent variation with the $\delta^{18}O_{planktic\ foraminifera}$ (Figure 30).

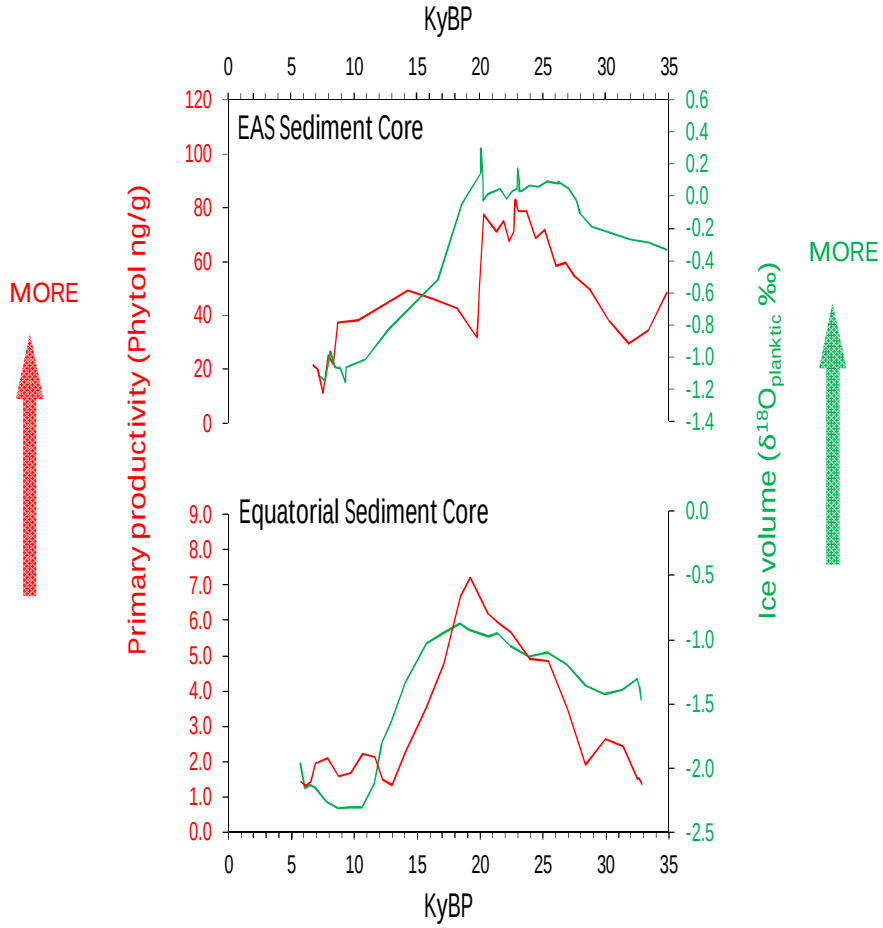

Figure 30. Variation in primary productivity (phytol) vis-à-vis global ice volume represented by $\delta^{18}O$ in the northern Indian Ocean

Although, the $\delta^{18}O_{planktic\ foraminifera}$ time-series presented here contain local monsoon variation related (local surface salinity and SST) gradient between LGM and Holocene, the overall variation is dictated by the ice-volume. Therefore, the phytol coherent behaviour with the $\delta^{18}O_{planktic\ foraminifera}$ clearly suggests that the marine productivity in the study region was, in fact, higher during the cold-LGM as compared to the warm- Holocene. This increase in marine productivity in the northern Indian Ocean possibly has contributed to the draw-down of the atmospheric CO_2 during the glacial climate. Thus, the present study provides an important clue about the role of tropical oceans in regulating CO_2 on glacial-interglacial climate

cycle, which needs to be further investigated. The LGM productivity increase by a factor of 2 as compared to the Holocene depicted by the lipids in the present study (Table 19) further signifies an increase in the burial of photosynthetic-C in the northern Indian Ocean sediment, which might have provided an important positive feedback for the LGM- carbon cycle.

CHAPTER 5

CONCLUSION

The salient observations from the present study are presented below.

- The reconstruction of paleoproductivity for the northern Indian Ocean clearly brings-out its relationship with past climate dynamics.
- The higher C_{org} and lipid contents in EAS than in EIO indicate regional difference in the productivity and also input of terrestrial-OM.
- The marine organic matter dominates in the sediment of the northern Indian Ocean (70 % to 99 %). The terrestrial organic matter constitutes a minor component and is composed of a mixture of C3- and C4-Type plant debris. The terrestrial-organic matter of C-4 nature increased during the LGM indicating that the LGM summer monsoon rains were significantly weaker and the dry winter monsoons became stronger.
- The northern Indian Ocean exhibited enhanced productivity (represented by phytol) during the LGM. The diatom production (brassicasterol) also increased during this period. The increase of marine productivity during the LGM was nearly by a factor of ~2. The enhanced diatom (opal) production during LGM further supports intensification of dry winters.
- The increased LGM-productivity in EIO could be associated with intensification of inter-monsoon equatorial westerly jets (also known as Wyrtki Jets). Where as, the increased LGM-productivity in the EAS supports previous interpretations which have linked increased entrainment of deep nutrient to photic zone due to intensification of winter-convection.
- The increase in marine productivity in the northern Indian Ocean during the LGM is likely to have contributed to the drawdown of atmospheric CO_2

which provides an important clue about the role of tropical oceans in regulating the atmospheric CO_2 on Glacial-Interglacial time-scales.

Thus, the sedimentary lipid biomarkers from the northern Indian Ocean clearly brought-out a relationship that the intensification of the LGM-winters have not only caused the marine productivity to increase, but also transported increased amount of C-4 type soil-organic matter to the adjacent seas. This process in turn helped in burial of increased amount of CO_2 in the marine sediment as organic matter during the LGM.

BIBLIOGRAPHY

Adhémar, J. A., 1842. Révolutions de la Mer: Déluges Périodiques, *Carilian-Goeury et V. Dalmont, Paris.*

Agnihotri, R., Sarin, M., Somayajulu, B. L. K., Jull, A. J. T., Burr, and G. S., 2003. Late-Quaternary biogenic productivity and organic carbon deposition in the eastern Arabian Sea. *Palaeogeography, Palaeoclimatology, Palaeoecology*, **197**(1): 43-60.

Almogi-Labin, A., Schmiedl, G., Hemleben, C., Siman-Tov, R., Segl, M., and Meischner, D.,et al., 2000. The influence of the NE winter monsoon on productivity changes in the Gulf of Aden, NW Arabian Sea, during the last 530ka as recorded by foraminifera. *Marine Micropaleontology*, **40**(3): 295-319.

Andersson, R. A., Kuhry, P., Meyers, P., Zebühr, Y., Crill, P., and Mörth, M., 2011. Impacts of paleohydrological changes on n-alkane biomarker compositions of a Holocene peat sequence in the eastern European Russian Arctic. *Organic Geochemistry*, **42**: 1065–1075

Baker, E.A., 1982. Chemistry and morphology of plant epicuticular waxes. In: *The Plant Cuticle*, Cutlet, D.F., Alvin, K.L., and Price, C.E., (Eds.), Linnean Society Symposium Series, Vol. 10, London. pp. 139-165

Banakar, V. K., Pattan, J. M., and Mudholkar, A. V., 1991. Abyssal sediment erosion in the Central Indian Basin: Evidence from radiochemical and radiolarian studies. *Marine Geology*, **96**(1): 167-173

Banakar, V. K, Nair, R. R., Tarkian, M., and Haake, B., 1993. Neogene oceanographic variations recorded in manganese nodules from the Somali Basin. *Marine Geology*, **110**(3): 393-402.

Banakar, V. K., Galy, A., Sukumaran, N. P., Parthiban, G., and Volvaikar, A. Y., 2003. Himalayan sedimentary pulses recorded by silicate detritus within a ferromanganese crust from Central Indian Ocean. *Earth and Planetary Science Letters*, **205**: 337–348.

Banakar, V. K., Oba, T., Chodankar, A. R., Kuramoto, T., Yamamoto, M., and Minagawa, M., 2005. Monsoon related changes in sea surface productivity and water column denitrification in the Eastern Arabian Sea during the last glacial cycle. *Marine Geology*, **219**: 99-108

Banakar., V. K., Mahesh, B. S., Burr, G., and Chodankar, A. R., 2010. Climatology of the Eastern Arabian Sea during the last glacial cycle reconstructed from paired measurement of foraminiferal δ18O and Mg/Ca. *Quaternary Research*, **73**, 535–540

Balch, W. M., Drapeau, D. T., and Fritz, J. J., 2000. Monsoonal forcing of calcification in the Arabian Sea. *Deep Sea Research II*, **47**: 1301-1337

Banse, K., and McClain, C. R., 1986. Winter blooms of phytoplankton in the Arabian Sea as observed by the Coastal Zone Color Scanner. *Marine Ecology Progress Series*, **34**: 201-211.

Banse, K., 1987. Seasonality of phytoplankton chlorophyll in the central and northern Arabian Sea. *Deep Sea Research*, **34** (5/6): 713-723

Barber, R. T., Marra, J., Bidigare, R. C., Codispoti, L. A., Halpern, D., Johnson, Z., Latasa, M., Goericke, R., and Smith, S. L., 2001. Primary productivity in

its regulation in the Arabian Sea during 1995. *Deep Sea Research*, **48**: 1127-1172

Barnola, J. M., Raynaud, D., Korotkevich, Y. S., and Lorius, C.,1987. Vostok ice core provides 160,000- year record of atmospheric CO_2. Nature, 329 :408-414

Bassinot, F. C., Labeyrie, L. D., Vincent, E., Quidelleur, X., Shackleton, N. J., and Lancelot, Y., 1994. The astronomical theory of climate and the age of the Brunhes-Matuyama magnetic reversal. *Earth and Planetary Science Letters*, **126**(1): 91-108

Beaufort, L., Lancelot, Y., Camberlin, P., Cayre, O., Vincent, E., Bassinot, F., and Labeyrie, L., 1997. Insolation cycles as a major control of Equatorial Indian Ocean Primary Production. *Science*, **278**: 1451-1454

Berner, R. A., Lasaga, A.C., and Garrels, R. M., 1983. The carbon-silicate geochemical cycle and its effect on atmospheric carbon dioxide over the past 100 million years. *American Journal of Science*, **283**: 641-683

Berner, R. A., 1994. GEOCARD II: A revised model for atmospheric CO_2 over Phanerozoic time. *American Journal of Science*, **294**:56-91

Bhattathiri, P. M. A., Pant, A., Sawant, Surekha, Gauns, M., Matondkar, S. G. P., and Mohanraju, R.,1996. Phytoplankton production and chlorophyll distribution in the eastern and central Arabian Sea in 1994-1995. *Current Science*, **71** (11): 857-862

Bianchi, G., 1995. Plant waxes. In: *Chemistry, Molecular Biology and Functions*, Hamilton, R.J. (Ed.). The Oil Press, Dundee, pp. 175-222.

Bindler, R., Renberg, I., and Klaminder, J., 2008. Bridging the gap between ancient metal pollution and contemporary biogeochemistry. *Journal of Paleolimnology*, **40**(3): 755-770.

Bligh, E. G., and Dyer, W. J., 1959. A rapid method of total lipid extraction and purification. Canadian Journal of Biochemistry and Physiology 37, 911-917

Bloor, W. R., 1943. In: *Biochemistry of the fatty acids and their compounds, the lipids*. Reinhold Publishing Corporation, Princeton. New Jersey

Boom, A., Marchant, R., Hooghiemstra, and Damste, J. S. S., 2002. CO_2 and temperature-controlled altitudinal shifts of C 4-and C 3-dominated grasslands allow reconstruction of palaeoatmospheric pCO_2. *Palaeogeography, Palaeoclimatology, Palaeoecology*, **177**(1-2): 151-168.

Boon, J. J., Rijpstra, W. I. C., deLange, F., de Leeuw, J. W., Yoshioka, M., and Shimizu, Y., 1979. Black Sea sterol- a molecular fossil for dinoflagellate blooms. *Nature*, **277**: 125-127

Boyd, P.W., Watson, A.J., Cliff, S.L., Edward, E.R., Trull, T., Murdoch, R., et al., 2000. *Nature*, **407**:695-702

Boyle, E.A., and Keigwin, L.D., 1982. Deep circulation of the North Atlantic over the last 200,000 years: Geochemical evidence. *Science*, **218**: 784-787

Bradley, R. S., 1991. In: *Paleoclimatology: Reconstructing Climates of the Quaternary,* Second Edition. Academic Press, United States of America

Brassell, S. C., Eglinton, G., Maxwell, J. R., and Philp, R. P., 1978. Natural background of alkanes in the aquatic environment. In: *Aquatic Pollutants: Transformation and Biological Effects*. Permagon Press, pp 69-86

Brassell, S.C., Brereton, R.G., Eglinton, G., Grimalt, J., Liebezeit, G., Marlowe, T., Pflaumann, U., and Sarnthein, M., 1986. Palaeoclimatic signals recognized by chemometric treatment of molecular stratigraphic data. *Organic Chemistry* **10**: 649-660.

Brassell, S. C., 1993. Applications of biomarkers for delineating marine paleoclimatic fluctutations during the Pleistocene. In: *Organic Geochemistry: Principles and Applcations. Plenum*, Engel, M. H., Macko, S. A., (Eds.) New York, pp. 699-738

Bray, E. E., and Evans, E. D., 1961. Distribution of n-paraffins as a clue to recognition of source beds. *Geochimica et Cosmochimica Acta*, **22**: 2-15.

Brink, K., Arnone, R., Coble, P., Flagg, C., Jones, B., Kindle, J., Lee, C., Phinney, D., Wood, M., Yentsch, C., Young, D., 1998. Monsoons boost biological productivity in Arabian Sea. *EOS, Transactions American Geophysical Unorthern Indian Oceann*: **79** (13): 165-172

Brock, J. C., McLain, C. R., Anderson, D. M., Prell, W. L., and Hay, W. W., 1992. Southwest monsoon circulation and environments of Recent planktonic foraminifera in the north-western Arabian Sea. *Paleoceanography*, **7**: 799–813

Brocker, W. S., 1982a. Glacial to interglacial changes in ocean chemistry. *Progress in Oceanography*,**11**: 151- 197

Broecker, W. S., 1982b. Ocean chemistry during glacial time. *Geochimica et Cosmochimica Acta*, **46**: 1689-1705

Canfield, D. E. 1994. Factors influencing organic carbon preservation in marine sediments. *Chemical Geology*, **114**(3): 315-329

Cayre, O., and Bard, E., 1999. Planktonic foraminiferal and alkenone records of the Last Deglaciation from the Eastern Arabian Sea. *Quaternary Research*, **52**: 337-342

Cayre, O., Beaufort, L., and Vincent, E., 1999. Paleoproductivity in the Equatorial Indian Ocean for the last 260,000 yr: a transfer function based on planktonic foraminifera. *Quaternary Science Reviews*, **18**(6): 839-857.

Chen, R. F., Jiang, Y., and Zhao, M., 2000. Solid-phase fluorescence determination of chlorins in marine sediments. *Organic Geochemistry*, **31** (12): 1755-1763

Chodankar, A. R., Banakar, V. K., and Oba, T., 2005. Past 100 ky surface salinity gradient response in the Eastern Arabian Sea to the summer monsoon variation recorded by $\delta^{18}O$ of *G.sacculifer*. *Global Planetary Change*, **47**: 135-142

Clark, R. C., and Blumer, M., 1967. Distributions of n-paraffins in marine organisms and sediment. *Limnology and Oceanography*, 12: 79-87

Clemens, S. C., and Prell, W. L., 1991. Late Quaternary Forcing of Indian Ocean Summer –Monsoon Winds: A Comparison of Fourier Model and General Circulation Model Results. *Journal of Geophysical Research*, **96**: 22683-22700

Conkright, M. E., Levitus, S., and Boyer, T. P., 1994. World Ocean Atlas Vol. 1, Nutrients. U.S. Department of Commerce National Oceanic and Atmospheric Administration, Washington D.C. 1994

Cotton, J. M., Sheldon, N. D., and Stromberg, C. A. E., 2012. High resolution isotopic record of C4 photosynthesis in a Miocene grassland. *Palaeogeography, Palaeoclimatology, Palaeoecology*, **337-338**: 88-98.

Cranwell, P. A., 1973. Chain length distribution of *n*-alkanes from lake sedeimnts in relation to post glacial environment change. *Freshwater Biology*, **3**: 259-265

Cranwell, P. and Volkman, J., 1981. Alkyl and steryl esters in a recent lacustrine sediment. *Chemical Geology*, **32**(1): 29-43

Cranwell, P. A., and Volkman, J. K., 1981. Alkyl and steryl esters in recent lacustrine sediment. *Chemical Geology*, **32**: 29-43

Croll, J., 1875. Climate and time in their geological relations. Appleton, New York

Cullen, J. L., 1981. Microfossil evidence for changing salinity patterns in the Bay of Bengal over the last 20 000 years. *Palaeogeography, Palaeoclimatology, Palaeoecology*, **35**: 315-356.

Currie, R. G., Fisher, A. E., Hargreaves, P. M., 1973. Arabian Sea upwelling. In*: The Biology of the Indian Ocean, Zeitschel, B. (ed)*. Springer-Verlag, New York, pp. 57-63.

Dai, A., and Trenberth, K. E., 2002. Estimates of fresh water discharge from continents: Latitudinal and seasonal variations. *Journal of Hydrometeorology*, **3**: 660-687

Danzeglocke, U., Jois, O., and Wenninger, B., 2008. CalPal 2007 online. http://www.calpal-online.de/, 2008-10-05.

Dezileau, L., Ulloa, O., Hebbeln, D., Lamy, F., Reyss, J-L., and Fontugne, M., 2004. Iron control of past productivity in the coastal upwelling system off the Atacama Desert, Chile. *Paleoceanography*, **19**: PA3012, doi:10.1029/2004PA001006

Didyk, B. M., Simoneit, B. R. T., Brassell, S. C., and Eglinton, G., 1978. Geochemical indicators of palaeoenvironmental conditions of sedimentation. *Nature*, **272**: 216-222.

Duan, Y., 2000. Organic geochemistry of recent marine sediments from the Nansha Sea, China. *Organic Geochemistry*, 31: 159-167

Duplessy, J. C., 1982. Glacial to interglacial contrast in the northern Indian Ocean. *Nature*,

Dutt, A. K., and Chatterjee, M., 2005. Bay of Bengal. *Encyclopedia of World Geography*, McColl, R. W., (Ed.). Facts on File Inc. New York), pp. 81-82 **295**: 494–498.

Eddy J. A., 1976. The Maunder Minimum. *Science*, **192:** 1189-1202.

Eglinton, G., and Calvin, M., 1967. Chemical fossils. *Scientific American*, **216**: 32-43

Eglinton, G., and Hamilton, R.J., 1967. Leaf epicuticular waxes. *Science*, **156**: 1322-1335

Ehleringer, J. R. and Cerling, T. E., 2002. C3 and C4 photosynthesis. *Encyclopedia of Global Environmental Change*. The Earth system: biological and ecological dimensions of global environmental change **2**: 186-190.

Emeis, K.-C., Anderson, D. M., Doose, H., Kroon, D., and Schulz-Bu, D., 1995. Sea-surface temperatures and the history of monsoon upwelling in the northwest Arabian Sea during the last 500,000 years. *Quaternary Research*, **43**(3): 355-361

EPICA Community Members, 2006. One to one coupling of glacial climate variability in Greenland and Antarctica. *Nature*, **444**: 195-198.

Falkowski, P., Scholes, R. J., Boyle, E., Canadell, J., Canfield, D., Elser, J., Gruber, N., Hibbard, K., Hogberg, P., Linder, S., Mackenzie, F. T., Moore III, B., Pederson, T., Rosenthal, Y., Seitzinger, S., Smetacek, V., and Steffan, W.,

2000. The global carbon cycle : A test of our knowledge of earth as a system. *Science*, **290** : 291-296

Fahy, E., Subramaniam, S., Brown, H.A., Glass, C.K., Merrill, A.H. Jr., Murphy, R.C., Raetz, C.R., Russell, D.W., Seyama, Y., Shaw, W., et al., 2005. A comprehensive classification system for lipids. *Journal of Lipid Research*, **46**: 839-862.

Fekete, B. M., Vorosmarty, and C. J., Grabs, W., 2002. High resolution fields of global runoff combining observed water balances. *Global Biogeochemical cycles*, **16** (3): doi:10.1029/1999GB001254

Fernandes, V., Rodrigues, V., Ramaiah, N., and Paul, J. T., 2008. Relevance of bacterioplankton abundance and production in the oligotrophic equatorial Indian Ocean. *Aquatic Ecology*, **42** : 511-519

Fieux, M., and Stommel, H., 1976. Historical sea surface temperature in the Arabian Sea. *Annales de l'Institut Oceanographique Paris*, 52: 5-15.

Findlater, J., 1971. mean monthly airflow at low levels over the western Indian Ocean. *Geophysical Memoirs*, **115**: 53

Findlater, J., 1974. The low level, cross equatorial air current of the western Indian Ocean during the northern summer. *Weather*, **29**: 411-416

Gadgil, S., 1988. Recent advances in monsoon research with particular reference to the Indian monsoon. *Australian Meteorological Magazine*, **36**: 193-204

Gadgil, S., 2003. The Indian monsoon and its variability. *Annual Review of Earth and Planetary Sciences*, **31**; 429-467.

Gagosian, R. B., Peltzer, E. T., and Merrill, J. T., 1986. The importance of atmospheric input of terrestrial organic material to deep sea sediments. *Organic Geochemistry*, **10**: 661–669.

Galy, V., Francois, L., France-Lanord, C., Faure, P., Kudrass, H., Palhol, F., and Sing, F., 2008. C4 plants decline in the Himalayan basin since the Last Glacial Maximum. *Quaternary Science Reviews* **27:** 1396– 1409.

Ganapati, P. N., and Raman, A. V., 1973. Pollution in Visakhapatnam harbour. *Current Science*, **42**: 490-492.

Ganeshram, R. S., T. F. Pedersen, S. E. Calvert, and J. W. Murray., 1995. Large changes in oceanic nutrient inventories from glacial to interglacial periods. *Nature*, **376**: 755–758.

Gooday, A. J., Levin, L. A., Aranda da Silva, A., Bett, B. J., Cowie, G. L., Dissard, D., Gage, J. D., Hughes, D. J., Jeffreys, R., Lamont, P. A., Larkina, K. E., Murtya, S. J., Schumacher, S., Whitcraft, C., and Woulds, C., 2009. Faunal responses to oxygen gradients on the Pakistan margin: A comparison of foraminiferans, macrofauna and megafauna. *Deep Sea Research Part II: Topical Studies in Oceanography*, **56**(6): 488-502

Groves, D. G., and Hunt, L. M., 1980. *Ocean World Encyclopedia*. McGraw Hill Book Company, New York

Gurr, M.I., Harwood, J. L., and Frayn, K. N., 2008. In: *Lipid Biochemistry: An Introduction*. Blackwell Publishing Company

Haake, B., Ittekkot, V., Rixen, T., Ramaswamy, V., Nair, R. R., and Curry, W. B., 1993. Seasonality and interannual variability of particle fluxes to the deep Arabian Sea. *Deep Sea Research I*, **40** (7): 1323-1344.

Haiyan, J., Jianfang, C., Huanxin, W., Hongliang, L. I., Weiyan, Z., Jie, X, Youcheng, B., and Kui, W., 2010. Variations in paleoproductivity and the environmental implications over the past six decades in the Changjiang Estaury. *Acta Oceanologica Sinica*, **29** (3): 38-45

Halley, E., 1686. A historical account of the trade winds, amd monsoons, observable in the seas between and near the tropics with an attempt to assign the physical cause of the said winds. *Philosophical Transactions of the Royal Society*, **16**: 153-168.

Harji, R. R., Yvenat, A., and Bhosle, N. B., 2008. Sources of hydrocarbons in sediments of the Mandovi estuary and the Marmugoa harbour, west coast of India. *Environment International*, **34** : 959-965

Harris, P. G., M, Zhao., A, Rosell-Mele., R, Tiedemann., M, Sarnthein., and J. R. Maxwell., 1996. Chlorin accumulation rate as a proxy for Quaternary marine primary productivity. *Nature*, **383**: 63-65

Hayakawa, K., N. Handa, Ikuta N., and Fukuchi, M., 1996. Downward fluxes of fatty acids and hydrocarbons during a phytoplankton bloom in the austral summer in Breid Bay, Antarctica. *Organic Geochemistry*, **24**(5): 511-521

Hedges, J. I., Kiel, R. G., 1995. Sedimentary organic matter preservation: an assessment and speculative synthesis. *Marine Chemistry*, **49**: 81-115

Hedges, J. I., Keil, R.G., and Benner, R., 1997. What happens to terrestrial organic matter in the ocean? *Organic Geochemistry*, **27**: 195–212

Higginson, M. J., Maxwell, J. R., and Altabet, M. A., 2003. Nitrogen isotope and chlorin paleoproductivity records from the Northern South China Sea: remote vs. local forcing of millennial- and orbital-scale variability. *Marine Geology*, **201**(1): 223-250

Hoefs, J., 1996. In: *Stable Isotope Geochemistry*, fourth edition. Springer, Heidelberg pp. 134.

Horikawa, K., Murayama, M., Minagawa, M., Kato, Y., and Sagawa, T., 2010. Latitudinal and downcore (0–750 ka) changes in *n*-alkane chain lengths in the eastern equatorial Pacific. *Quaternary Research*, 73: 573-582

Imbrie, J., Hays, J. D., Martinson, D. G., McIntyre, A., Mix, A. C., Moorley, J. J., Pisias, N. G., Prell, W. L., and Shackleton, N. J., 1984. The orbital theory of Pleistocene climate: support from a revised chronology. In: *Milankvovitch and climate, Part-1* Berger, A. (Ed.). Springer, NY, pp. 269-305

IPCC AR4 SYR., 2007. Core Writing Team; Pachauri, R.K., and Reisinger, A., (Eds.) Climate Change 2007: Synthesis of working groups I, II and III to the Fourth Assessment Report (AR) of the Inter-govermental Panel on Climate Change. Geneva, Switzerland: IPCC. ISBN 92-9169-122-4.

Ishiwatari, R., Yamada, K., Matsumoto, K., Houtatsu, M., and Naraoka, H., 1999. Organic molecular and carbon isotopic records of the Japan Sea over the past 30k yr. *Paleoceanography*, **14**: 260–270

Ishiwatari, R., Yamamoto S., and Uemura, H., 2005. Lipid and lignin/cutin compounds in Lake Baikal sediments over the last 37 kyr: implications for glacial–interglacial palaeoenvironmental change. *Organic Geochemistry*, **36**: 327-347

Ittekot, V., Haake, B., Bartsch, M., Nair, R. R., and Ramaswamy, V., 1992. Organic carbon removal in the sea: The continental connection; In Upwelling Systems:

Evolution since the Early Miocene (ed. C. P. Summerhayes et al.,), 64: 167-176. Geological Society Special Publication, London.

Ittekot, V., 1993. The abiotically driven biological pump in the ocean and short term fluctuations in atmospheric CO_2 contents. *Global and Planetary Change*, **8**: 17-25

Ivanova, E., Schiebel, R., Singh, A. D., Schmiedl, G., Niebler, H-S., and Hemleben, C., 2003. Primary production in the Arabian Sea during the last 135 000 years. *Palaeogeography, Palaeoclimatology, Palaeoecology*, **197**(1): 61-82

Joseph, S., Wallcraft, A. J., Jensen, T. G., Shenoi, S. S. C., and Nayak, S., 2012. Weakening of spring Wyrtki jets in the Indian Ocean during 2006–2011. *Journal of Geophysical Research: Oceans (1978–2012)*, **117**: doi: 10.1029/2011JC007581**117**(C4).

Kabanova, Y. G., 1968. Primary production of the northern part of the Indian Ocean. *Oceanology* (English translation), **8**: 214- 225.

Kallel, N., L. D. Labeyrie, A. Juillet-Leclerc, and J.-C. Duplessy., 1988. A deep hydrological front between intermediate and deep-water masses in the glacial Indian Ocean. *Nature*, 333: 651 – 655

Kantha, L., Rojsiraphisal, and T., Lopez, J., 2008. The north Indian Ocean and its variability as seen in a numerical hindcast of the years 1993-2004. *Progress in Oceanography*, **76**: 111-147.

Karl, D. M., Bidigare, R. R., and Letelier, R. M., 2001. Long-term changes in plankton community structure and productivity in the North Pacific Subtropical Gyre:The domain shift hypothesis. *Deep-Sea Research II*, **48**: 1449-1470

Kaufman., A.J., Jacobsen, S.B., Knoll, and A.H., 1993. The Vendian record of Sr- and C-isotopic variations in sea water: Implications for tectonics and paleoclimate. *Earth and Planetary Science Letters*, **120**: 409-430.

Kelkar, R. R., 2009. In: *Monsoon Prediction.* B S Publications, Hyderabad

Kenneth, J. P., 1982. In: Marine Geology. Prentice-Hall, Englewood Cliffs, NJ, pp. 813

Kenneth, J. P., and Stott, L. D., 1991. Abrupt sea-warming, palaeoceanographic changes and benthic extinctions at the end of the Palaeocene. *Nature*, **353**: 225 - 229

Kirschvink, J. L., 1992. Late Proterozoic low-latitude global glaciation: the Snowball Earth. In: *The Proterozoic Biosphere: A Multidisciplinary Study*, J. W. Schopf., C. Klein., (Eds.). Cambridge University Press, pp. 51-52

Knies, J., 2005. Climate-induced changes in sedimentary regimes for organic matter supply on the continental shelf off northern Norway. *Geochimica et Cosmochimica Acta*, **69**(19): 4631-4647

Kurian, S., Agnihotri, R., Borole, D. V., Naqvi, S. W. A., Farreira, A. M., Vale, C., 2009. Possible solar control on primary production along the west coast on decadal to centennial timescale. *Journal of Quaternary Science*, **24**: 109-116

Kutzbach, J. E., Guetter, P. J., Ruddiman, W. F., and Prell, W. L., 1989. Sensitivity of climate to late Cenozoic uplift in southern Asia and the American west: Numerical experiments. *Journal of Geophysical Research*, **94**: (D15), 18 393–18 407

Lamb, H. H., 1965. The early medieval warm epoch and its sequel. *Palaeogeography, Palaeoclimatology, Palaeoecology*, **1**: 13-37.

Laws, E. A., Popp, B. N., Bidigare, R. R., Kennicutt, M. C., and Macko, S. A., 1995. Deprndence of phytoplankton carbon isotopic composition on growth rate and $[CO_2]_{aq}$: Theoretical considerations and experimental results. *Geochimica Cosmochimica Acta*, **59**: 1131-1138

Levin, L. A., Gage, J. D., Martin, C., and Lamont, P. A., 2000. Macrobenthic community structure within and beneath the oxygen minimum zone, NW Arabian Sea. *Deep Sea Research II*, 47: 189-226

Lipp, J. S., Morono, Y., Inagaki, F., and Hinrichs, K-U., 2008. Significant contribution of Archaea to extant biomass in marine subsurface sediments; *Nature*, **454**, 991-994

Lisiecki, L. E., and Raymo, M. E., 2005. A Pliocene-Pliestocene stack of 57 globally distributed benthic $\delta^{18}O$ records. *Paleoceanography* **20**, PA1003: doi: 10.1029/2004PA001071

Liu, X., Liu, Z., Clemens, S., Prell, W., and Kutzbach, J., 2007. A coupled model study of Glacial Asian Monsoon Variability and Indian Ocean Dipole. *Journal of the Meteorological Society of Japan*, **85** (1): 1-10

Luis, A., and Kawamura, H., 2004. Air-Sea interaction, coastal circulation and primary production in the Eastern Arabian Sea: A Review. *Journal of Oceanography*, **60**: 205-218

Mackenzie, A.S., 1984. Application of biological markers in petroleum geochemistry, Brooks, J., and Welte, D.H. (Eds.). In: *Advances in Petroleum Geochemistry, Vol 1*. Academic Press, London.

Madhupratap, M., Prasanna Kumar, S., Bhattathiri, P. M .A., Dileep Kumar, M., Raghukumar, S., Nair, K. K. C., and N. Ramaiah., 1996. Mechanism of the biological response to winter cooling in the northeastern Arabian Sea, *Nature*, **384**: 549–552

Madureira, L. A. S., Conte, M. H., and Eglinton, G., 1995. Early diagenesis of lipid biomarker compounds in North Atlantic sediments. *Paleoceanography*, **10**(3): 627-642**.**

Mahesh, B. and Banakar, V. K., 2014. Change in the intensity of low-salinity water inflow from the Bay of Bengal into the Eastern Arabian Sea from the Last Glacial Maximum to the Holocene: Implications for monsoon variations. *Palaeogeography, Palaeoclimatology, Palaeoecology*, **397**: 31-37.

Marlowe, I. T., Green, J. C., Neal, A. C., Brassell, S. C., Eglinton, G., and Course, P, A., 1984. Long chain (n-C_{37}-C_{39}) alkenones in Prymnesiophyceae. Distribution of alkenones and other lipids and their taxonomic significance. *British Phycological Journal*, **19**; 203-216

Martin, J.H., Coale, K.H., Johnson, K.S., Fitzwater, S.E., Gordon, R.M., Tanner, S., et al., 1994. Testing the iron hypothesis in ecosystems of the equatorial Pacific Ocean, *Nature*, **371**:123-124

Matthes, F., 1939. Report of Committee on Glaciers. *Transactions of American Geophysical Unorthern Indian Oceann*, **20**: 518-535

McCreary, J P., Murtugudde, R., Vialard, J., Vinaychandran, P. N., Wiggert, J. D., Hood, R. R.., Shankar, D., Shetye, S. 2009. Biophysical processes in the Indian Ocean. *Geophysical Monograph Series*, 185

McElroy, M. B., 1983. Marine biological controls on atmospheric CO_2 and climate. *Nature*, **302**: 328– 329

Méjanelle, L. and Laureillard, J., 2008. Lipid biomarker record in surface sediments at three sites of contrasting productivity in the tropical North Eastern Atlantic. *Marine Chemistry*, **108**(1): 59-76.

Meyers., P. A., 1997. Organic geochemical proxies of paleoceanographic, paleolimnologic, and paleoclimatic processes. *Organic Geochemistry*, **27**: 213–250

Meyers, P.A., 2003. Applications of organic geochemistry to paleolimnological reconstructions: a summary of examples, from the Laurentian Great Lakes. *Organic Geochemistry*, **34**: 261–289

Milankovitch, M., 1920. Theorie Mathematique des Phenomenes Thermique par la Radiation Solaire. *Academie Yougoslave des Sciences et des Arts de Zagreb, Gauthier-Villars, Paris*

Milankovitch, M., 1938. Astronomische Mittel Zur Erforschung der Erdgeschichtlichen Klimate. *Handbook der Geophysik*, **9**: 593-698

Müller, A. 1997. Hydrodynamics and nutrient distribution in bottom sediments of the Archipelago Sea, southwestern Finland. *Boreal Environment Research*, **2**(3): 229-237.

Nagura, M., and McPhaden M., 2010. Wyrtki jet dynamics: Seasonal variability. *Journal of Geophysical Research*, **115**: C07009, doi:10.1029/2009JC005922.

Naidu, P. D., and Malmgrem, B. A., 1995. A 2,200 years periodicity in the Asian monsoon system. *Geophysical Research Letters*, **22** (17): 2361-2364.

Naidu, P. D., and Malmgren, B. A., 1999. Quaternary carbonate record from the equatorial Indian Ocean and its relationship with productivity changes. *Marine Geology* **161**: 49-62

Naini, B. R. and Talwani, M., 1982. Structural framework and the evolutionary history of the continental margin of western India, In: *Studies in Continental Margin Geology Vol. 34*, Watkins, J. S., Drake, C. L., (Eds.). American Association of Petroleum Geologists, pp. 167–191

Nair, R. R., Ittekot, V., Manganini, S. J., Ramaswamy, V., Haake. B., Degems, E. T., Desai, B. N., and Hanjo, S., 1989. Increased particle flux to the deep ocean related to monsoon. *Nature*, **338**: 749-751

Ninnemann, U. S., and C. D. Charles., 2002. Changes in the mode of Southern Ocean circulation over the last glacial cycle revealed by foraminiferal stable isotopic variability. *Earth and Planetary Science Letters*, **201**(2): 383 – 396

Olson, D. B, Hitchcock, G. L., Fine, R. A., and Warren, B. A., 1993. Maintenance of the low-oxygen layer in the central Arabian Sea. *Deep Sea Research Part II*, **40**: 673-685

Overpeck, J., Anderson, D., Trumbore, S., Prell, W., 1996. The southwest Indian Monsoon over the last 18000 years. *Climate Dynamics*, **12**: 213-225

Pailler, D., Edouard, B., Rostek, F., Zheng, Y., Mortlock, R., and Cerege, A., 2002. Burial of redox-sensitive metals and organic matter in the equatorial Indian Ocean linked to precession. *Geochimica et Cosmochimica Acta*, **66**: 849-865

Paropkari, A. L., Babu, C. P., Mascarenhas, A., 1993. New evidence for enhanced preservation of organic carbon in contact with oxygen minimum zone on the western continental slope of India. *Marine Geology*, **111**(1): 7-13.

Paul, M. R., and Ramammirthan, C. P., 1963. Hydrography of the Laccadives offshore waters- A study of the winter conditions. *Journal of the Marine Biological Association of India*, **V** (2):159-169.

Pattan, J., Masuzawa, T., Naidu, P. D., Parthiban, G., and Yamamoto, M., 2003. Productivity fluctuations in the southeastern Arabian Sea during the last 140 ka. *Palaeogeography, Palaeoclimatology, Palaeoecology*, **193**(3): 575-590

Pearson, A. and Eglinton, T. I., 2000. The origin of *n*-alkanes in Santa Monica Basin surface sediment: a model based on compound-specific $\Delta^{14}C$ and $\delta^{13}C$ data. Organic Geochemistry, **31**(11): 1103-1116.

Petit, J.-R., Jouzel, J., Raynaud, D., Barkov, N. I., Barnola, J. M., Basile, I., Bender, M., Chappellaz, J., Davis, M., Delaygue, G., Delmotte, M., Kotlyakov, V. M., Legrand, M., Lipenkov, V. Y., Lorius, C., Pepin, L., Ritz., C., Saltzman, E., Stievenard, M., 1999. Climate and atmospheric history of the past 420,000 years from the Vostok ice core, Antarctica. *Nature*, **399**(6735): 429-436.

Piotrowski, A. M., Banakar, V.K., Scrivner, A.E., Elderfield, H., Galy, A., and Dennis, Aileen., 2009. Indian Ocean circulation and productivity during the Last Glacial Cycle. *Earth and Planetary Science Letters*, **285**:179-189.

Pourmand, A., Marcantonorthern Indian Ocean, F., Bianchi, T. S., Canuel, E. A., and Waterson, E. J., 2007. A 28-ka history of sea surface temperature, primary productivity and planktonic community variability in the western Arabian Sea. *Paleoceanography*, **22**(4): 1- 14.

Poynter, J G., Farrimond, P., Brassell, S. C., and Eglinton, G., 1989. Molecular stratigraphic study of sediments from holes 658A and 660A, Leg 108, Ruddiman, W., and Sarnthein, M., (Eds.) *Proceedings of the Ocean Drilling Program, Scientific Results*, **108**: 387-394

Prabhu, C. and Shankar, R., 2005. Palaeoproductivity of the eastern Arabian Sea during the past 200ka: A multi-proxy investigation. *Deep Sea Research Part II: Topical Studies in Oceanography*, **52**(14): 1994-2002

Prahl, F. G., Ertel, J. R., Goni, M. A., Sparrow, M. A., and Eversmeyer, B., 1994. Terrestrial organic carbon contributions to sediments on the Washington margin. *Geochimica et Cosmochimica Acta*, **58:** 3035–3048

Prahl, F. G., and Wakeham, S. G., 1987. Calibration of unsaturation patterns in long-chain ketone composition for paleo-temperature assessment. *Nature*, **330**: 367-369.

Prahl, F. G., Dymond, J., and Sparrow, M. A., 2000. Annual biomarker record for export production in the central Arabian Sea. *Deep Sea Research II*, **47**: 1581-1604

Prasanna Kumar, S., Madhupratap, M., Dileep Kumar, M., Gauns, M, Muraleedharan, P.M., Sarma, V. V. S. S., DeSouza, S. N., 2000. Physical control of primary productivity on a seasonal scale in Central and Eastern Arabian Sea. Proc. Ind. Acd. Sci. (EPS), 109, 433-441.

Prasanna Kumar, S., Ramaiah, N., Gauns, M,, Sarma, V. V. S. S., Muraleedharan, P. M., Raghukumar, S., Dileep Kumar, M., and Madhupratap, M., 2001. Physical forcing of biological productivity in the Northern Arabian Sea during the Northeast Monsoon. Deep Sea Research II, 48: 1115-1126

Prakash Babu, C., Brumsack, H-J., Schnetger., 1999. Distribution of organic carbon in surface sediments along the eastern Arabian Sea: a revisit. *Marine Geology*,**162**(1): 91-103.

Prell, W.L., Hutson, W.H., Williams, D.F., Be, A.W.H., Geitzenauer, K., and Molfino, B., 1980. Surface circulation of the Indian Ocean during the last

glacial maximum: Approximately 18,000 yr BP. *Quaternary Research,* **14**: 309-336

Punyu, V. R., Banakar, V. K., and Garg, A., 2014. Equatorial Indian Ocean productivity during the last 33kyr and possible linkage to Westerly Jet variability. *Marine Geology,* **348**: 44-51.

Qasim, S. Z., 1977. Biological productivity of the Indian Ocean. *Indian Journal of Marine Sciences,* **6** : 122-137.

Qasim, S. Z., 1982. Oceanography of the northern Arabian Sea. *Deep Sea Research II,* **29**: 1041-1068

Qasim, S. Z., 1998. In: *Glimpses of the Indian Ocean*. Universities Press (India) Limited

Rai, A. K., and Das, S. S., 2011. Late Quaternary changes in surface productivity and oxygen minimum zone (OMZ) in the northwestern Arabian Sea: Micropaleontologic and sedeimentary record at ODP site 728A. *Journal of Earth System Science*,**120** (1): 113-121

Rajagopalan, G., Sukumar, R., Ramesh, R., Pant, R. K., and Rajagopalan, G., 1997. Late Quaternary vegetational and climatic changes from tropical peats in southern India-An extended record up to 40,000 years BP. *Current Science*, **73**: 60-63

Ramage, C., 1971. Monsoon Meteorology. *International Geophysics Series*, **15**: 296 Academic Press, San Diego, California

Raman, A. V., 1995. Pollution effects in Visakhapatnam harbour, India: an overview of 23 years of investigations and monitoring. *Helgoland Marine Research*, **49**: 1-4

Rao, T. S. S., and Griffiths, R. C., 1998. Understanding the Indian Ocean-Perspectives on Oceanography.UNESCO, Paris, France

Rao, R. R., Sivakumar, R., 2003. Seasonal variability of sea surface salinity and salt budget of the mixed layer of the north Indian Ocean. *Journal of Geophysical Research*, **107**: Doi:10.1029/2001JC00907

Redfield, A. C., Ketchum, B. H., Richards, F. A., 1963. The influence of organisms on the composition of seawater; In: *The Sea,* M. N. Hill (Ed.), Vol. 2. Wiley, New York, NY, pp. 26-77

Reichert, G. J., Lourens, L. J., Zachariasse, W. J., 1998. Temporal variability in the northern Arabian Sea Oxygen Minimum zone (OMZ) during the last 225,000 years. *Paleoceanography*, **13** (6): 607-621.

Reid, J. L., Brinton, E., Fleminger, A., Venrick, E. L., and McGowan, J. A., 1978. Ocean circulation and marine life. In: *Sir George Deacon (Ed.). Advances in Oceanography*. Plenum Press, New York

Reid, J. L., 2003. On the total geostrophic circulation of the Indian Ocean: Flow patterns, tracers, and transports. Progress in Oceanography, 56: 137-186.

Resplandy, L., Levy, M., Bopp, L., Echevin, V., Pous, S., Sarma, V. V. S. S and Kumar, D., 2012. Controlling factors of the OMZ in the Arabian Sea. *Biogeosciences Discussions*, **9**: 5509- 5550

Rieley, G., Collier, R. J., Jones, D. M., and Eglinton, G., 1991. The biogeochemistry of Ellesmere Lake, UK-I: source correlation of leaf wax inputs to the sedimentary lipid record. *Organic Geochemistry*, **17**: 901-912

Rochford, D. J., 1964. Salinity maximum in the upper 100 meters of the north Indian Ocean. *Australian Journal of Marine and Freshwater Research*, **15**: 1-24

Rogers, A. D., 2000. The role of the oceanic oxygen minima in generating biodiversity in the deep sea. *Deep Sea research II*, **47**: 119-148

Rommerskirchen, F., Eglinton, G., Dupont, L., and Rullkotter, J., 2006. Glacial/interglacial changes in southern Africa: compound-specific δ13C land plant biomarker and pollen records from southeast Atlantic continental margin sediments. *Geochemistry, Geophysics, Geosystems*, **7**: Q08010. doi:10.1029/2005GC001223

Rontani, J-F., and Volkman, J. K., 2003. Phytol degradation products as biogeochemical tracers in aquatic environments. *Organic Geochemistry*, **34**: 1-3

Rostek, F., Ruhland,G., Bassinot, F. C., Beaufort, F., Müller, P. J., and Bard, E., 1994. Fluctuations of the Indian monsoon regime during the last 170,000 years: evidence from sea surface temperature, salinity and organic carbon records. *Global Precipitations and Climate Change*, **26**: 27-51.

Rostek, F., Bard, E., Beaufort, L., Sonzogni, C., and Ganssen, G., 1997. Sea surface temperature and productivity records for the past 240 kyr in the Arabian Sea. *Deep Sea Research II*, **44** (6-7): 1461-1480.

Ruttenberg, K. C., 1993. Reassessment of the oceanic residence time of phosphorus. *Chemical Geology*, **107**: 405–409

Ryther, J., and Menzel, D.W., 1965. On the production, composition, and distribution of organic matter in the Western Arabian Sea. *Deep-Sea Research* **12**: 199-209

Ryther, J. H., Hall, J. R., Pease, A. K., Bakun, A., and Jones, M. M., 1966. Primary organic production in relation to the chemistry and hydrography of the Western Indian Ocean. *Limnology and Oceanography*, **11** : 371-380

Sachs, J. P., Sachse, D., Smittenberg, R., Zhang, Z. H., Battisti, D. S., and Golubi, S., 2009. Southward movement of the Pacific intertropical convergence zone AD 1400-1850. *Nature Geosciences,* **2**:519-525.

Saraswat, R., Nigam, R., Weldeab, S., Mackensen, A., and Naidu, P. D., 2005. A first look at past sea surface temperatures in the equatorial Indian Ocean from Mg/Ca in foraminifera. *Geophysical Research Letters*, **32**(24): L24605, doi:10.1029/2005GL024093

Sardans, J., Rivas-Ubach, A., and Penuelas, J., 2012. The C: N: P stoichiometry of organisms and ecosystems in a changing world: a review and perspectives. *Perspectives in Plant Ecology, Evolution and Systematics*, **14**(1): 33-47.

Sarmiento, J. L., and Gruber, N., 2006. Ocean Biogeochemical Dynamics. Princeton University Press, Princeton, N. J

Sarma, K. V. L. N. S., Ramana, M. V., Krishna, K. S., Ramprasad, T., and Desa, M., 2000. Morphological features in the Bay of Bengal. *Journal of Indian Geophysical Unorthern Indian Oceann*, **4** (2): 185-190

Sarma, V. V. S. S., 2002. An evaluation of physical and biogeochemical processes regulating perennial suboxic conditions in the water column of the Arabian Sea. *Global Biogeochemical Cycles*, **16** (4): 1082, doi:10.1029/2001GB001461

Sawant, S., and Madhupratap, M., 1996. Seasonality and composition of phytoplankton in the Arabian Sea. *Current Science*, **71** (11): 869-873

Schefuß, E., Versteegh, G. J. M., Jansen, J. H. F., Sinninghe Damsté, J. S., 2001. Marine and terrigenous lipids in southeast Atlantic sediments (Leg 175) as paleoenvironmental indicators: Initial results. *In: Wefer, G; Berger, WH;*

Richter, C (eds.) Proceedings of the Ocean Drilling Program, Scientific Results, College Station, TX (Ocean Drilling Program), **175**, 1-23, doi:10.2973/odp.proc.sr.175.228.2001

Schott, F. A. and McCreary Jr, J. P., 2001. The monsoon circulation of the Indian Ocean. *Progress in Oceanography*, **51**(1): 1-123.

Schott, F. A., Dengler, M., Schoenefeldt, R., 2002. The shallow overturning circulation of the Indian Ocean. *Progress in Oceanography*, **53**: 57-10

Schouten, S., Hoefs, M. J. L., and Daamste, J. S. S., 2000. A molecular and stable carbon isotopic study of lipids in late Quaternary sediments from the Arabian Sea. *Organic Geochemistry*, **31**: 509-521.

Schubert, C. J., Villanueva, J., Calvert, S. E., Cowie, G. L., von Rad, U., Schulz, H., Berner, U., and Erlenkeuser, H., 1998. Stable phytoplankton community structure in the Arabian Sea over the past 200,000 years. *Nature*, **394**: 563–566

Schulte, S., Rostek, F., Bard, E., Rullkotter, J., and Marchal, O., 1999. Variations of oxygen-minimum and primary productivity recorded in the sediments of the Arabian Sea. *Earth and Planetary Science Letters*,**173**: 205-221

Schulte, S., Mangelsdorf, K., and Rullkoetter, J., 2000. Organic matter preservation on the Pakistan margin as revealed by biomarker geochemistry. *Organic Geochemistry*, **31**: 1005-1022

Schulte, S., and Bard, E., 2003. Past changes in biologically mediated dissolution of calcite above the chemical lysocline recorded in Indian Ocean sediments. *Quaternary Science Reviews*, **22**: 1757–1770

Schulz, H., Rad, U. V., Stackelberg, U. V., 1996. Laminated sediments from the oxygen-minimum zone of the northeastern Arabian Sea. *Geological Society, London, Special Publications*, **116**(1): 185-207.

Schwabe, H., 1843. Solar Observations during 1843. *Astronomische Nachriten*, **20** (495)

Senan, R., Sengupta, D., and Goswami, B. N., 2003. Intraseasonal "monsoon jets" in the equatorial Indian Ocean. *Geophysical Research Letters*, **30**(14). doi: 10.1029/2003GL017583

Sengupta, R., and Qasim, S. Z., 1995. The Indian Ocean- An environmental overview. IOC/UNESCO workshop on regional Co-operation in Marine Science in the Central Indian Ocean and Adjacent Seas and Gulfs, Colombo, 8-13 July, 1985, pp. 9-41.

Shackleton, N.J., Imbrie, J., and Hall, M.A., 1983. Oxygen and carbon isotope record of east Pacific core V19-30: Implications for the formation of deep water in the late Pleistocene North Atlantic. *Earth and Planetary Science Letters*, **65**: 233-244

Shackleton, N. J., 2000. The 100,000 year ice-age cycle identified and found to lag temperature, carbon dioxide and orbital eccentricity. *Science*, **289**: 1897-1902

Shankar, D., 2000. Seasonal cycle of sea level and currents along the coast of India. *Current Science*, **78** (3): 279-288

Shankar, D., Vinaychandran, P. N., and Unnikrishnan, A. S., 2002. The monsoon currents in the north Indian Ocean. *Progress in Oceanography*, **52**: 63-120

Shetye, S. R., Gouveia, A. D., Shenoi, S. S. C., Michael, G. S., Sundar, D., Almeida, A. M., Santanam, K., 1991. The coastal current off western Indian during the northeast monsoon. *Deep Sea Research*, **38** (12): 1517-1529

Shetye, S. R., Gouveia, A. D., and Shenoi, S. S. C., 1994. Circulation and water masses of the Arabian Sea. *Proceedings of the Indian Academy of Science (Earth and Planetary Sciences)*:**103** (2): 107-123

Sigman, D. M., and Boyle, E. A., 2000. Glacial/interglacial variations in atmospheric carbon dioxide. *Nature*, **407**: 859-869

Sigman, D. and Haug, G., 2003. The biological pump in the past. *Treatise on Geochemistry*, **6**: 491-528

Sigman, D. M., Mathis, H. P., 2012. The Biological Productivity of the Ocean: Section 2; Nature Education

Simoneit, B.R.T., 1984. Organic matter of troposphere-III. Characterization and sources of petroleum and pyrogenic residues in aerosols over the Western United States. *Atmospheric Environment*, 18: 51-67.

Singh, A. D., Jung, S. J., Darling, K., Geneshram, R., Ivanochko, T., and Kroon, D., 2011. Productivity collapses in the Arabian Sea during glacial cold phases. *Paleoceanography*, **26**: PA3210, doi:10.1029/2009PA001923

Sirocko, F., and Ittekot, V., 1992. Organoc carbon accumulation rates in the Holocene and glacial Arabian Sea: Implications for O_2 consumption in deep-sea and atmospheric CO_2 variations. *Climate Dynamics*, **7**: 167-172

Sirocko, F., Brunck, H., and Pfahl., 2012. Solar influence on winter severity in central Europe. Geophysical Research Letters, **39**: L16704, doi:10.1029/2012GL052412

Smith, H. J., Wahlen, M., Mastroianni, D., and Taylor, K. C., 1997a. The CO_2 concentration of air trapped in GISP2 ice from the Last Glacial Maximum-Holocene transition. *Geophysical Research Letters*, **24** (1): 1-4

Smith, H. J., Wahlen, M., Mastroianni, D., Taylor, K. C., and Mayewski P., 1997b. The CO_2 concentration of air trapped in Greenland Ice Sheet Project 2 ice formed during periods of rapid climate change. *Journal of Geophysical Research*, **102**: 26,577-26582

Smith, R. L., and J. S. Bottero., 1977. On upwelling in the Arabian Sea. In*: A voyage of Discovery*, *George Deacon 70th Anniversary Volume*, Angel, N., (Ed.). Pergamon Press

Smith, S.L., and Codispoti, L.A., 1980. Southwest monsoon of 1979: chemical and biological response of Somali coastal waters. *Science*, **209**: 597-600.

Smith, S. L., 2001. Understanding the Arabian Sea: Reflections on the 1994-1996 Arabian Sea Expedition. *Deep Sea Research Part II*, **48**: 1385–1402

Smittenberg, R.H., Saenger, C., Dawson, M.N., and Sachs, J.P., 2011. Compound – specific D/H ratios of the marine lakes of Palau as proxies for West Pacific Warm pool hydrologic variability. *Quaternary Science Reviews*, **30**:921-933

Sonzogni, C., Bard, E., and Rostek, F., 1998. Tropical sea-surface temperatures during the last glacial period: a view based on alkenones in Indian Ocean sediments. *Quaternary Science Reviews*, **17**(12): 1185-1201

Sukumar, R., Suresh, H.S., and Ramesh, R., 1995. Climate change and its impact on tropical montane ecosystems in Southern India. *Journal of Biogeography*, **22**:533-536.

Swallow, J. C., 1984. Some aspects of physical oceanography of the Indian Ocean. *Deep Sea Research*, **31**: 639-650

Tamburini, F., Adatte, T., Follmi, K., Bernasconi, S. M., and Steinmanna, P., 2003. Investigating the history of East Asian monsoon and climate during the last

glacial–interglacial period (0–140 000 years): mineralogy and geochemistry of ODP Sites 1143 and 1144, South China Sea. *Marine Geology*, **201**(1): 147-168.

Tchernia, P., 1980. In: *Descriptive Regional Oceanography*. Permagon Press

Ternois, Y., Kawamura, K., Keigwin, L., Ohkouchi, N., and Nakatsukai, T., 2001. A biomarker approach for assessing marine and terrigenous inputs to the sediments of Sea of Okhotsk for the last 27,000 years. *Geochimica et Cosmochimica Acta*, **65** (5): 791–802

Thamban, M., Rao, V. P., and Raju, S. V., 1997. Controls on organic carbon distribution in sediments from the eastern Arabian Sea margin. *Geo-Marine Letters*, **17**(3): 220-227

Tiwari, M., R. Ramesh, Somayajulu, B. L. K., Jull, A. J. T., and Burr, G. S., 2006. "Paleomonsoon precipitation deduced from a sediment core from the equatorial Indian Ocean." *Geo-Marine Letters*, **26**(1): 23-30.

Tolosa, I., LeBlond, N., Copin-Montegut, C., Marty, J., de Mora, S., and Prieur, L., 2003. Distribution of sterol and fatty alcohol biomarkers in particulate matter from the frontal structure of the Alboran Sea (SW Mediterranean Sea). *Marine Chemistry*, **82**: 161–183.

Tomczak , M and Godfrey, J. S., 1994. In: *Regional Oceanography: an introduction*, Permagon, United Kingdom

Tschumi, J., and Stauffer, B., 2000. Reconstructing past atmospheric CO_2 concentration based on ice- core analyses: open questions due to insitu production of CO_2 in the ice. *Journal of Glaciology*, **46** (152)

Tudhope, A. W., Lea, D. W., Shimmield, G. B., Chilcott, C. P., and Head, S., 1996. Monsoon climate and Arabian Sea coastal upwelling recorded in massive corals from Southern Ocean. *Palaios*, **11**: 347-361

Valdiya, K. S., 1993. Uplift and geomorphic rejuvenation of the Himalaya in the Quaternary Period. *Current Science* **64**: 873-885

Van Campo, E., Duplessy, J. C., Rossignol-Strick, M., 1982. Climatic conditions deduced from a 150-kyr oxygen isotope-pollen record from the Arabian Sea. *Nature*, **296**: 56-59.

Van Campo, E. 1986. Monsoon fluctuations in two 20,000-yr BP oxygen-isotope/pollen records off southwest India. *Quaternary Research*, **26**(3): 376-388.

Vinaychandran, P. N., Saji, N. H., and Yamagata, T., 1999. Response of the Equatorial Indian Ocean to an unusual wind event during 1994. *Geophysical Research Letters* **26**: 1613-1616

Vogts, A., Moossen, M., Rommerskirchen, F., and Rullkötter, J., 2009. Distribution patterns and stable carbon isotopic composition of alkanes and alkan-1-ols from plant waxes of African rain forest and savanna C3 species. *Organic Geochemistry*, **40**: 1037–1054

Volkman, J. K., 1986. A review of sterol markers for marine and terrigenous organic matter. *Organic Geochemistry*, **9**: 83-99

Volkman, J. K., Barretti, S. M., Balckburn, S I., Mansour, M. P., Sikes, E. L., and Gelin, F., 1998. Microalgal biomarkers: A review of recent research developments. *Organic Geochemistry*, **29**: 1163-1179

Volkman, J. K., Barrett, S. M., Blackburn, and S. I., 1999. Eustigmatophyte microalgae are potential sources of C29 sterols, *n*-C23–*n*-C28 *n* alkanols and

C28–C32 *n*-alkyl diols in freshwater environments. *Organic Geochemistry*, **30**: 307-318

Volkman J K., 2006. Lipid markers for marine organic matter. In: *The Handbook of Environmental Chemistry. Vol 2 : Reactions and Processes*, Volkman, J. K., (Ed.). Berlin: Springer Verlac

Wagener, A. L. R., Meniconi, M. F. G., Hamacher, C., Farias, C. O., da Silva, G. C., Gabardo, I. T., and Scofield, A. L., 2012. Hydrocarbons in sediments of a chronically contaminated bay: The challenge of source assignment. *Marine Pollution Bulletin*, **64**: 284-294.

Wahlen, M., Allen, D., and Deck, B., 1991. Initial measurements of CO_2 concentrations (1530 to 1940 AD) in air occluded in the GISP 2 ice core from Central Greenland. *Geophysical Research Letters*, **18** (8): 1457-1460

Wakeham, S. G., Peterson, M. L., Hedges, J. I., and Lee, C., 2002. Lipid biomarker fluxes in the Arabian Sea, with a comparison to the equatorial Pacific Ocean. *Deep-Sea Research* II, **49**: 2265–2301

Walker, G. T., 1920. Probable amount of monsoon rainfall in 1920. *Monthly Weather Review*, **48**: 415

Walsh, J. J., Premuzic, E. T., and Whitledge, T. E., 1981. Fate of nutrient enrichment on continental shelves as indicated by C/N content of bottom sediments. In: Nihoul, J.C.J. (Ed.), Echohydrodynamics. Elsevier, pp. 13–49.

Wiggert, J., Jones, B., Dickey, T. D., Brink, K. H., Weller, R. A., Marra, J., and Codispoti, L. A., 2000. The Northeast Monsoon's impact on mixing, phytoplankton biomass and nutrient cycling in the Arabian Sea. *Deep Sea Research Part II: Topical Studies in Oceanography*, **47**(7): 1353-1385

Wiggert, J. D., Hood, R. R., Banse, K., and Kindle, J. C., 2005. Monsoon-driven biogeochemical processes in the Arabian Sea. *Progress in Oceanography*, **65**: 176–213

Wyrtki, K., 1971. *Oceanographic Atlas of the International Indian Ocean Expedition*, National Science Foundation, Washington, D. C., pp. 531

Wyrtki, K., 1973. An equatorial jet in the Indian Ocean. *Science*, **181**: 262-264

Xie, S., Yi, Y., Huang, J., Hu, C., Cai, Y., Collins, M., and Baker, A. 2003. Lipid distribution in a subtropical southern China stalagmite as a record of soil ecosystem response to paleoclimate change. *Quaternary Research*, **60**: 340-347

You, Y., 2000. Implications of the deep circulation and ventilation of the Indian Ocean on the renewal mechanisms of North Atlantic Deep Water. *Journal of Geophysical Research*, **105**: 23,895-23,926.

You, Y., and Tomczak, M., 1993.Thermocline circulation and ventilation in the Indian Ocean derived from water mass analysis. *Deep Sea Research (I)*, **40**: 13-56.

Zhou, W., Zheng, Y., Meyers, P. A., Jull, A. J. T., and Xie, S., 2010. Postglacial climate-change record in biomarker lipid compositions of the Hani peat sequence, Northeastern China. *Earth and Planetary Science Letters*, **294**: 37–46